Project funded by EUROPEAN UNION

BSB 966

Available methodologies for REDA

Deliverable No: D.T1.2.1

GA T1 IMPLEMENTATION (A harmonized approach for Rapid Earthquake Damage), A.T1.2 (Feasibility study of available methodologies for REDA)

COORDINATED BY:

Ovidius University of Constanta (OUC)

INVOLVED PARTNERS:

- The Legal Successor of TEICM, International Hellenic University (IHU-TEICM)
- Institute of Engineering Seismology & Earthquake Engineering - Research Unit of Earthquake Planning & Protection Organization (ITSAK-EPPO)
- Democritus University of Thrace (DUTh)
- Gebze Technical University (GTU)
- Institute of Geology and Seismology (IGS)

PROJECT DETAILS:

Programme	Black Sea Joint Operational Programme 2014-20
Priority and Measure	2. Promote coordination of environmental protection and joint reduction of marine litter in the Black Sea Basin
Objective	2.1 Improve joint environmental Monitoring
Project Title	Rapid Earthquake Damage Assessment Consortium
Project Acronym	REDACt
Contract No	BSB-966
Lead Partner	The Legal Successor in rights and Duties of TEICM_SARF, IHU SARF, GREECE
Total Budget	974.860,00 Euro (€)
Time Frame:	
Start Date – End Date	01/07/2020 – 31/12/2022
Project Coordinator	Papatheodorou K. (IHU-TEICM)

DELIVERABLE CONTRIBUTORS:

OUC: TOMA-DANILA Dragos, TIGANESCU Alexandru, VINTILĂ Dragos-Florian, CIOFLAN Carmen Ortanza, TEPES Florin Onea
IHU-TEICM: PAPATHEODOROU Konstantinos, KIRTAS Emmanouil, PANAGOPOULOS Georgios, KOLIOPOULOS Panagiotis
ITSAK-EPPO: THEODOULIDIS Nikolaos, MARGARIS Basil, KARAKOSTAS Christos, KONSTANTINIDOU Kiriaki
DUTh: KLIMIS Nikos, PAPATHANASSIOU George, PETALA Eleni
GTU: ZULFIKAR Can, YASIN Fahjan, CETINDEMIR Oguzhan, AKRAM M. Rizwan, BIRO Yesim
IGS: TROIAN Sergiu

RECORD OF REVISIONS

Issue/Rev	Date	Page(s)	Description of Change	Release
1	10.12.2020	112	Release of the first consolidate draft by OUC	I.01
2	20.12.2020	124	Review by all project partners	I.02
3	15.01.2021	129	Release of the second consolidated draft by OUC	I.03
4	30.01.2021	128	Release of the first deliverable version by OUC	I.04
5	31.01.2021	132	Minor editing corrections	I.05
6	31.01.2021	132	Approved!	I.05

DOCUMENT RELEASE SHEET

Responsible Partner:	Ovidius University, Constanta, Romania	
Approval	Emmanouil Kirtas	Signature 31.01.2021
Approval	Nikolaos Theodoulidis	Signature 31.01.2021
Approval	Nikolaos Klimis	Signature 31.01.2021
Approval	Can Zulfikar	Signature 31.01.2021
Approval	Dragos Vintila	Signature 31.01.2021
Approval	Sergiu Tojan	Signature 31.01.2021e
Approved by the Project Coordinator:	Konstantinos Papatheodorou	Signature 31.01.2021
Distribution:	ALL PARTNERS	

Konstantinos Papatheodorou

Digitally signed by Konstantinos Papatheodorou
DN: c=GR, l=Thessaloniki, o=International Hellenic University, ou=Class B - Private Key created and stored in software CSP, sn=Papatheodorou, givenName=Konstantinos, serialNumber=6173517149, cn=Konstantinos Papatheodorou, email=conpap@teicm.gr
Date: 2021.04.16 10:14:27 +03'00'

TABLE OF CONTENTS

1 BACKGROUND OF THE DOCUMENT 8

1.1 SCOPE AND OBJECTIVES 8
1.2 RELATED DOCUMENTS 8
1.2.1 INPUT 8
1.2.2 OUTPUT 8

2 INTRODUCTION 8

3 OVERVIEW OF REDA METHODOLOGIES 9

3.1 HAZARD EVALUATION 9
3.2 SHAKEMAP METHODOLOGY 14
3.3 GEOTECHNICAL HAZARD MODELLING 18
3.3.1 LIQUEFACTION 18
LIQUEFACTION SEVERITY NUMBER LSN 41
3.3.2 LANDSLIDES 42
3.4 DAMAGE ESTIMATION METHODOLOGIES FOR BUILDINGS 52
3.5 INFRASTRUCTURE LOSS ESTIMATION METHODS 59
3.5.1 FRAGILITY FUNCTIONS FOR TYPICAL BRIDGE STRUCTURES 59
3.5.2 FRAGILITY FUNCTIONS FOR BURRIED PIPELINES 73
3.6 SOCIO-ECONOMIC CONSEQUENCE ESTIMATION 78

4 AVAILABLE REDA SOFTWARE 82

4.1 REDA SOFTWARE OR SYSTEMS 82
4.2 AFAD-RED 97
TYPICAL BRIDGE STRUCTURES DAMAGE ASSESSMENT IN AFAD-RED 98
4.3 CAPRA SOFTWARE COLLECTION 103
4.4 ELER 105
4.5 HAZUS 106
4.6 MAEVIZ 108
4.7 OPENQUAKE 109
4.8 PAGER 111
4.9 SELENA 115
4.10 OTHER SOFTWARE 117

5 METHODOLOGY SELECTION FOR REDA 117

6 CONCLUSIONS 120

REFERENCES 122

LIST OF FIGURES

FIGURE 1. FOUR BASIC STEPS OF PSHA (REITER, 1991) 12
FIGURE 2. ILLUSTRATION OF THE SEISMIC HAZARD CURVES WITH PERCENTILES DETERMINED BY PSHA APPROACH (ABRAHAMSON AND BOMMER, 2005). 14
FIGURE 3 SCHEMATIC MAIN PRINCIPLES OF SHAKEMAP® V3.5 AND THE BAYESIAN INFERENCE SHAKE-MAP PROCEDURES. SHAKEMAP® V4 DOES NOT CORRECT TO ROCK CONDITIONS BEFORE 17
FIGURE 4. GEOMORPHOLOGICAL ORIENTED MAP OF LIQUEFACTION MANIFESTATIONS AT THE AREA OF CHRISTCHURCH 19
FIGURE 5. SPATIAL CORRELATION OF LATERAL SPREADING PHENOMENA AND THE TYPE OF DEPOSITS AT THE AREA OF AVON RIVER (BASTIN ET AL., 2017) 20
FIGURE 6. DETAILED PRESENTATION OF LIQUEFACTION-INDUCED GROUND FAILURES (BASTIN ET AL., 2020) 20
FIGURE 7. RANGES OF WC/LL AND PLASTICITY INDEX FOR VARIOUS SUSCEPTIBILITY CATEGORIES ACCORDING TO BRAY AND SANCIO (2006) 27
FIGURE 8. CPT-BASED SOIL BEHAVIOR TYPE CHART (ROBERTSON, 1990) 28
FIGURE 9. MAPS OF THE OBSERVED LIQUEFACTION FEATURES AND THE PREDICTED PROBABILITY OF LIQUEFACTION FOR THE 1989 LOMA PRIETA EARTHQUAKE (ZHU ET AL., 2015) 33
FIGURE 10. PROBABILITY MAPS PREDICTED FROM MODEL 1 FOR EARTHQUAKES IN THE USA (ZHU ET AL., 2017). 36
FIGURE 11. PROBABILITY MAPS PREDICTED FROM MODEL 2 FOR A) WENCHUAN 2008, B) NORTHRIDGE 1994, C) HECTOR MINE 1999, D) CHI-CHI 1999, E) NEPAL 2015, F) BHUJ 2001 EARTHQUAKES (ZHU ET AL., 2017). 36
FIGURE 12. LPI-BASED PROBABILITY CURVE (PAPATHANASSIOU, 2008) 40
FIGURE 13. DISCRIMINATING BETWEEN OCCURRENCE AND NON-OCCURRENCE OF GROUND RUPTURING DUE TO LIQUEFACTION 0.2G PGA); AND (B) BOUNDARY CURVES PROPOSED FOR IDENTIFICATION OF LIQUEFACTION-INDUCED DAMAGE (ISHIHARA, 1985) 42
FIGURE 14 FLOW CHART FOR STEPS INVOLVED IN THE PROPOSED APPROACH TO OBTAIN THE DISPLACEMENT PREDICTIONS (BOXES IN LIGHT RED SIGNIFY AVAILABLE DATA) (SAADE ET AL., 2016) 48
FIGURE 15. MAIN COMPONENTS AND PHASES CONSIDERED IN ANALYTICAL FRAGILITY ASSESSMENT METHODOLOGIES AND ASSOCIATED UNCERTAINTIES MAIO & TSIONIS (2015) 54
FIGURE 16. FRAGILITY CURVES FOR MASONRY (THIN LINES) AND REINFORCED CONCRETE (THICK LINES) BUILDING TYPOLOGIES CONVERTED TO PGA (LEFT) AND SA(0.3S) (RIGHT) (MICHEL ET AL., 2018) 58
FIGURE 17. COMPARISON OF CONVERTED AND REFERENCE FRAGILITY CURVES TO SPECTRAL ACCELERATION AT A LARGER PERIOD (FROM SA(0.5S) TO SA(T>0.5 S)) (SUZUKI AND IERVOLINO, 2020) 58
FIGURE 18 PERCENTAGE OF VARIOUS SEISMIC INTENSITY PARAMETERS USED FOR DEVELOPMENT OF FRAGILITY RELATIONSHIPS. 74
FIGURE 19 COMPARISON OF FRAGILITY CURVES DEVELOPED BY VARIOUS RESEARCHERS (RR AGAINST PGV) 75
FIGURE 20 COMPARISON OF REPAIRS RATE VS. PGV BASED ON K1 76
FIGURE 21 SCENARIO-BASED SEISMIC RISK ASSESSMENT IN TERMS OF LOSS CURVES AND DAMAGE MAPS: (I) HAZARD SIMULATION IN TERMS OF PGA, PGV, AND PGD; (II) VULNERABILITY FUNCTIONS; (III) LOSS CURVES; (IV) FRAGILITY FUNCTIONS; AND (V) DAMAGE MAPS. 78
FIGURE 22. POST-EARTHQUAKE RESTORATION CURVES FOR VARIOUS RESTORATION LEVELS FOR MOMENT FRAME REINFORCED CONCRETE BUILDINGS DESIGNED ACCORDING TO THE OLD GREEK CODES (KAPPOS ET AL., 2009) 79
FIGURE 23. THE COMMUNITY-LEVEL RECOVERY FUNCTION FOR ONE OF THE ZONES UNDER ANALYSIS, SHOWING HOW THE NORMALIZED RECOVERY LEVEL EVOLVES WITH TIME AFTER THE EARTHQUAKE (OPENQUAKE INTEGRATED RISK MODELLING TOOLKIT DOCUMENTATION) 80
FIGURE 24. AN EVACUATION VULNERABILITY EXAMPLE FOR THE MUNICIPALITY OF AGHIA PARASKEVI (ATHENS, GREECE). THE COLOR CORRESPONDS TO THE RATIO OF POPULATION EVACUATED TO THE BLD (BULK LANE

DEMAND). ORANGE COLOR REPRESENTS A VALUE OF 300 PERSONS PER LANE WHILE RED OF MORE THAN 500 (KONTOES ET AL., 2012) 81
FIGURE 25. ANALYSIS OPTION FOR TRANSPORTATION SYSTEM 98
FIGURE 26. VULNERABILITY FOR BRIDGE STRUCTURES 98
FIGURE 27. VULNERABILITY TYPES FOR BRIDGE STRUCTURES. (LOG-NORMAL DISTRIBUTION PARAMETERS) 99
FIGURE 28. LOSS ESTIMATION METHOD FOR TRANSPORTATION SYSTEM 99
FIGURE 29. UPLOADING THE SHAPE FILE AND BRIDGE AND TUNNELS INVENTORY 100
FIGURE 30. SHAPE FILE FOR THE BRIDGES IN TURKEY 100
FIGURE 31. ATTENUATION RELATIONSHIP EQUATIONS 101
FIGURE 32. ATTENUATION RELATIONSHIPS MODULE IN AFAD-RED 102
FIGURE 33. RESULTS, IN THE FORM OF GIS MAPS 102
FIGURE 34. RESULTS: REPORTING OPTIONS 103

LIST OF TABLES

TABLE 1. LIST OF FORMER DELIVERABLES ACTING AS INPUTS TO THIS DOCUMENT........8
TABLE 2. LIST OF OTHER DELIVERABLES FOR WHICH THIS DOCUMENT IS AN INPUT. 8
TABLE 3. ASSESSMENT OF LIQUEFACTION SUSCEPTIBILITY OF THE GEOLOGICAL UNITS, BASED ON THE SEDIMENTATION PROCESS AND THE AGE OF DEPOSITION (YOUD AND PERKINS, 1978)........22
TABLE 4. SUSCEPTIBILITY OF DETAILED GEOMORPHOLOGICAL UNITS TO LIQUEFACTION SUBJECTED TO GROUND MOTION OF THE MMS INTENSITY VIII (WAKAMATSU, 1992)........24
TABLE 5. VALUES OF PARAMETERS A, B AND C DEPENDING THE TYPE OF GEOLOGICAL DEPOSITS AND THE DEPTH OF WATER TABLE (HOLZER ET AL. 2011). 30
TABLE 6. REGRESSION PARAMETERS OBTAINED FOR EACH GROUP (MATSUOKA ET AL., 2015)........32
TABLE 7. SUMMARY OF ALL CANDIDATE EXPLANATORY VARIABLES (ZHU ET AL. 2017) 34
TABLE 8. COEFFICIENTS OF TOP PERFORMING COASTAL MODELS AND GLM-ZEA15G (ZHU ET AL., 2017)........35
TABLE 9. PARAMETERS FOR RELATING MODEL PROBABILITIES TO AREAL LIQUEFACTION PERCENT........37
TABLE 10 RESULTS OF THE REGRESSION ON THE GLOBAL DATASET (NOWICKI ET AL., 2014)........44
TABLE 11 BEST FIT MODEL COEFFICIENTS (JESSEE ET AL., 2018) 46
TABLE 12 LIST OF EQUATIONS FOR COEFFICIENTS C1(MC) AND C2(MC) (B < 45°). 47
TABLE 13 LIST OF EQUATIONS FOR COEFFICIENTS C1 AND C2 (B > 450). 48
TABLE 14 LITERATURE REVIEW; REFERENCES, BRIDGE TYPES, METHODOLOGY, INTENSITY MEASURE, DAMAGE PARAMETERS, DAMAGE STATES (REPRODUCED AND UPDATED FROM TSIONIS AND FARDIS 2014 IN SYNER-G PROJECT) 64
TABLE 15 FRAGILITY EQUATIONS DEVELOPED BY VARIOUS RESEARCHERS........74
TABLE 16 MODIFICATION FACTOR VALUES FOR DIFFERENT SOIL-PIPE CONDITIONS........76
TABLE 17 DAMAGE STATES FOR PIPELINES 77
TABLE 18. EXPECTED NUMBER OF CASUALTIES IN THE THESSALONIKI, RISKUE SCENARIO (PITILAKIS ET AL., 2006) 80
TABLE 19. COMPARISON OF SOFTWARE CAPABLE OF REDA IMPLEMENTATION........82
TABLE 20. DAMAGE TO LOSS MODEL FOR DEVELOPMENT OF VULNERABILITY MODEL (HAZUS)........97

1 BACKGROUND OF THE DOCUMENT

1.1 SCOPE AND OBJECTIVES

The deliverable consists of a state-of-the-art report dedicated to the evaluation of the world-wide available methodologies for REDA, highlighting which of them could be implemented in the areas of the project, based also on the situation reflected by the previous deliverable.

1.2 RELATED DOCUMENTS

1.2.1 Input

Table 1. List of former deliverables acting as inputs to this document

Document ID	Descriptor
D.T.1.1.1	Evaluation of REDA Capabilities in each partner country

1.2.2 Output

Table 2. List of other deliverables for which this document is an input.

Document ID	Descriptor
D.T1.3.1	System specifications for a harmonized REDA
D.T1.4.1	REDA system operational requirements
D.T2.1.1	Data requirements and specifications
D.T2.2.1	Data processing and harmonization
D.T2.3.1	REDA system

2 INTRODUCTION

Over the time, multiple methodologies devoted to the estimation of structural damage, human and economic damage due to earthquakes have been developed. The demand of such methodologies is both scientific but also practical, with results being of high interest in emergency management, risk reduction strategies or the insurance sector. In its sense, intensity – a subjective descriptor of earthquake effects, was used in evaluating the potential effects of earthquakes long before magnitude calculation. Initially, simple methods for estimating what could the losses be after an earthquake were developed using equations based on damage observations and correlations. Given also the capabilities of years ago computational technology, operational limitations had an important impact in methodological design. As time passed and new equipment and technologies became available but also important data from seismic events, for elaborating models and providing validation, more attention was drawn to the understanding of earthquake effects on buildings (as "not earthquakes kill people so much, but building behavior") and then linking potential damage with probability of injury or economic losses. Coupled with progress in seismic instrumentation equipment, building information modeling or shaketable increased capacities, progress was significantly made in understanding building behavior during various types of earthquakes and methods for representing potential damage as a function were developed –fragility functions. In order to make a link of structural damage with socio-economic loss, consequence functions were developed. Vulnerability functions – capable of directly reflecting losses for a specific building typology, were also elaborated, as a more direct approach. Either way, now there are multiple methodologies and software for estimating rapidly after an earthquake damage levels, but among the challenges are:

- how to better account for local site effects?
- how to describe more accurately, using fragility functions or other methods, the variability in the distribution of structures in different areas but also variability within the building typology?
- how to quantify and express uncertainty?
- how to consider structure degradation, habitability and economical evolution effects throughout the time in vulnerability models?
- how to quickly integrate real observation in new or altered vulnerability models?

Through our analysis we will evaluate the current state-of-the-art in methods and software for rapid earthquake damage assessment (REDA), trying to understand which path should the REDACt system take in order for it to be scientifically reliable, actual but also innovative.

3 OVERVIEW OF REDA METHODOLOGIES

3.1 HAZARD EVALUATION

Seismic hazard analysis is based on two main parts. The first is the identification of the seismic source zones and the second is the characterization of the seismic ground motion at the site of the interest. Two commonly used approaches of seismic hazard analysis are deterministic seismic hazard analysis (DSHA) and probabilistic seismic hazard analysis (PSHA). In the process of selecting the appropriate approach, authors have to consider the purpose of the hazard or risk assessment, whether the site of the interest is in high, moderate or low seismic risk region and available input data. However, in the scientific community, it remains a big question which procedure is best to choose.

(a) The deterministic seismic hazard analysis (DSHA) is used in cases the consequences of failure are intolerable and a suitable protection is required. Then the worst event that can be reasonably expected to occur at the site is usually evaluated. This event can be regarded, for example, as the maximum credible earthquake (MCE) maximizing the effects at the spectral frequencies for which the critical facility & infrastructure is more sensitive for its structural safety and serviceability. Thus, the MCE is defined on an engineering basis but without relation to its probability of occurrence.

DSHA is an approach in which the hazard is estimated as maximum ground motion based on parameters of a single earthquake or set of earthquakes. To perform DSHA three basic elements have to be specified (Reiter, 1991): earthquake source, controlling earthquake of the particular size and level of seismic ground motion characteristic at selected distance. Consequently, seismic hazard can be expressed as a resulting value of specified ground motion characteristics following the occurrence of causative earthquake originating from particular source at a specified distance. DSHA is comprised of four basic steps:

1. The identification of seismic source zones. Individual sources may have character of points, lines, areas or volumes. In order to identify these sources, the seismological, geological, geotechnical and geophysical database are compiled. The content of these databases can vary based on the purpose of the analysis.
2. The selection of the controlling earthquake. Maximum earthquake in terms of magnitude is assigned to each source zone. Also, the closest distance of each source zone from the site of the interest is determined. Controlling earthquake is the one whose characteristics at the site of interest are dominant in comparison with characteristics of the maximum earthquakes from other source zones. Selection of the controlling earthquake may be a difficult task (Baker, 2008). If faults in vicinity of the site are poorly mapped, seismic source zone is considered to be areal and earthquake can occur in any part of this zone. If the site is found to be exactly in the

seismic source zone, it is assumed, that the location of the maximum earthquake is right under the study site.

3. The selection of the appropriate ground motion prediction model (GMPM). GMPMs, previously known as attenuation relationships, estimate the value of chosen ground motion characteristic for an earthquake characterized by source parameters, distance and site conditions (Douglas 2018).
4. The estimation of the seismic hazard at the site of the interest. Basically, it is the combination of the steps mentioned above and estimation of the ground motion characteristic according to magnitude and distance of the causative earthquake using GMPM.

(b) The Probabilistic seismic hazard analysis (PSHA) allows estimation of the probability that selected ground motion parameters will be exceeded, at a given site, within a certain time interval (Cornell, 1968). It represents a powerful tool that integrates over all earthquake occurrences, in space and time, surrounding a selected study site. Unfortunately, the concept of a causative earthquake is lost when performing a PSHA. That is, there is no specific earthquake, in terms of magnitude and source-to-site distance, reproducing the uniform hazard spectrum (UHS) at the selected exceedance probability within a reference time return period.

Unlike DSHA, probabilistic seismic hazard analysis is not constrained on maximum earthquake but rather comprises effects of all earthquakes of all magnitudes up to a predefined source-to-site distance, which can affect ground motion at the site of interest (Kramer, 1996; Baker, 2008). PSHA allows inclusion of various alternatives of input data into computation, along with their associated uncertainties. Seismic hazard can be expressed as the annual probability of exceeding selected level of ground motion characteristic. The results of the analysis can be used to estimating seismic risk.

Four basic steps of the PSHA are illustrated in **Error! Unknown switch argument.**. The prerequisite of this computation is the compilation of the aforementioned databases for the site of interest, similarly as for DSHA. The content of the databases can vary, due to the purpose of the analysis. The data of the database should comprise following information about the earthquakes: date and time of the origin of the earthquake, coordinates of the epicenter, depth of the focus, all determined magnitudes and seismic moment, maximum and epicentral intensity along with the type of the scale, description of the observed damage, isoseismal map, estimation of the uncertainty for each of the parameters mentioned, information about felt foreshocks and aftershocks. Beneficial is also knowledge on focal mechanism, data from the broadband seismometers and strong motion accelerographs.

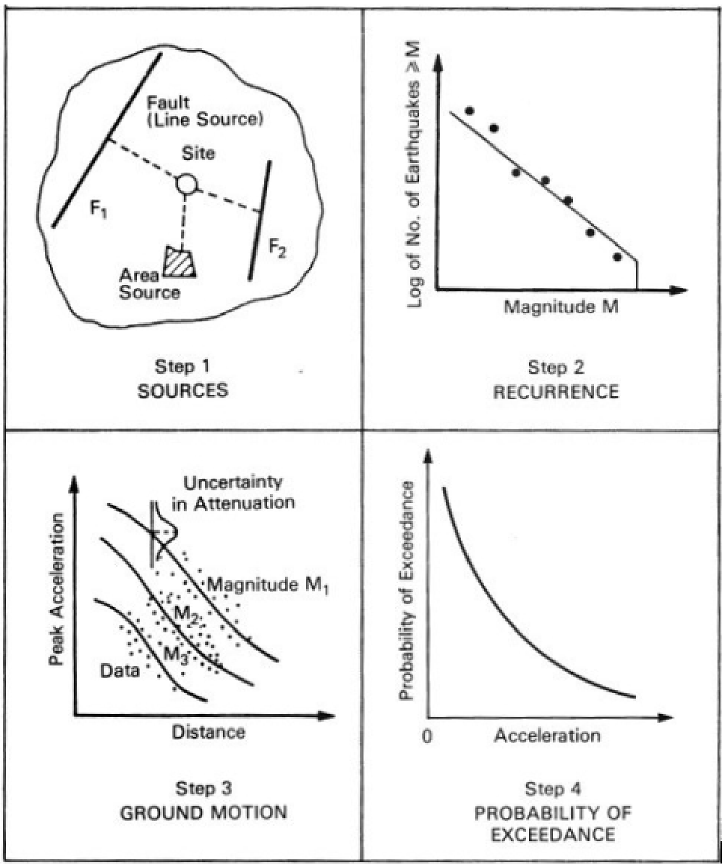

Figure 1. Four basic steps of PSHA (Reiter, 1991)

Steps in PSHA:

1. The identification of seismic source zones. In this step the PSHA is analogous to DSHA, individual sources may have character of points, lines, areas or volumes. Seismotectonic model is composed of the synthesis of seismological, geological, geotechnical and geophysical databases. Consequently, two types of seismic sources can be distinguished. Seismogenic structures are defined from the data of geological and seismological databases based on the features for which exists direct or indirect evidence that were active in the last tectonic regime. Diffuse seismicity zones are those where no apparent correlation can be made between earthquakes with any specific geological structures.
2. The determination of the recurrence law and maximum magnitude, together with associated uncertainties, for each source zone. Recurrence law is the relation between the magnitude of the event with its occurrence frequency inside the source zone during selected period of time T (usually is considered annually). This step is significantly different from the DSHA. Prior to computation of the parameters in recurrence law it is inevitable to process the seismological database. Consistent type of the magnitude, usually Mw, for each earthquake have to be determined (homogenization),

foreshocks, mainshocks and aftershocks have to be separated (declustering). Estimation of the temporal and spatial completeness of the database in the terms of magnitude have to be performed. Most frequently the Gutenberg and Richter (1944) recurrence law is used in the form:

$$\log N_m = a - bm \quad (1)$$

where Nm is the annual rate of exceedance of magnitude m and m ≥ 0 (Reiter, 1991). Parameter 10a is mean yearly number of earthquakes with magnitude larger or equal to zero and value b determines the ratio of strong to weak earthquakes in each seismic source.

3. The determination of earthquake effects. Since in PSHA earthquakes of all magnitudes and from all distances in seismic source zones are included in the computation, equations related to selected ground motion characteristic have to be considered along with the estimated uncertainties. The effects are estimated using empirical GMPMs for selected ground motion characteristic. GMPMs are usually function of magnitude, source-to-site distance and other relevant parameters (e.g. local conditions, style of faulting) (Douglas 2018). These models comprise also random error term, assumed as normally distributed with zero mean and standard deviation σ. This term represents the aleatory uncertainty of ground motion.
4. The estimation of the seismic hazard at the study site. This step is significantly different compared to DSHA. In PSHA effects of all earthquakes of all magnitudes and distances along with uncertainties, contribute to hazard output. The result of PSHA is seismic hazard curve which can be expressed as annual probability of exceedance of specified level of ground motion characteristic at the site of the interest. Alternatively, the curve can be expressed as annual frequency (or mean return period) in which a specified level of ground motion characteristic will be exceeded at the site. The results are not determined as single values but as probability distribution function. Therefore, usually median, 84 percentile and mean hazard curves are estimated (**Error! Unknown switch argument.**). The 84 percentile is presented as mean plus one standard deviation. The one-standard- deviation bounds should enclose about 2/3 of the observed values if the uncertainties are normally distributed. A thorough explanation of the methodology of computing percentiles can be found in background documents of the relevant software CRISIS 2007 (Ordaz et al., 2007).

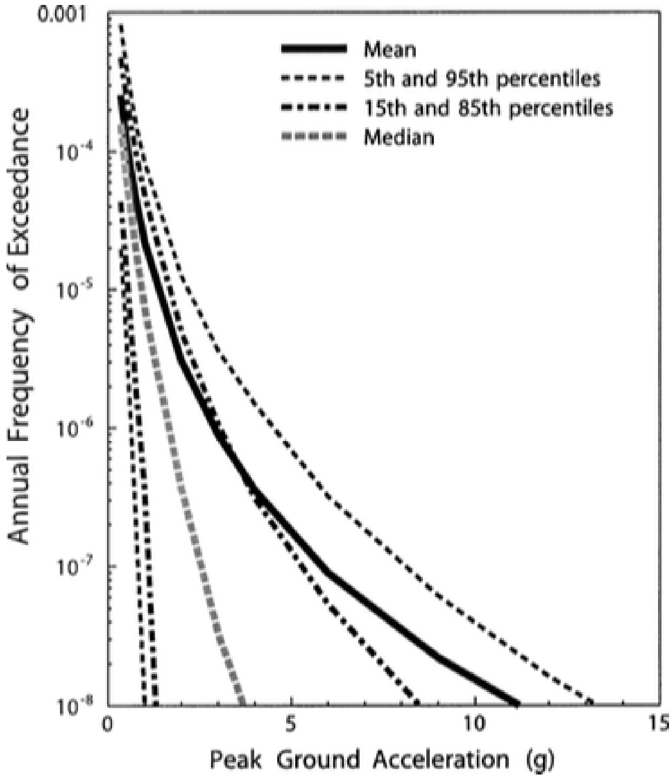

Figure 2. Illustration of the seismic hazard curves with percentiles determined by PSHA approach (Abrahamson and Bommer, 2005).

3.2 SHAKEMAP METHODOLOGY

The most widespread system for generating maps reflecting the ground motion distribution of parameters and instrumental intensity is the ShakeMap developed by USGS (Wald et al., [5,9]). This system is also installed, with minor modifications, both in Romania and Greece at the moment. An informative summary on the general methodology of ShakeMap was provided in the review paper of Guerin-Marthe et al. (2020); given its usefulness in our purpose, we replicate most of the paper's content below.

"The still widely used version 3.5 of ShakeMap is based on a weighted interpolation algorithm (Worden et al., 2010). At the locations of observations, the global bias introduced by the observations with respect to the initial Ground Motion Model (GMM)/ GMPE estimate is computed: the bias is corrected by finding the magnitude that reduces the errors between the observed and the predicted ground motions, when the GMM is evaluated for the adjusted magnitude. The bias-adjusted GMM is applied in order to estimate corrected ground parameters over a spatial grid. At each grid point, the ground-motion parameter of interest is updated through a weighted average between the bias-adjusted GMM estimate and the interpolated observations: the GMM estimate is weighted by the inverse of the variance provided by the GMM, while each observation is weighted by the term $1/\sigma^2_{obs}$ (i.e., σ_{obs} is the standard deviation assigned to the observation - it increases with the distance between the observation and the grid point, based on a ground-motion spatial correlation model).

Based on the interpolation scheme proposed by Worden et al. (2010), the mean updated ground-motion parameter Y at grid point (x,y) is expressed as:

$$\overline{Y_{xy}} = \frac{\frac{Y_{GMM,xy}}{\sigma^2_{GMM}} + \sum_{i=1}^{n} \frac{Y_{obs,xy,i}}{\sigma^2_{obs,xy,i}} + \sum_{j=1}^{m} \frac{Y_{convobs,xy,j}}{\sigma^2_{convobs,xy,j}}}{\frac{1}{\sigma^2_{GMM}} + \sum_{i=1}^{n} \frac{1}{\sigma^2_{obs,xy,i}} + \sum_{j=1}^{m} \frac{1}{\sigma^2_{convobs,xy,j}}}$$

where $Y_{GMM,xy}$ is the bias-corrected GMM estimate at the point (x,y), and $Y_{obs,xy,i}$ (resp. $Y_{convobs,xy,j}$) is the ith ground-motion measurement out of n (resp. the jth macroseismic observation out of m) scaled to the point (x, y). The scaling from the observation's location to each grid point (x,y) is performed using the relative source-to-distance factors provided by the GMM:

$$\begin{cases} Y_{obs,xy,i} = Y_{obs,i} \times \left(\frac{Y_{GMM,xy}}{Y_{GMM,obs,i}} \right) \\ Y_{convobs,xy,j} = Y_{convobs,j} \times \left(\frac{Y_{GMM,xy}}{Y_{GMM,convobs,j}} \right) \end{cases}$$

Similarly, the total variance of the updated ground-motion parameter Y at grid point (x,y) is expressed as:

$$\sigma^2_{Y,xy} = \frac{1}{\frac{1}{\sigma^2_{GMM}} + \sum_{i=1}^{n} \frac{1}{\sigma^2_{obs,xy,i}} + \sum_{j=1}^{m} \frac{1}{\sigma^2_{convobs,xy,j}}}$$

where

σ_{GMM} is the standard deviation of the intra-event error term associated with the GMM: when enough observations are present, it is assumed that the inter-event error term is well enough constrained by the bias correction; $\sigma_{obs,xy,i}$ is the standard deviation associated with an observation location at a given distance d from the grid point (x,y): for instance;

$\sigma_{obs,xy,i} = \sigma_{GMM} \,.\, f(d)$, where f is decreasing function with distance d.

Usually, if d tends towards zero, $\sigma_{obs,xy,i}$ tends towards zero (i. e., the observed value becomes the dominant term in near field); and if d tends towards infinity, $\sigma_{obs,xy,i}$ tends towards infinity (i.e., the GMM estimate becomes the dominant in far field).

The functional form and values taken by f depend on the spatial correlation model that is associated with the ground-motion parameter of interest. By default, Worden et al. (2010) propose a radius of 10 km, within which we have $\sigma_{obs,xy,i} < \sigma_{GMM}$; another radius of 15 km is defined, beyond which it is assumed that $\sigma_{obs,xy,}i = \infty$. The radius of influence of observations has a strong influence on the local shape of the shake-map; and further sensitivity studies should be performed in order to assess its link with the spatial correlation of the ground-motion parameters. On the other hand, the standard deviation $\sigma_{convobs,xy,j}$, related to the uncertainty associated with macroseismic observations, is decomposed into the distance-based standard deviation $\sigma_{obs,xy,j}$ (as detailed above), and the standard deviation of the Ground Motion to Intensity Conversion Equation (GMICE) (i.e. uncertainty from converting the macroseismic intensity into a ground-motion parameter):

$$\sigma^2_{convobs,xy,j} = \sigma^2_{obs,xy,j} + \sigma^2_{conv}$$

The simple equations used by the algorithm prevent the build-up of computational complexity, since the optimization of the first presented equation allows the computation time to remain linearly proportional to the number of grid points. This shake-map system is flexible enough to produce updated maps of various types of ground-motion parameters (e.g., PGA, PGV, SA at different periods), as long as the ad-hoc GMMs are available. Shake-maps in terms of macroseismic intensity are also provided, thus making a direct use of the macroseismic testimonies that are collected after the earthquake event.

It should be noted that the recent version change of ShakeMap® (from version 3.5 to 4) has introduced a different interpolation scheme (Worden and Wald, 2020), namely the use of the multi-variate normal (MVN) distribution. The vector of ground-motion parameters Y (assumed to be normally distributed) is divided into Y_1 (m prediction sites, or grid points) and Y_2 (n observations sites), with the following expressions for the mean and variance:

$$\mu_{\mathbf{Y}} = \begin{bmatrix} \mu_{\mathbf{Y}_1} \\ \mu_{\mathbf{Y}_2} \end{bmatrix} \quad \mathbf{\Sigma}_{\mathbf{Y}} = \begin{bmatrix} \mathbf{\Sigma}_{\mathbf{Y}_1\mathbf{Y}_1} & \mathbf{\Sigma}_{\mathbf{Y}_1\mathbf{Y}_2} \\ \mathbf{\Sigma}_{\mathbf{Y}_2\mathbf{Y}_1} & \mathbf{\Sigma}_{\mathbf{Y}_2\mathbf{Y}_2} \end{bmatrix}$$

Then, given a set of observations $Y_2 = y_2$, a vector of residuals is defined as $\zeta = y_2 - \mu Y_2$. Thanks to the MVN, it is possible to express the mean and variance of the set of predictions Y_1, as follows:

$$\mu_{\mathbf{Y}_1|\mathbf{y}_2} = \mu_{\mathbf{Y}_1} + \mathbf{\Sigma}_{\mathbf{Y}_1\mathbf{Y}_2} \cdot \mathbf{\Sigma}_{\mathbf{Y}_2\mathbf{Y}_2}^{-1} \cdot \zeta$$

$$\mathbf{\Sigma}_{\mathbf{Y}_1\mathbf{Y}_2|\mathbf{y}_2} = \mathbf{\Sigma}_{\mathbf{Y}_1\mathbf{Y}_1} - \mathbf{\Sigma}_{\mathbf{Y}_1\mathbf{Y}_2} \cdot \mathbf{\Sigma}_{\mathbf{Y}_2\mathbf{Y}_2}^{-1} \cdot \mathbf{\Sigma}_{\mathbf{Y}_2\mathbf{Y}_1}$$

The initial mean values of Y_1 are obtained from a GMM, and the variance-covariance matrix is assembled from the standard-deviations associated with the GMM and from the spatial correlation structure of the ground motion parameter(s) of interest. Therefore, the results from the previous two equations may be directly used as the updated ground-motion distribution for the generation of the shake-map. Worden et al. also show that this approach enables the consideration of multiple types of ground-motion parameters (e.g., PGA, SA at different periods) simultaneously: thanks to the cross-correlation structure between some ground-motion parameters (esp. spectral responses), it is possible to gain knowledge and constrain shake-maps when only parameters of a given type have been recorded, for instance."

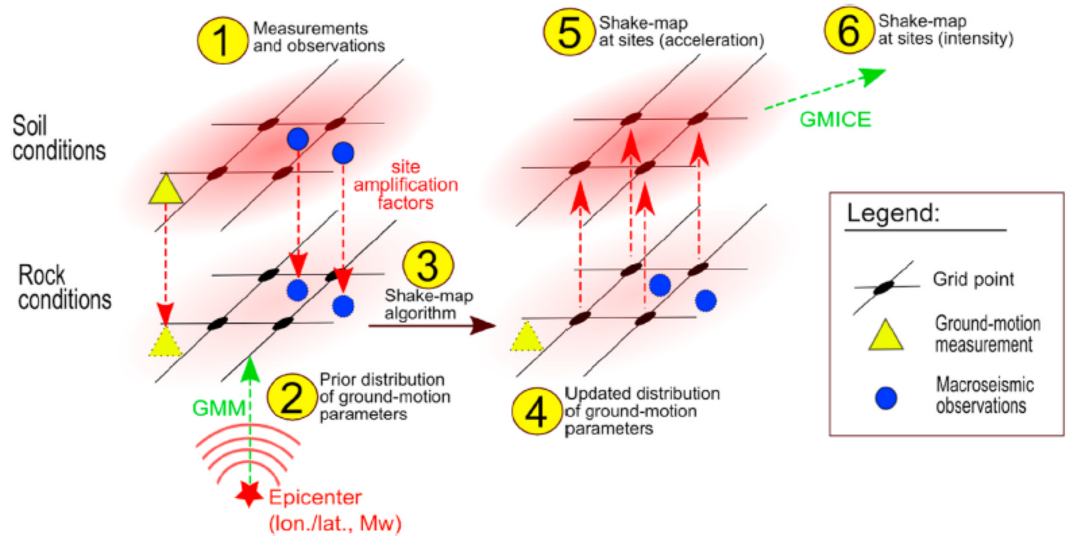

Figure 3 Schematic main principles of ShakeMap® v3.5 and the Bayesian inference shake-map procedures. ShakeMap® v4 does not correct to rock conditions before

Interpolation (from Guerin-Marthe et al., 2020)

Other ways of generating shake-maps have been investigated by Douglas (2007) and Guerin-Marthe et al. (2020).

3.3 GEOTECHNICAL HAZARD MODELLING

3.3.1 LIQUEFACTION

Assessment of liquefaction susceptibility

In this section, the most widely used approaches for the assessment of liquefaction susceptibility are presented. Initially, a discrimination of these published methodologies is taken place based on the scale of the project. The regional scale approaches are mainly oriented and suggested to be used for projects dealing with scales smaller than 1:25,000, while the local scale or site-specific projects aim to assess the liquefaction susceptibility on scales higher than 1:25,000 i.e. urban environment. The latter methodologies are based on the information provided by laboratory testing performed on recovered soil samples from borings, while the former approaches are based on geological-geomorphological maps where the spatial distribution of surficial geological formations is provided.

Regional scale

The liquefaction susceptibility of a geological unit can be evaluated on the basis of its depositional environment; the depositional process affects the sediment's liquefaction susceptibility, since fine- and coarse-grained soils sorted by fluvial or wave actions are more susceptible than unsorted sediments (Youd, 1998). In the same direction, Youd and Perkins (1978) stated that the younger, looser and more segregated the deposit, the greater the susceptibility, while they defined as non-liquefiable the Pre-Pleistocene sediments.

Furthermore, Papathanassiou and Pavlides (2011), as well as Knudsen and Bott (2011), studied the spatial distribution of liquefaction occurrences, at a regional/state scale, triggered by earthquakes in Greece and California, respectively. They concluded that the manifestation of liquefaction phenomena is strongly related to the type and age of sediments, as well as their proximity to water bodies. Papathanassiou and Pavlides (2011) concluded that 68% of liquefaction-induced surface disruption sites in Greece were documented at a distance of 0-50 m from a water body, 31% between 50 and 100 m and only 1% farther than 100 m. Regarding the type of the surficial geological unit where liquefaction phenomena were reported, 89% of liquefaction occurrences are related to recent formations that mainly consisted of alluvial and fluvial deposits. In addition, 5% of liquefaction manifestations observed in coastal, fluvial, deltaic, marsh deposits, while 6% reported in artificial fills. In addition, Knudsen and Bott (2011) concluded that liquefaction tends to occur in young sediments, near water bodies and on low to flat grounds. They found that 90% of liquefied surface evidences were reported in areas characterized as historical or late Holocene surficial deposits, with 73% in artificial fills or near streams and 67% at an elevation less than 10 m.

Moreover, the earthquakes that recently occurred in New Zealand (2010-2011) and Italy (2012) confirmed the strong correlation of the sedimentary depositional environment with the liquefaction occurrences. Wotherspoon et al. (2012) studied the liquefaction-induced failures at the town of Kaiapoi, New Zealand and concluded that the most significant ones occurred in areas where river channels had been reclaimed or in old channels that have had flow diverted away.

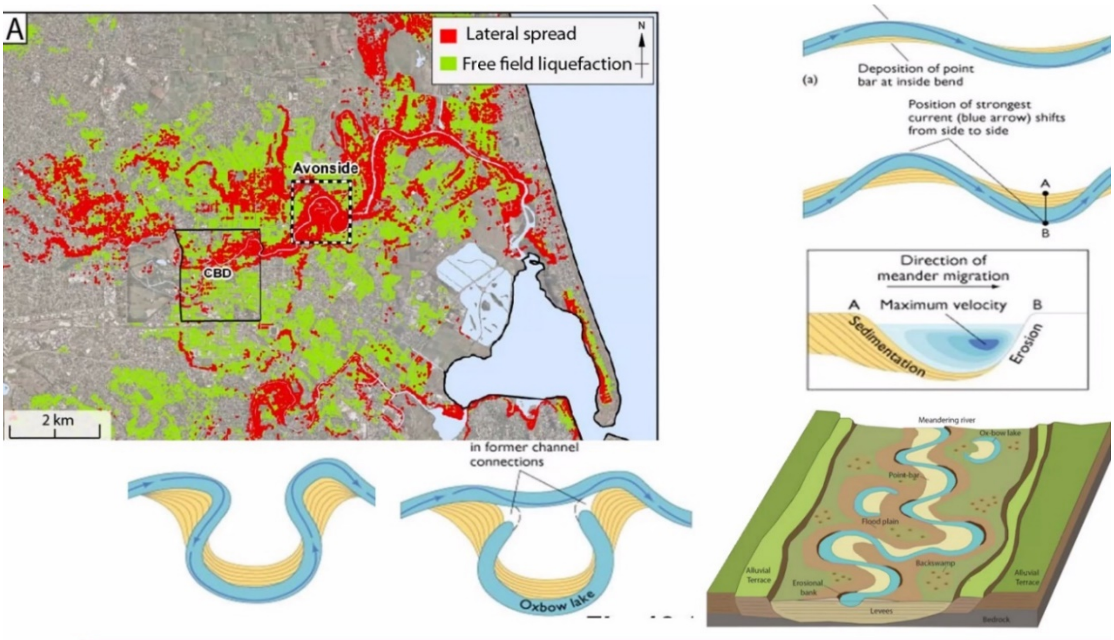

Figure 4. Geomorphological oriented map of liquefaction manifestations at the area of Christchurch

Bastin et al. (2015, 2017) concluded that the severity and distribution of earthquake-induced liquefaction phenomena were strongly influenced by the distance from a free-face and the depositional environment, by considering that liquefaction phenomena (including lateral spreading) are mainly concentrated around modern waterways and areas underlain by Holocene to recent deposits. For the study area of Avonside, New Zealand they pointed out that the most susceptible to liquefaction sediments were recent fluvial and paleo-channel deposits, and that severe liquefaction occurrences were reported within 50 m of a free-face.

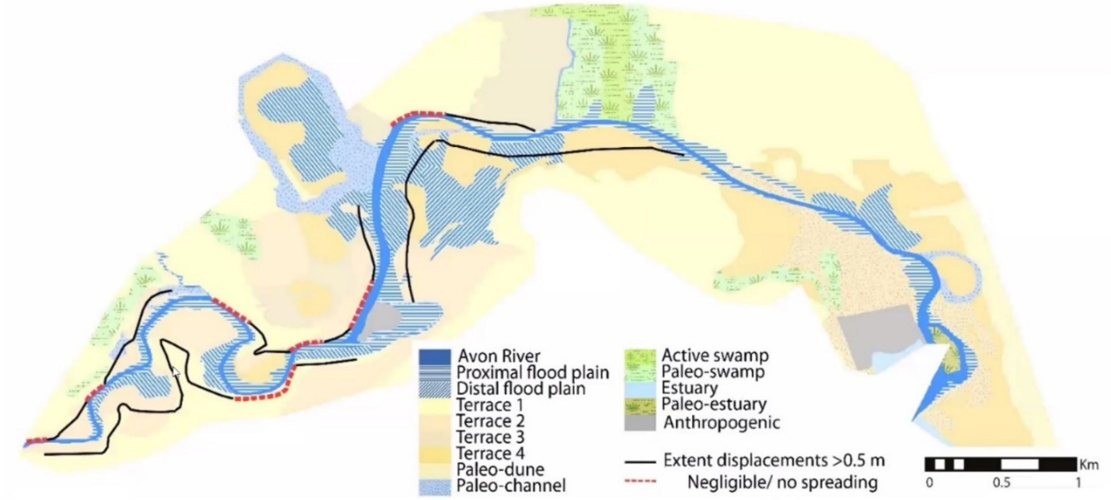

Figure 5. Spatial correlation of lateral spreading phenomena and the type of deposits at the area of Avon river (Bastin et al., 2017)

Recently, Villamor et al. (2016) suggested that liquefaction manifestations triggered by the 2010-2011 Canterbury Earthquake Sequence (CES) are strongly correlated with specific environments within the alluvial systems. More specifically, they studied the sites of Hardwick and Marchand near Lincoln, New Zealand and concluded that ridges of scroll bars on the inside bends of meander loops hosted most of the liquefaction manifestations e.g. sand blows and sand fissures, while this correlation was not presented in the swales. Finally, Bastin et al. (2018, 2020), considering data collected from the 2016 Kaikoura M7.8 Earthquake, proposed that liquefaction occurrences were strongly correlated with the point-bar and paleochannel deposits.

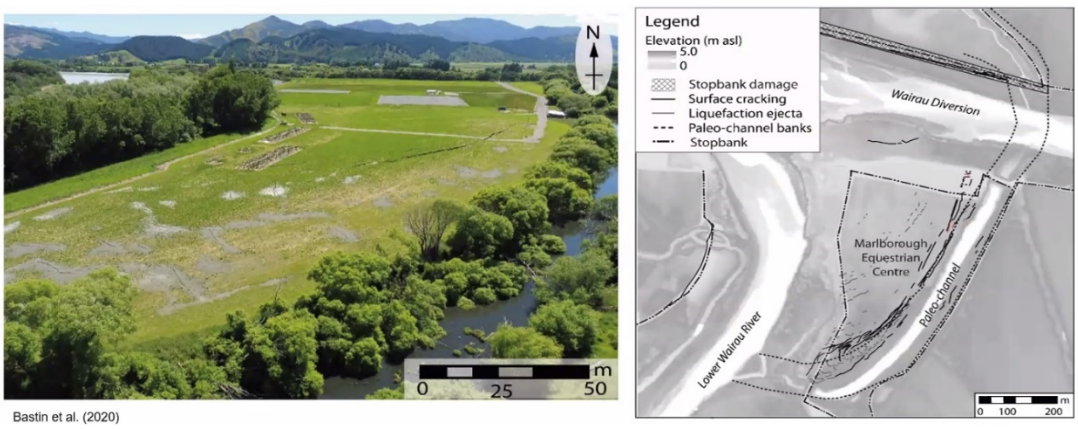

Figure 6. Detailed presentation of liquefaction-induced ground failures (Bastin et al., 2020)

Regarding the earthquake-induced liquefaction phenomena at the Emilia-Romagna region, Italy that were triggered by the 20th and 29th May 2012 earthquakes, it has been shown that a strong correlation with the type of geological units also exists. Di Manna et al. (2012) and Papathanassiou et al. (2015) suggested that numerous liquefaction phenomena were induced, being more severe than expected for such moderate magnitude earthquakes. These liquefaction features were mainly concentrated along a narrow zone of 3-4 km long and 1 km wide, described as a paleo-river channel. Civico et al. (2015) performed a detailed study within this area using an airborne Lidar data and highlighted the correlation between the depositional environment and the density of liquefaction phenomena. They concluded that more than 50% of the observed liquefaction features were mapped on fluvial landforms, namely alluvial ridges, levee ridges, crevasse splays and abandoned riverbeds.

Moreover, an additionally parameter that is taken into account for the assessment of liquefaction susceptibility is the occurrence of historical liquefaction occurrence. This has to be investigated since it is known that liquefaction tends to occur repeatedly at the same site. Thus, maps showing the localities of past liquefaction may be considered as likely to liquefaction area in future earthquakes (Youd, 1984). However, lack of evidence does not provide adequate proof that a site is immune to liquefaction (Youd, 1988).

Regarding the approaches that can be used for the assessment of the liquefaction susceptibility on regional scale, Youd and Perkins (1978) qualitatively defined the liquefaction susceptibility of the geological units, based on the sedimentation process and the age of deposition and stated that the Pre-Pleistocene sediments should be classified as non-liquefiable. The proposed classification is illustrated on table 3.

Furthermore, a well-known procedure that can be appropriately used for the characterization of an area as liquefiable at small scale maps was proposed by the California Department of Conservation, Division of Mines and Geology (CDMG, 1999). According to these guidelines, a zone is considered as prone to liquefaction when meeting the following criteria:

- evidence of historical liquefaction occurrences
- data from in-situ tests and analyses indicate that the soils are likely to liquefy

In case of lacking of the above data, a site is considered as susceptible to liquefaction when:

- area containing soils of late Holocene age, the groundwater is less 13 meters deep and the peak ground acceleration (PGA) having a 10% probability of being exceeded in 50 years is greater than 0.1g
- soils of Holocene age where the depth of groundwater table is less than 10 meters and the PGA (10% in 50 years) is greater than 0.2g

- areas containing soil deposits of latest Pleistocene age, where the PGA has a 10% probability of being exceeded in 50 years is greater or equal to 0.3g and the depth of the groundwater table is less than 6 meters.

Table 3. Assessment of liquefaction susceptibility of the geological units, based on the sedimentation process and the age of deposition (Youd and Perkins, 1978)

Type of Deposit (1)	General Distribution of Cohesionless sediments in deposits (2)	Likelihood that Cohesionless Sediments, When Saturated, Would be Susceptible to Liquefaction (by Age of Deposit) <500 yr (3)	Holocene (4)	Pleistocene (5)	Pre-Pleistocene (6)
(a) Continental Deposits					
River Channel	Locally Variable	Very High	High	Low	Very Low
Floodplain	Locally Variable	High	Moderate	Low	Very Low
Alluvial Fan and Plain	Widespread	Moderate	Low	Low	Very Low
MarineTerraces/ Plains	Widespread	-----	Low	Very Low	Very Low
Delta and Fan-delta	Widespread	High	Moderate	Low	Very Low
Lacustrine and Playa	Variable	High	Moderate	Low	Very Low
Colluvium	Variable	High	Moderate	Low	Very Low
Talus	Widespread	Low	Low	Very Low	Very Low
Dunes	Widespread	High	Moderate	Low	Very Low
Loess	Variable	High	High	High	Unknown
Glacial Till	Variable	Low	Low	Very Low	Very Low
Tuft	Rare	Low	Low	Very Low	Very Low
Tephra	Widespread	High	High	?	?
Residual Soils	Rare	Low	Low	Very Low	Very Low
Sebkha	Locally Variable	High	Moderate	Low	Very Low
(b) Coastal Zone					
Delta	Widespread	Very High	High	Low	Very Low
Esturine	Locally Variable	High	Moderate	Low	Very Low
Beach					
High Wave Energy	Widespread	Moderate	Low	Very Low	Very Low
Low Wave Energy	Widespread	High	Moderate	Low	Very Low
Lagoonal	Locally Variable	High	Moderate	Low	Very Low
Fore Shore	Locally Variable	High	Moderate	Low	Very Low
(c) Artificial					
Uncompacted Fill	Variable	Very High	-----	-----	-----
Compacted Fill	Variable	Low	-----	-----	-----

Recently, Witter et al. (2006) stated that susceptible to liquefaction areas can be identified through detailed geological, geomorphological and hydrological mapping.

Regarding seismic loading, appropriate parameters for the assessment of the liquefaction susceptibility (corresponding either to the maximum intensity and/or the peak ground acceleration) have been introduced by Kuribayashi and Tatsuoka (1975) and Wakamatsu (1992). According to their results, liquefaction phenomena can be triggered by seismic shaking with intensity in excess of V (JMA scale) or VIII (MM scale) (TC4 1999).

For this intensity value, Wakamatsu (1992) classified sedimentary deposits, using geomorphological criteria, in 3 categories of liquefaction susceptibility, namely “likely”, “possible” and “not likely”.

Areas classified in the “not likely” liquefaction susceptibility class correspond to zones where liquefaction-induced failures are not expected. On the contrary, zones covered by geomorphological units such as natural levee, former river channel, sandy dry river channel and artificial fills were classified as the highest level of liquefaction potential, (i.e. liquefaction likely, TC4 1999). At these areas, further investigation using in-situ tests should be performed for evaluating the physical and mechanical parameters of subsoil layers.

Table 4. Susceptibility of detailed geomorphological units to liquefaction subjected to ground motion of the MMS intensity VIII (Wakamatsu, 1992)

Geomorphological conditions		**Liquefaction potential**
Classification	**Specific conditions**	
Valley plain	Valley plain consisting of gravel or cobble	Not likely
	Valley plain consisting of sandy soil	Possible
Alluvial fan	Vertical gradient of more than 0.5%	Not likely
	Vertical gradient of less than 0.5%	Possible
Natural levee	Top of natural levee	Possible
	Edge of natural levee	Likely
Back marsh		Possible
Abandoned river channel		Likely
Former pond		Likely
Marsh and swamp		Possible
Dry river bed	Dry river bed consisting of gravel	Not likely
	Dry river bed consisting of sandy soil	Likely
Delta		Possible
Bar	Sand bar	Possible
	Gravel bar	Not likely
Sand dune	Top of dune	Not likely
	Lower slope of dune	Likely
Beach	Beach	Not likely

	Artificial beach	Likely
Interlevee lowland		Likely
Reclaimed land by drainage		Possible
Reclaimed land		Likely
Spring		**Likely**
Fill	Fill on boundary zone between sand and lowland	**Likely**
	Fill adjoining cliff	**Likely**
	Fill on marsh or swamp	**Likely**
	Fill on reclaimed land by drainage	**Likely**
	Other type fill	possible

The Chinese building code (CNS 2001) stated that soil is considered non-liquefiable or the consequences of liquefaction can be neglected for Pleistocene deposits for shaking intensities 7 to 9; Moss and Chen (2008) note that Chinese Intensity 7 through 9 is approximately equal to Modified Mercalli Intensity VI through X.

The selection of one of the above approaches depends on the amount and type of collected data, but mainly on the scale (spatial accuracy) of the corresponding information available on the geological maps.

Summarizing, it should be pointed out that the liquefaction susceptibility maps do not predict liquefaction-related ground failures, although ground failures may accompany liquefaction and are more likely to occur in areas with higher liquefaction susceptibility (Tinsley et al., 1985).

Considering the parameters that should be taken into account for the assessment of liquefaction susceptibility of surficial geological formations on regional scale, in areas where the expected peak ground acceleration of the ground motion is >0.1g, it can be stated that i) the age and ii) the depositional environment of the sediments, and iii) the distance from a water body are the most critical proxies; almost all the liquefaction manifestations were reported in a short distance from a river, lake and seashore.

Local scale

In order to examine the susceptibility to liquefaction of the subsoil layers on a local scale, samples from boreholes should be tested in the laboratory regarding the grain-size characteristics and the values of Atterberg limits of the soil element. In general, it was believed that sands were more susceptible than silts or gravels, but laboratory test to fine-grained soils from liquefied soils collected after the earthquakes of Kocaelli, Turkey and Chi-Chi, Taiwan in 1999, showed that cohesive soils could also liquefied under specific conditions. Recently, ejection of coarse material i.e. gravel and sand, on liquefied areas i.e. Lefkada, Greece (Papatheodorou et al., 2007), Lyxouri, Greece (Papathanassiou et al., 2016) indicated that gravelly soils may also liquefied under specific conditions. In the following paragraph, a brief description of the most applied methodologies considering the liquefaction susceptibility of soil layers on local scale are presented.

Initially, Tsuchida (1971) defined boundaries curves for potentially liquefiable soils based on their grain size distribution curves. Few years later, Wang (1979), as well as Seed and Idriss (1982) suggested that the classification of a soil element depends on the Atterberg limits and the percentage of clay-size material. Andrews and Martin (2000) re-evaluated the liquefaction field case histories and transported the “Modified Chinese Criteria” to US conventions. However, Seed et al. (2003) suggested that the “modified Chinese criteria” and the liquefaction susceptibility criteria proposed by Andrews and Martin (2000) should be considered as conservative. This approach was mainly based on the use of data provided by post-earthquake in-situ tests at liquefied sites triggered by the two devastating earthquakes of Kocaeli and Taiwan in 1999. Seed et al. (2003) concluded that the plasticity behaviour of fine size particles of soils is more important than the percent clay size, and there are numerous cases of liquefaction with more than 10% clay-size fines. According to these recommendations, soils with fines content more than 35% are characterized potentially liquefiable when its liquid limit is less than 37 and the plasticity index is less than 12 ($LL \leq 37$ and $PI \leq 12$), and the water content (w_c) is high relative to their Liquid Limit ($w_c > 0.8$ LL). Soils with (i) $PI \leq 20$ and (ii) $LL \leq 47$ are transitional and require further testing if w_c /LL>0.85, and soils whose properties lie outside these bounds are not susceptible to liquefaction but might be vulnerable to strength loss.

Boulanger and Idriss (2006) proposed that soils with $PI < 3$ exhibit “sand-like” behavior; soils with $PI \geq 7$ exhibit “clay-like” behavior, but if a soil is classified as CL-ML according to the Unified Soil Classification System (USCS) (ASTMD-2487-11; ASTM, 2011), this criterion may be reduced to $PI \geq 5$. Also, soils with $3 < PI < 6$ may exhibit intermediate behavior and should be tested further. Idriss and Boulanger (2008) proposed that in the absence of cyclic laboratory testing on undisturbed samples, soils with PI<7 can be conservatively assumed to exhibit "sand-like" behavior and be evaluated using the simplified procedure. Thus, soils with PI<7 can practically be considered as soils of sand-like behavior that are susceptible to liquefaction, and when PI≥7 as clay-like behavior that are judged as not susceptible to liquefaction (Donahue et al., 2007). It should be pointed out that the latter soils can still have the potential for generating earthquake-induced deformations, but the quantitative evaluation of the failures requires the use of procedures dealing with cyclic softening.

Finally, Bray and Sancio (2006), based on data provided by Adapazari silts and clays from the Kocaeli 1999 event, that have been tested in laboratory, recommended that a fine-grained soil can be characterized as susceptible to liquefaction when the Plasticity Index PI≤12 and water content to liquid limit ratio (w_c/LL) ≥0.85. Soils with 12 < PI < 18 and w_c /LL >0.8 may be "moderately susceptible" to liquefaction and require further testing; and soils whose properties fall outside these bounds are not susceptible to liquefaction but may undergo deformation.

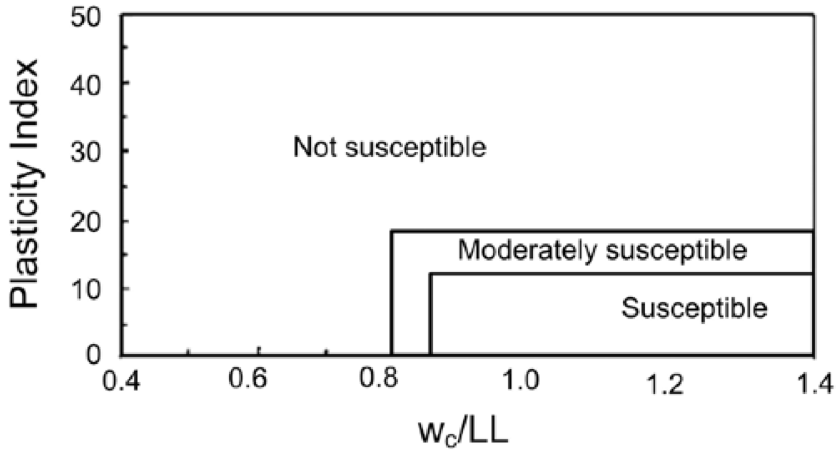

Figure 7. Ranges of wc/LL and plasticity index for various susceptibility categories according to Bray and Sancio (2006)

Consequently, fine-grained soils, previously characterized as non-liquefiable based on the liquefaction susceptibility criteria proposed by Wang (1979), Seed and Idriss (1982) and Andrews and Martin (2000), are currently considered as potentially liquefiable according to the more recent recommendations of Seed et al. (2003), Boulanger and Idriss (2006) and Bray and Sancio (2006). Despite the fact that the above research groups recommend slightly different susceptibility criteria, it is clear that fine-grained soils can undergo severe strength loss due to increased pore water pressure that temporarily reduce the effective stress in soil (Donahue et al., 2007).

Regarding the data provided by CPTs, classification of soil units follows the normalized CPT soil behavior type index I_c, as proposed by Robertson and Wride (1998), which is a function of tip resistance and sleeve friction ratio for cohesionless soils with high fines content. The value of I_c that was suggested as a boundary between susceptible and non-susceptible to liquefaction soils (clay) is 2.6. However, as it is pointed out by Maurer et al. (2017), because I_c boundaries between soil types are approximate and may need regional refinement (e.g., Yi 2014), the I_c < 2.6 criterion may in some cases be inappropriate (e.g., Zhang et al. 2002; Li et al. 2007; Pease, 2010). For this reason, Youd et al. (2001) recommended that soils with I_c > 2.4 be sampled and tested to evaluate their susceptibility.

The I_c is defined as follows:

$$I_C = \sqrt{(3.47 - \ log_{10}Q)^2 + (1.22 + log_{10}F)^2}$$

where Q and F are the normalized CPT penetration resistance and normalized CPT friction ratio, respectively.

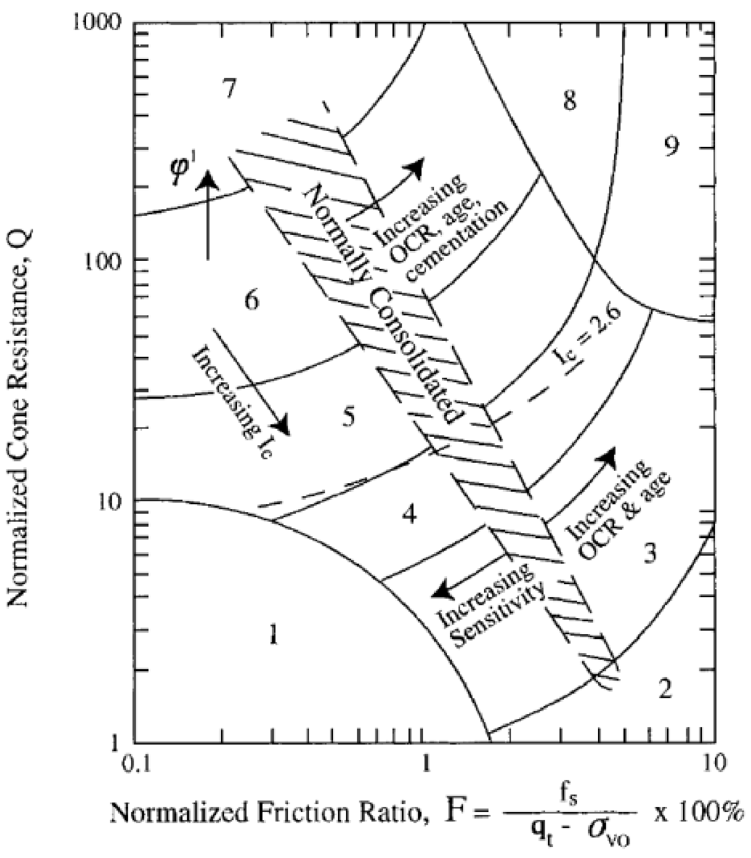

1. Sensitive, fine grained
2. Organic soils - peats
3. Clays - silty clay to clay
4. Silt mixtures - clayey silt to silty clay
5. Sand mixtures - silty sand to sandy silt
6. Sands - clean sand to silty sand
7. Gravelly sand to dense sand
8. Very stiff sand to clayey sand*
9. Very stiff, fine grained*

**Heavily overconsolidated or cemented*

Figure 8. CPT-based Soil Behavior Type chart (Robertson, 1990)

CPT soundings offer advantages over other methods of estimating liquefaction resistance in both the detection of thin layers that may affect liquefaction triggering and subsequent pore pressure redistribution and in the reproducibility of results. CPT results are less dependent on the equipment operator or setup than most other in situ test methods, and CPT can be performed with relative speed and economy. CPT-based simplified procedure has disadvantages too; soil samples are typically not recovered during CPT sounding, and consequently cannot directly be characterized or tested further in the laboratory.

Evaluation of liquefaction potential

Regional scale

The procedures presented in this section are focused on the development of maps showing the spatial distribution of liquefaction hazard on a regional scale, which can consequently be incorporated in relevant rapid response maps and loss estimates.

Holzer et al. (2011) proposed a method for computing the probability of liquefaction occurrences on a regional scale and particularly, a method for developing liquefaction probability curves that would enable surficial geologic maps to be transformed into liquefaction hazard maps. More specifically, these curves are related to 14 different types of surficial geologic deposits that according to Holzer et al. (2011) are the principal types in which liquefaction occurred in historical earthquakes. Thus, the probability of surface manifestations of liquefaction for each surficial geologic unit is inferred from complementary cumulative frequency distributions of LPI. Distributions were computed for a specific earthquake magnitude, PGA, and water table condition. The probability of liquefaction is the frequency at LPI> 5, the empirical threshold value for surface manifestations of liquefaction determined by Toprak and Holzer (2003). The proposed methodology was developed using a scenario of earthquake magnitude M 7, however it can also be used for other magnitudes by scaling the seismic demand by the magnitude scaling factor (MSF) as it was defined by Youd et al. (2001). The probability of surface manifestations of liquefaction (p) is computationally simplified by curve fitting the relation between probability and PGA/MSF and can be computed using the following regression:

$$p = \frac{a}{1 + \left(\frac{\frac{PGA}{MSF}}{b} \right)^{c}}$$

In particular, it is the probability that a surficial geologic unit will exhibit surface manifestations of liquefaction conditioned on PGA and M and it is usually computed for a specified water table depth; 1.5 and 5m following the procedure proposed by Holzer et al. (2011).

Table 5. Values of parameters a, b and c depending the type of geological deposits and the depth of water table (Holzer et al. 2011).

Study Area	Type of Geologic Deposit	Location	WT = 1.5 m			WT = 5 m		
			a	b	c	a	b	c
1	Alluvial fan	Greater Oakland, CA	0.0645	0.3366	−6.2881	0	—	—
2	Alluvial fan	Santa Clara Valley, CA	1.8336	1.2479	−2.5577	0.2268	0.6571	−3.4305
	Alluvial fan, young levee		0.6503	0.2981	−3.7789	0.5886	0.4586	−3.5751
3	Beach ridge (Holocene)	Greater Charleston, SC	0.9542	0.1861	−3.8421	0.9382	0.2530	−4.2631
	Beach ridge (Pleistocene)		0.9903	0.2503	−7.4332	0.8520	0.3475	−6.4186
4	Beach ridge	Upper Peninsula, MI	0.5648	0.3872	−5.8965	2.1841	1.2806	−3.3766
5	Delta, topset beds	Sheyenne River, Richland County, ND	0.9759	0.2530	−8.0436	0.9236	0.3192	−8.0451
	Delta, foreset beds		0.3498	0.4307	−9.5162	0	—	—
6	Dunes, eolian	Indiana Dunes National Lakeshore, IN	0.8915	0.2510	−5.1627	0.6635	0.3584	−5.3073
7	Floodplain (flood basin)	Evansville, IN	0.3405	0.3705	−2.3085	0.0699	0.2244	−5.5514
	Floodplain (levee)		1.0802	0.2741	−2.7483	1.7482	0.7912	−1.9527
8	Floodplain (point bar)	Mississippi River, AR, MO, and MS	0.9514	0.2231	−4.7039	0.8717	0.3339	−5.2697
	Floodplain (aban. chan.)		0.7781	0.2107	−5.7692	0.6539	0.2858	−5.5505
	Floodplain (flood basin)		0.6018	0.2397	−3.2337	0.5062	0.3226	−3.9267
9	Floodplain (point bar)	Ouachita River, AR	1.0023	0.1940	−4.1876	0.9702	0.3372	−4.3742
10	Floodplain (point bar)	Red River, AR	0.9741	0.2370	−6.7458	0.9671	0.3417	−7.1810
11	Floodplain (point bar)	Rio Grande, TX	0.8479	0.2743	−6.5802	0.8056	0.4038	−7.1731
12	Floodplain (point bar)	Wolf River, TN	1.0079	0.2924	−4.8917	0.8432	0.4223	−6.4632
13	Lacustrine	Richland County, ND	0.0707	0.4644	−12.2006	0	—	—
14	Lagoonal	Brazoria and Matagorda Counties, TX	0.7539	0.2383	−4.3654	0.6221	0.3571	−4.3517
15	Sandy artificial fill	Greater Oakland, CA	0.7826	0.2315	−4.6645	0.4385	0.3939	−3.4294
16	Valley train, Pvl1	Mississippi Valley, AR and MO	1.0155	0.2784	−6.8479	0.8240	0.3988	−3.4256
	Valley train, Pvl2		0.8816	0.3084	−3.1019	0.9858	0.4176	−6.9698

Matsuoka et al. (2015) proposed a method to quantitatively and easily estimate the liquefaction occurrence probability using engineering-based geomorphologic classifications compiled in a 7.5-arcsec map. This probability is defined as the liquefaction occurrence ratio (number of liquefaction grid cells divided by total number of grid cells of the region) on a regional scale. They established their suggestion on the correlation of the seismic intensity describing by the Japanese Meteorological Agency (JMA) with the geomorphological characteristics of the geological formations i.e. sediments. The soil deposits were classified in four groups:

- Group-1: Liquefaction began at a seismic intensity (JMA) around 5.0. [Natural levee (NTL), abandoned river channels (ARC), lower slope of a dune (LSD), lowland between coastal dunes and/or bars (LDB), reclaimed land (REC), and filled land (FLL)]
- Group-2: Liquefaction did not occur at a seismic intensity of ~5.0, but as the seismic intensity increased, the liquefaction occurrence ratio increased rapidly. [Alluvial fan (ALF), alluvial fan with a slope angle of less than 1/100 (AFS), and marine sand and gravel bars (BAR)]

- Group-3: Some liquefaction occurred at a seismic intensity of ~5.4, but the liquefaction occurrence ratio did not increase significantly even as the seismic intensity increased. [Back marsh (BKM), delta and coastal lowland (DEL), and sand dune (DUN)]
- Group-4: Liquefaction occurred at a seismic intensity of ~6.0, and the ratio increased rapidly as the seismic intensity increased. [Gravelly terrace (GVT), valley bottom lowland (VBP), valley bottom lowland with a slope angle less than 1/100 (VPS)]

They pointed out that ALF deposits experienced liquefaction for gradients of 1/100 or less and they subdivided ALF and VBP based on the slope angle.

In addition, they assigned the following specific characteristics for each of the group:

- Group-1: Shallow groundwater level and loose sand deposits.
- Group-2: Shallow groundwater level and sand or sandy gravel deposited widely, but firm compared to the sand in Group-1.
- Group-3: Groundwater level and sand distribution varied. Shallow groundwater level, but a localized distribution of loose sand (cohesive soil was predominant) (BKM, DEL). Loose, clean sand (sand with a small fine fraction) distributed widely, and generally deep groundwater level (DUN).
- Group-4: Soil material varied. Sandy gravel deposited widely (GVT, VBP). Cohesive soil was predominant with localized sand distribution (VPS).

Thus, they concluded that when the seismic intensity (JMA) exceeded 5.0, the sediments classified in Group-1 were the most susceptible to liquefaction and the liquefaction occurrence ratio increased as the seismic intensity increased. Although the seismic intensity at which liquefaction became pronounced was higher for Group-2 (seismic intensity of around 5.4), the trend for the increase in the ratio was similar to Group-1. In Group-3, liquefaction occurred at a rather low seismic intensity (~5.4), but the increase in the ratio was slow as the seismic intensity increased (Matsuoka et al., 2015). They justified this outcome by suggesting that the possible reasons might be the deposition of clay and the deep ground water level. In Group-4, liquefaction occurred when the seismic intensity was around 6.0, but the trend for the ratio was similar to Group 1.

Furthermore, they constructed a regression to estimate liquefaction occurrence probability from the seismic intensity by taking into account the classification of soil deposits in these four groups.

$$P_{liq}(I) = \Phi[I - \mu)/\sigma]$$

Where the $P_{liq}(I)$ represents the liquefaction probability of a 250-m grid cell at JMA-scale Seismic intensity I, μ is the mean value, and σ denotes the standard deviation. According to Matsuoka et al. (2015), this regression quantitatively and easily determined the large-area liquefaction potential estimation for each geomorphologic classification for a range of earthquake magnitude Mw from 6.0 to 8.1.

Table 6. Regression parameters obtained for each group (Matsuoka et al., 2015)

Group	Geomorphologic map unit and ID	Mean value, μ	Standard deviation, σ
1	Natural levee (NTL) Sand dune connect to lowland (LSD) Lowland between coastal dunes and/or bars (LDB) Abandoned river channels/Former pond and swamp (ARC) Reclaimed land (REC) Filled land (FLL)	7.00	0.82
2	Alluvial fan (ALF, AFS) Marine sand and gravel bars (BAR)	7.22	0.81
3	Back marsh (BKM) Delta and coastal lowland (DEL) Sand dune (DUN)	7.97	0.97
4	Valley bottom lowland (VBP, VPS) Gravelly terrace (GVT)	7.24	0.64
5	All others	9.97	1.24

Furthermore, the last decade geoscientists and engineers focus on the correlation of geological, geomorphological and climatic factors in order to assess the liquefaction hazard on a regional scale. Afterwards, these probabilistic liquefaction maps can be integrated with event-specific shaking intensity maps for rapid response and loss estimation.

In particular, Zhu et al. (2015) have developed a logistic regression model to predict the probability of liquefaction occurrence as a function of simple and globally available geospatial features (e.g., derived from digital elevation models), standard earthquake-specific intensity data (e.g. peak ground acceleration), and spatially continuous data as a proxy for important subsurface parameters. Applying a probabilistic modeling framework, their geospatial liquefaction model estimates the spatial extent and variability of liquefaction occurrence (Zhu et al., 2015).

The model of Zhu et al. (2015) is developed with respect to the areal extent of liquefaction, which can identify broad zones likely to liquefaction and not to achieve a model that can explain the liquefaction features at a site-by-site scale. The Global Geospatial Liquefaction (GGL) model is developed using logistic regression and is based on the following variables: compound topographic index (CTI), slope-derived shear wave velocity (V_{S30}), and magnitude weighted peak ground acceleration (PGA_M). The CTI is a hydrologic parameter that provides a proxy for soil saturation and V_{S30} is a geotechnical parameter that is commonly used as a proxy for soil stiffness. Zhu et al. (2015) used the magnitude scaling factor (MSF) as a proxy for earthquake duration; the PGA_M is PGA divided by MSF. The resolution of the developed maps is at 30 arc-sec resolution, which is roughly a 900 m x 900 m pixel.

The model outputs the probability of liquefaction (P), which is given by

$$P = \frac{1}{1 - e^{-x}}$$

where $x = 24.10 + 2.07\, ln(PGA_M) + 0.36CTI - 4.78 ln\,(V_{s30})$

Zhu et al. (2015) concluded that the model performance is good in native soils where liquefaction coincides with river channels but does not always capture the liquefaction potential of artificial fill (**Error! Unknown switch argument.**).

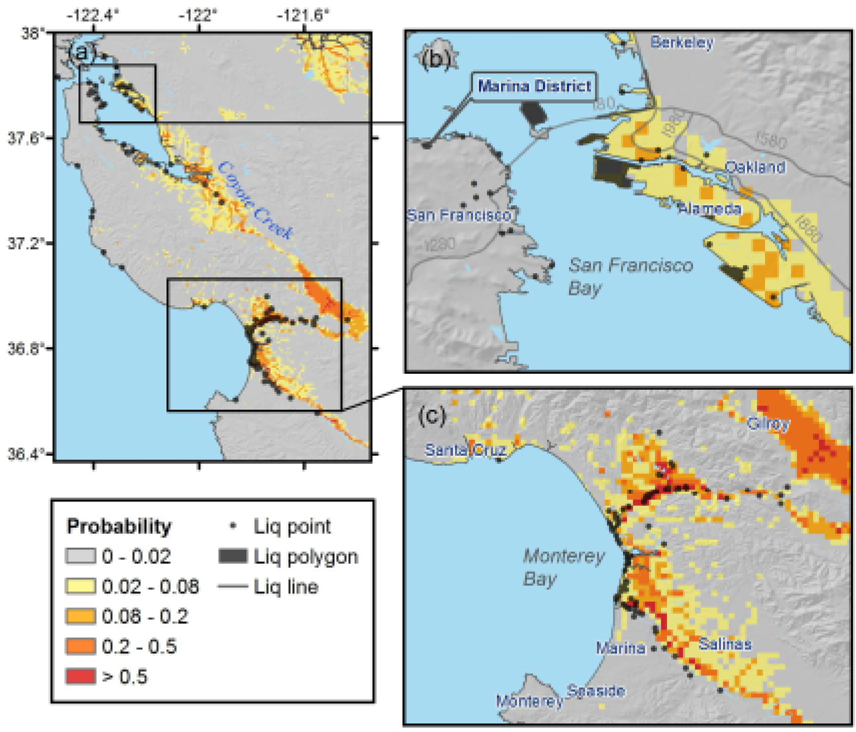

Figure 9. Maps of the observed liquefaction features and the predicted probability of liquefaction for the 1989 Loma Prieta earthquake (Zhu et al., 2015)

Zhu et al. (2017) updated the previous GGL model by taking into account previous works, such as Youd and Perkins (1978), which characterized the relationship between geologic depositional environments and liquefaction susceptibility, and Wald and Allen (2007), which identified a first-order approximation of soil conditions from topography. In particular, they inspected 14 broadly available geospatial proxies and concluded that the most promising are slope-derived V_{S30}, modeled water table depth, distance to coast, distance to river, distance to the closest water body, and precipitation, while they found that peak ground velocity (PGV) performs better than PGA as the shaking intensity parameter. The spatial resolution for all variables is 30 arcsec (approximately 900 x 900m).

Table 7. Summary of all candidate explanatory variables (Zhu et al. 2017)

Variable Description	Variable Name	Density	Saturation	Load
Shear-wave velocity over the first 30 m (slope derived)	V_{S30}	•		
Elevation	*elev*	•		
Topographic slope	*slope*	•		
Roughness	*rough*	•		
Topographic position index	TPI	•		
Terrain roughness index	TRI	•		
Distance to the nearest coast	*dc*	•	•	
Compound topographic index	CTI		•	
Global water table depth	*wtd*		•	
Distance to the nearest river	*dr*		•	
Distance to the nearest water body	*dw*		•	
Elevation above the nearest water body	*hwater*		•	
Mean annual precipitation	*precip*		•	
Aridity index	AI		•	
Peak ground acceleration	PGA			•
Peak ground velocity	PGV			•
Magnitude	M_w			•
Magnitude-scaling factor	MSF			•

They proposed two models, one for coastal areas and one for noncoastal areas. The latter model is based on the proxies of PGV, V_{S30}, water table depth (wtd), distance to the closest water body (dw), and precipitation and is recommended by the authors for global implementation.

They used logistic regression to model the probability of liquefaction which lies in the range between zero and one:

$$P = \frac{1}{1 + e^{-x}}$$

Where $x = \beta o + \beta_1 x_1 + \cdots + \beta_\kappa x_{\kappa,}, x_1, x_2, \ldots, x_\kappa$ are the explanatory variables, and β_0; β_1; …; β_k are the coefficients estimated from the regression.

They concluded that the estimated probability of liquefaction seems negatively correlated with ln(PGA) and ln(PGV) when PGA is beyond 0.3g and PGV is beyond 50 cm/s. In addition, they heuristically assigned zero to the predicted probability for both models when PGV < 3 cm/s. Similarly, they assigned zero to the probability when V_{S30} > 620 m/s. They stated that a threshold of 0.3 of liquefaction probability is more conservative in that it overpredicts liquefaction, whereas a threshold of 0.4 is a more balanced classifier.

Table 8. Coefficients of top performing coastal models and GLM-Zea15g (Zhu et al., 2017)

	GLM-Zea15g	Model 1	Model 2	Units
Intercept	24.10	12.435	8.801	
ln(PGV)		0.301	0.334	cm/s
$\ln(V_{S30})$	−4.784	−2.615	−1.918	m/s
precip		5.556×10^{-4}	5.408×10^{-4}	mm
$\ln(PGA_{M,SM})$	2.067			*g*
$\sqrt{dc}$		−0.0287		km
dr		0.0666		km
CTI	0.355			
dw			−0.2054	km
wtd			−0.0333	m
$\sqrt{dc} \times dr$		−0.0369		
AUC (all events)*	0.755	0.801	0.788	
Brier score (all events)*	0.232	0.162	0.166	
AUC (noncoastal)	0.655	0.793	0.811	
Brier score (noncoastal)	0.106	0.091	0.104	

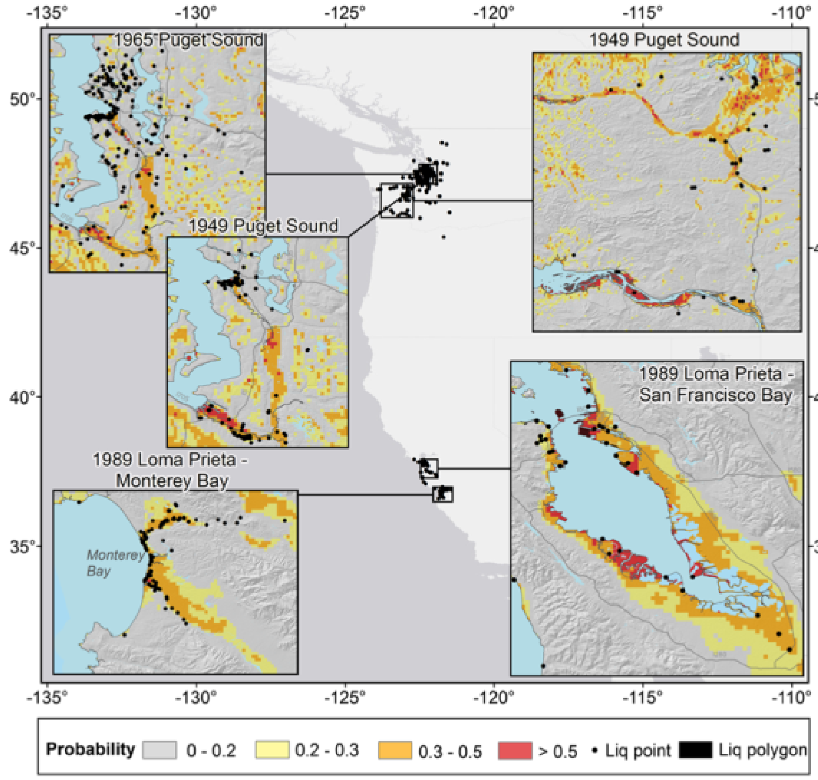

Figure 10. Probability maps predicted from model 1 for earthquakes in the USA (Zhu et al., 2017).

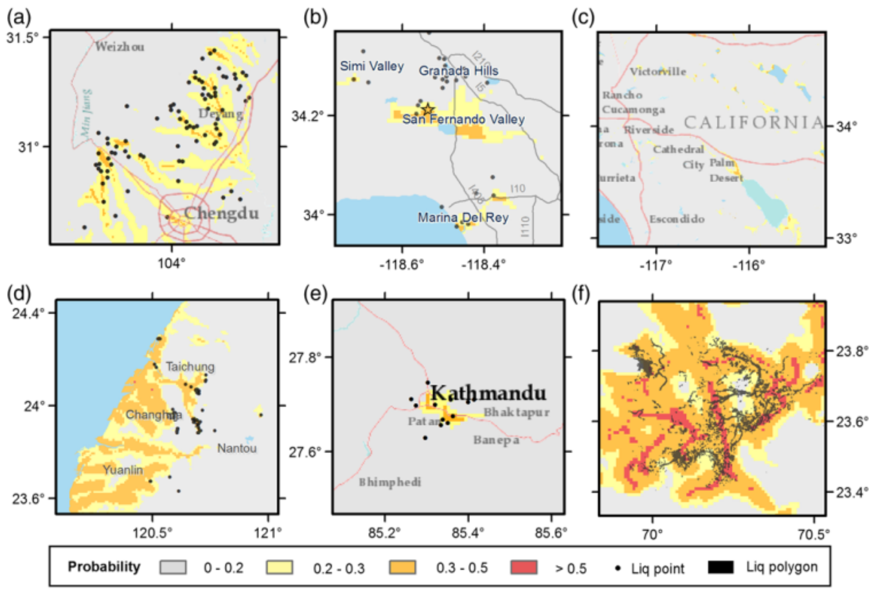

Figure 11. Probability maps predicted from model 2 for a) Wenchuan 2008, b) Northridge 1994, c) Hector Mine 1999, d) Chi-Chi 1999, e) Nepal 2015, f) Bhuj 2001 earthquakes (Zhu et al., 2017).

Moreover, they proposed an equation that can be used for predicting the spatial extent of liquefaction within a probability class. For models 1 and 2, they fit a logistic function which has the same form as the equation developed for computing the probability of liquefaction occurrences, except that in this case they found that squaring the denominator improves the fit

$$L(P) = \frac{a}{(1 + be^{-cP})^2}$$

in which L is the areal liquefaction percent, P is the predicted probability, and the parameters a, b, and c are given in **Error! Unknown switch argument.**. This equation can either be used to convert the predicted probability to liquefaction percent or to define simplified classes. For example, to define a class in which the percent liquefaction is between 10% and 20% from the probabilities predicted by model 2, one would insert the value of 10 and 20 for LP into equation and solve for P with the model 2 coefficients from **Error! Unknown switch argument.**, which would yield probabilities of 0.37–0.47 (Zhu et al., 2017).

Table 9. Parameters for relating model probabilities to areal liquefaction percent

parameters	**Model 1**	**Model 2**
a	42.08	49.15
b	62.59	42.40
c	11.43	9.165

Local scale

Having assessed the liquefaction susceptibility of the soil layers, and estimated the seismic parameters, PGA and M, a quantitative evaluation of liquefaction potential can be performed by taking into account data provided by borings with in-situ tests (vSPT).

In particular, the ability of a soil element to resist liquefaction is defined as liquefaction factor of safety, fs, and two variables are required for its calculation: the cyclic resistance ratio CRR and the earthquake induced cyclic stress ratio CSR at a specific depth for a given design earthquake. The factors of safety against liquefaction of the susceptible to liquefaction layers can be computed using simplified procedures proposed by several researchers e.g. Seed and Idriss (1971), Seed et al. (1985), Youd et al. (2001), Idriss and Boulanger (2012) and Cetin et al. (2016). Soil layers with factors of safety greater than 1.0 are considered as non-liquefiable.

$$fs = \frac{CRR_{7.5}}{CSR_{7.5}}$$

The CRR, according to Youd et al. (2001) is approximated with the following equation:

$$CRR_{7.5} = \frac{1}{34 - N_{1(60)}} + \frac{N_{1(60)}}{135} + \frac{50}{\left[10 \times N_{1(60)} + 45\right]^2} - \frac{1}{200}$$

The calculation of $N_{1(60)}$ is influenced by the measured standard penetration resistance N, the overburden pressure factor Cn, the correction for hammer energy ratio (ER) Ce, the correction for borehole diameter, Cb the correction factor for rod length Cr and the correction for samplers with or without liners. Afterwards, a “fine content” correction is applied to the calculated $N_{1(60)}$ value in order to obtain an equivalent clean sand value $N_{1(60)cs}$.

The CSR defines the seismic demand and is expressed as:

$$CSR = 0.65 \times \left(\frac{a_{\max}}{g}\right) \times \left(\frac{\sigma_{vo}}{\sigma'_{vo}}\right) \times r_d$$

where, σ_{vo}: total vertical stress at depth z, σ'_{vo}: effective vertical stress at the same depth, a_{max}: peak horizontal ground acceleration, g: gravity acceleration and r_d: stress reduction factor.

Finally, the CSR values will be divided by the magnitude scaling factor, MSF.

$$MSF = \left(\frac{Mw}{7.5}\right)^{2.56}$$

Liquefaction Potential Index LPI

Furthermore, the overall liquefaction potential of a soil column, defined as Liquefaction Potential Index (LPI), has been suggested to be computed based on the methodology proposed by Iwasaki et al., (1982) using the following equation:

$$LPI = \int_0^z F(z)W(z)dz$$

where z is the depth below the ground surface in meters and is calculated as w(z)=10-0.5z; F(z) is a function of the factor of safety against liquefaction, fs, where F(z) =1-fs when fs<1 and if fs>1, then F(z)=0. The index is proportional to the thickness of the liquefiable layer, the thickness of the non-liquefiable crust layer and the factor of safety against liquefaction. For the calculation of the LPI per borehole only soil layers with fs<1 that satisfies at the same time the liquefaction susceptibility criteria are taken into account.

The LPI values have the capability of characterizing liquefaction potential of soil column of 20m from ground surface. According to Toprak and Holzer (2003), the “simplified procedure” predicts what will happen to a soil element, whereas the LPI predicts the performance of the whole soil column and the consequences of liquefaction at the ground surface. Papathanassiou (2008) stated that the advantage of LPI is that it quantifies the likely of liquefaction of the site, by providing a unique value for the entire soil column, instead of several factors of safety per layer and accordingly assess the spatial probability of liquefaction potential. According to the threshold values proposed by Iwasaki et al. (1978), the liquefaction potential should be characterized as 'low' at sites where 0 < LPI < 5, 'high' where LPI is in the range 5-15 and 'very high' above 15.

Sonmez (2003) developed a modified scale by adding a threshold value of 1.2 instead of 1 for the calculation of Fs and introduced two new categories of liquefaction failure potential by distinguishing LPI = 0 as 'non liquefiable', 0 to 2 as 'low', 2 to 5 as 'moderate', 5 to 15 as 'high' and >15 as 'very high'.

Papathanassiou (2008) proposed an LPI-based probabilistic approach for the evaluation of liquefaction-surface evidences and, by taking into account a cut-off value of 50% probability, he defined a threshold value of LPI = 14 for discriminating the cases of liquefaction surface manifestation from the non-liquefaction ones.

The probability of liquefaction surface manifestation is computed based on the following equation:

$$\Pr ob(liquefaction) = \left(\frac{1}{1 + e^{-(-3.092 + 0.218 \times LPI)}} \right)$$

In this model, the LPI value is the independent variable while the occurrence or not of liquefaction phenomena is the dependent one.

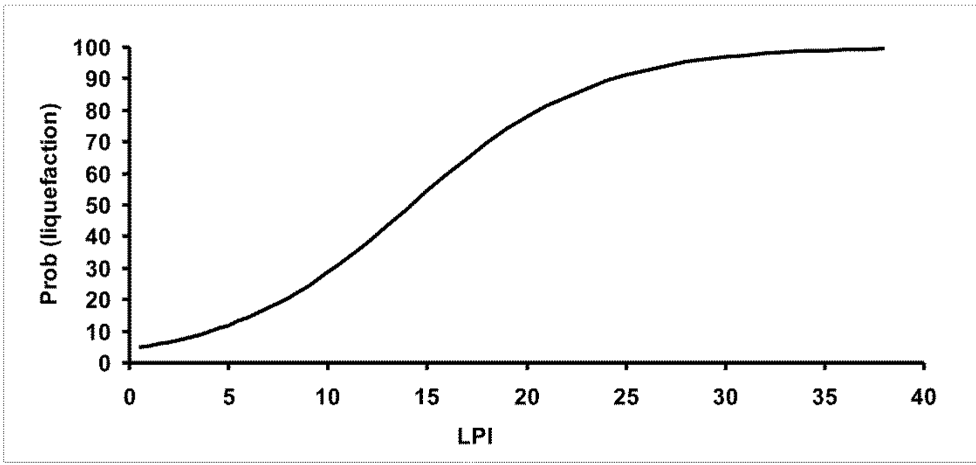

Figure 12. LPI-based probability curve (Papathanassiou, 2008)

The above classifications have been developed exclusively using SPT data, while the one proposed by Papathanassiou (2008) took additionally into account the susceptibility to liquefaction criteria proposed by Seed et al. (2003) for the classification of the soil layers. The fact that Papathanassiou (2008) followed the recently published susceptibility criteria, and accordingly took into acount silty soils for the computation of LPI, is the main reason for this higher threshold value of LPI = 14. Moreover, Maurer et al. (2014) concluded that this high LPI value might be explained by the fact that Papathanassiou (2008) analyzed soils with high fines content. The same conclusion was also used to explain the high LPI threshold proposed by Lee et al. (2003), which is briefly presented in the next paragraph.

An important confirmation of the Iwasaki et al. (1978) classification was provided by Toprak and Holzer (2003) which compared LPI values with the liquefaction-induced failures of several earthquakes, obtained from CPTs instead of SPTs. They concluded that sand boils likely occur where LPI ≥ 5 and lateral spreading phenomena will occur where LPI ≥ 12. They also suggest that LPI ≥ 5 can be used as a threshold for the surface manifestation of liquefaction. Furthermore, Lee et al. (2003) by implementation of the Robertson and Wride (1998) method, in order to determine the factor of safety, suggest that liquefaction risk is 'high' for sites with LPI > 21 and 'low' for sites with LPI < 13. Juang et al. (2008) computed LPI with the concept of probability of surface manifestation of liquefaction (PG) and recommended the following classification of risk for surface manifestation of liquefaction; 'extremely low' when PG < 0.1, 'low' for 0.1 < PG < 0.3, 'medium' when 0.3 < PG < 0.7, 'high' when 0.7 < PG < 0.9 and 'extremely high' for PG > 0.9.

Juang et al. (2008) concluded that the two threshold values (5 and 15) assumed in the Iwasaki criterion are likely not universally applicable and that the LPI scale should be rigorously re-calibrated anytime a component model of the LPI procedure is modified. Moreover, this discrepancy between the existing calibrations proposed by several authors, as briefly reviewed above, may be also due to different types of considered liquefiable layers, e.g. clean sand or silty sands and sandy silts. Furthermore, Maurer et al. (2014) pointed out the inportance of having consistency in the way threshold LPI values are determined and how LPI values are computed to assess liquefaction hazard.

Liquefaction Severity Number LSN

The LSN is a recently developed parameter by Tonkin and Taylor (2013), proposed to be used in order to reflect damaging effects of shallow liquefaction and is proposed to be considered as a probabilistic measure indicating risk assessment (Tonkin and Taylor, 2013). The LSN could be considered as an extension of the philosophy at the basis of the LPI and represents an alternative method for assessing the response of structures to liquefaction. The LSN rating represents the intensity of liquefaction by using volumetric densification strain as a proxy (e_V), with depth weighting by a hyperbolic (1/z) rather than a linear reduction (van Ballegooy et al., 2012). According to Tonkin and Taylor (2013), the LSN is higher for liquefying soils closer to the ground surface in comparison to liquefying layers at depth. The equation that should be used for computing the LSN is:

$$LSN = 1000 \cdot \int_0^h \frac{e_v}{z} dz$$

where the volumetric densification strain in the subject layer, e_V, is estimated by the approach proposed by Zhang et al. (2002) and z is the depth from the surface to the layer of interest in meters. As shown in equation, the integration depth is commonly posed equal to 20m because the contribution of the underlying layers would be negligeable.

Based on the observed land damages caused by Christchurch 2010-2011 earthquakes and the results provided by thousands CPTs performed in the epicentral area, Tonkin and Taylor (2013) developed a first classification of LSN associating 'little-to-no expression of liquefaction' to 0 < LSN <10, 'minor expression of liquefaction and sand boils' to 10 < LSN < 20, 'moderate-to-severe expression of liquefaction and likely settlement' when 20 < LSN < 30 and 'major expression of liquefaction, damage to ground surface and severe settlement of structures' when 30 < LSN < 40. Finally, for LSN values greater than 50, 'severe damage and widespread evidence of liquefaction at the surface' is reported.

Furthermore, Ishihara recognizing the influence of the non-liquefied capping layer on mitigating the surficial manifestation of liquefaction, he plotted observations of liquefaction surface effects using the thicknesses of the non-liquefied capping layer, H1, and the liquefied strata, H2. Based on this diagram, he proposed boundary curves for predicting liquefaction manifestation as a function of H1, H2, and peak ground acceleration (PGA). Ishihara (1985) initially proposed a single boundary curve using data from sites subjected to a PGA of 0.2g while incorporating the work of others, a series of curves was then proposed corresponding to different PGAs. The proposed boundary curves indicate that for a given PGA, there is a limiting H1 beyond which surface manifestations are not form, regardless of H2 (Maurer et al. 2014).

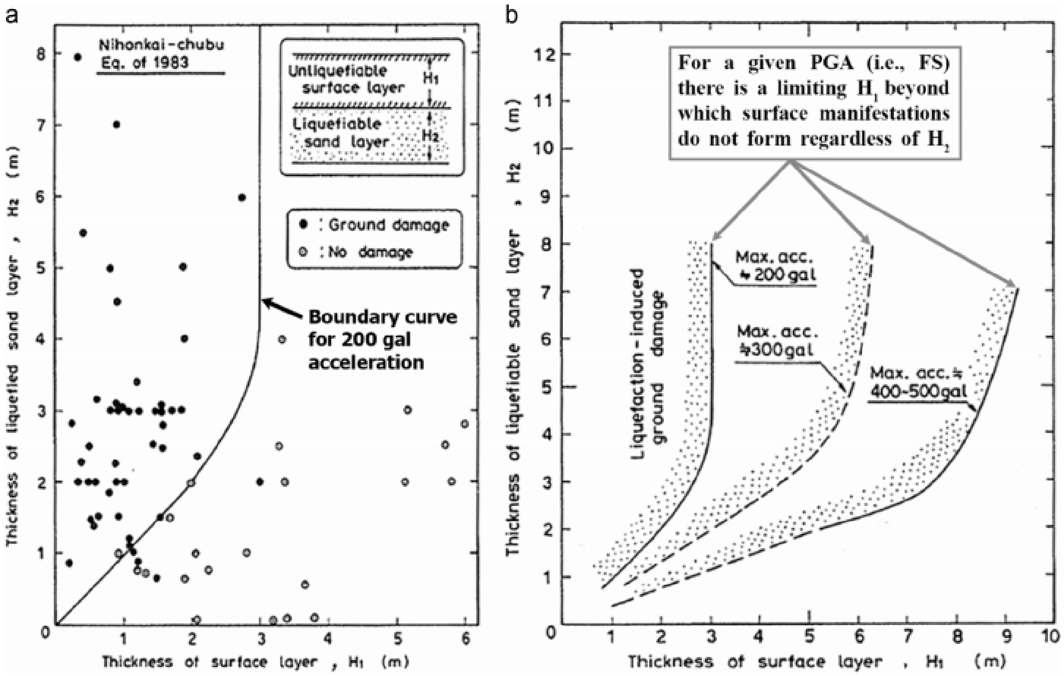

Figure 13. Discriminating between occurrence and non-occurrence of ground rupturing due to liquefaction 0.2g PGA); and (b) boundary curves proposed for identification of liquefaction-induced damage (Ishihara, 1985)

3.3.2 LANDSLIDES

Landslide Hazard Assessment (LHA) on a regional scale is a useful tool, that can support decisions regarding strategic planning for disaster prevention, but it can also make part of a REDA system. Landslide Hazard maps can be used to estimate the potential risks, prioritize areas in terms of the necessity to apply preventive measures and plan local investigations (slope stability analyses) which require a more detailed planning for funding and implementation. Such a strategic planning can provide the State Regional and local administration with the tool to effectively plan landslide disaster mitigation measures in both their financial and technical aspects. In case of a seismic event, it will provide in “near real-time”, maps where likely landslides are expected to have occurred, as soil or rock instabilities are considered as “potential damage”.

Numerous methods based on two different quantitative methodological approaches exist for assessing Landslide Hazard on regional scale, each one of them with a number of advantages and disadvantages. The multitude of existing methods and the different methodological approaches that exist in international bibliography, result into non comparable outputs, which is a major issue in cross-border areas and cross-border cooperation. Taking into consideration the existing lack of accessible landslide inventories, the scarceness of reliable data and meta-data and the requirements of a REDA system, a small number of methods feasible to be implemented under the existing conditions is initially adopted for a regional scale landslide hazard assessment.

For the needs of the present project two different methodological approaches for LHA have been selected. The first is a statistically based method, whilst the second one belongs to the category of physically based models. Implementation of these methodologies is feasible under the existing conditions in the broader project implementation area. These methodologies will be reasonably adapted to specific conditions and their outputs reliability and accuracy will be once again verified in the framework of this project.

In the following paragraphs, the statistically based models being essentially oriented to a regional scale assessment of landslide hazard, are presented. In this case, an empirical landslide probability model initially developed by Nowicki et al (2014) and improved by Jessee et al. (2018) who proposed an updated model regarding the near-real time assessment of seismically induced landslides, has been selected. Another method which also belongs to the statistically based methods, yet combined with two failure criteria for soils or rock masses, is the one proposed by Saade et al (2016), which is also going to be incorporated into the models used by REDACt.

On a second stage, a physically based method resulting in the calculation of the factor of safety, based on modelling slope failure processes, is presented. Namely, the infinite slope model used to describe shallow landslides or to the deterministic model for planar and circular failures are being presented.

The statistical approach is rather oriented to regional scale assessment of landslide hazard, especially when spatial variability of mechanical parameters that determine slope stability is not reliable or adequate, thus reducing the reliability and accuracy of the applied methods. On the other hand, if required data and their spatial variability are appropriate and sufficient, calculation of landslide hazard in terms of a factor of safety, provides more “engineer oriented” outputs which are definitely better conceived in engineered projects of seismic scenarios and decision making, during or just after, a seismic event.

Methods based on statistical approach

Empirical landslide probability model

Nowicki et al. (2014) developed an empirical landslide probability model, combining shaking estimates with broadly available landslide susceptibility proxies, i.e., topographic slope, surface geology, and climate parameters. As a core layer for the seismic shaking, they used deterministic estimates of the ground motion from earthquake events (e.g., peak acceleration and velocity) produced by the U.S. Geological Survey (USGS) ShakeMap system.

For their research, they applied the statistical analysis of logistic regression, which is appropriate for a process involving only a binary outcome (slide or no slide) and allows the observed outcomes to be fitted to the logistic function using data representing multiple predictor variables. They included the following predictor variables in the regression: ground motion produced by the earthquake, topographic slope, material strength, and soil wetness. In particular, they used the maximum slope obtained by the SRTM elevation data, the angle of friction of the geological material as a parameter of strength and the CTI regarding the soil wetness. The resolution of the developed maps was 30 arcseconds (approximately 900m pixels).

Their study resulted to the following equation which is considered as the best fitting model:

$Z = a + b*x_1 + c*x_2 + d*x_3 + e*x_4 + f*x_5$

where x_1=PGA, x_2=max slope, x_3=friction, x_4=CTI and x_5 =PGA*max slope. The values of these variables are listed in **Error! Unknown switch argument.**.

Table 10 Results of the regression on the global dataset (Nowicki et al., 2014)

AIC	Coefficients	Estimate	Std. error	*p*-Value
101,771	Intercept	−3.6490	0.2389	<0.001
	PGA	0.0133	0.0016	<0.001
	Max Slope	0.0364	0.0016	<0.001
	Friction	−0.0635	0.0082	<0.001
	CTI	−0.0004	0.0001	<0.001
	PGA ∗ Slope	0.0019	0.0000	<0.001

PGA=peak ground acceleration, CTI=compound topographic index.

The predicted probability of landslide occurrence P(z) can be computed based on the following formula:

$P(z)=1/(1+\exp(-z))$

Recently, Jessee et al. (2018) proposed an updated model regarding the near-real time assessment of seismically induced landslides. This model is the outcome arisen from the statistical analysis of data provided by 23 seismically induced landslides that span a range of earthquake magnitudes and climate and tectonic settings. In order to develop this model, they used logistic regression for relating the spatial distribution of slope failures with factors representing the ground shaking, the topography, lithology, land cover type and the soil wetness. The resulted maps were validated following the high balance accuracy (correctly versus incorrectly classified pixels).

Their study resulted to the following equation which is considered as the best fitting model:

$$z = a + b \times ln(PGV) + c \times slope + d \times lithology + e \times land\ cover + f \times CTI + g \times ln\ (PGV) \times slope$$

The values of the coefficients are listed in **Error! Unknown switch argument.**.

The predicted probability of landslide occurrence P(z) can be computed based on the following formula

P(z)=1/(1+exp(-z))

In order to validate their model, Jessee et al. (2018) applied the developed analysis in several areas where earthquake-induced slope failures were documented, by taking into account a 50% probability threshold; every probability 50% and above is classified as a landslide. More specifically, they estimated that the balance accuracy for the Wenchuan, China map is 94.6%, while the relevant accuracy for the Haiti map is 93.7% (Jessee et al., 2018). In addition, they tested their model to the Chi-Chi Taiwan and Kobe Japan earthquakes, resulting to 92.5% and 93.1% accuracy, respectively.

Taking into account those results, they concluded that the developed model performs well but at the same time, some pixels exist where this statistical model either underestimate or overestimate the actual landslide risk.

Table 11 Best fit model coefficients (Jessee et al., 2018)

Variable code	Description	Estimate
(Intercept)	—	−6.30
log (pgv)	Ground shaking	1.65
gted75c	Slope	0.06
glim75c3	Metamorphics	−1.87
glim75c4	No data	−0.66
glim75c5	Acid plutonic rocks	−0.78
glim75c6	Basic plutonic rocks	−1.88
glim75c7	Intermediate plutonic rocks	−1.61
glim75c8	Pyroclastics	−1.05
glim75c9	Carbonate sedimentary rocks	−0.95
glim75c10	Mixed sedimentary rocks	−1.36
glim75c11	Siliciclastic sedimentary rocks	−1.92
glim75c12	Unconsolidated sediments	−3.22
glim75c13	Acid volcanic rocks	−1.54
glim75c14	Basic volcanic rocks	−1.50
glim75c15	Intermediate volcanic rocks	−0.81
cti	Spatially varying wetness	0.03
globcover14	Rainfed croplands	0.91
globcover20	Mosaic cropland	0.88
globcover30	Mosaic vegetation	0.78
globcover40	Closed to open broadleaved evergreen or semideciduous forest	0.68
globcover50	Closed broadleaved deciduous forest	0.30
globcover60	Open broadleaved deciduous forest/woodland	1.77
globcover70	Closed needleleaved evergreen forest	1.71
globcover90	Open needleleaved deciduous or evergreen forest	−1.26
globcover100	Closed to open mixed broadleaved and needleleaved forest	1.50
globcover110	Mosaic forest or shrubland/grassland	0.68
globcover120	Mosaic grassland/forest or shrubland	1.13
globcover130	Closed to open broadleaved or needleleaved, evergreen or deciduous shrubland	0.79
globcover140	Closed to open herabceous vegetation	1.03
globcover150	Sparse vegetation	0.54
globcover160	Closed to open broadleaved forest regularly flooded	2.34
globcover180	Closed to open grassland or woody vegetation on regularly flooded or waterlogged, soil, fresh, brackish, or saline water	1.19
globcover190	Artificial surfaces and associated areas	0.30
globcover200	Bare areas	−0.06
globcover220	Permanent snow and ice	−0.18
globcover230	No data (burnt areas, clouds, …)	−1.08
log (pgv)*gted75c	Interaction term	0.01

Furthermore, Jessee et al. (2018) proposed an equation for estimating the frequency of landslide occurrence that can be interpreted as the areal coverage Lp; the portion of each cell that is expected to have landslide occurrence.

$$L_p(P) = e^{(a+b\times P+c\times P^2+d\times P^3)}$$

where P is the predicted probability of landslide occurrence, a=-7.592, b=5.237, c=-3.042 and d=4.035.

Hybrid statistical model combined with failure criteria

Saade et al. (2016) conducted a parametric study aiming to identify the relationship between the critical acceleration of the slope, the slope angle, and the slope shear strength parameters. In order to achieve this, they used the two failure criteria of Mohr-Coulomb (MC) and Hoek-Brown (HB) and particularly the former one for soil slopes less than 45° and the latter one for steep slopes greater than 45o. In addition, they used the equations deriver by Li et al. (2008) in order to calculate the equivalent parameters for a particular set of material strength.

As an outcome, they proposed the following formula for soil slopes of less than 45° angle (MC criterion)

$$a_c = C1\frac{c}{\gamma H} + C2$$

where C1 and C2 are the coefficients of the proposed equation varied in function of the slope angle ß and a_c is the value of critical acceleration.

Table 12 List of equations for coefficients C1(MC) and C2(MC) (ß < 45°).

ϕ (deg)	Coefficient $C1_{(MC)}$	Coefficient $C2_{(MC)}$	$R^2_{adjusted}$
25	$1.3228\ln\left(\frac{\tan\beta}{\tan\phi}\right) + 2.9007$	$-0.306\ln(\tan\beta) - 0.135$	0.9113
30	$1.2843\ln\left(\frac{\tan\beta}{\tan\phi}\right) + 3.2438$	$-0.321\ln(\tan\beta) - 0.0582$	0.9394
35	$1.3716\ln\left(\frac{\tan\beta}{\tan\phi}\right) + 3.5366$	$-0.352\ln(\tan\beta) + 0.0125$	0.9558
40	$1.1993\ln\left(\frac{\tan\beta}{\tan\phi}\right) + 3.7779$	$-0.359\ln(\tan\beta) + 0.1066$	0.9503
45	$1.0874\ln\left(\frac{\tan\beta}{\tan\phi}\right) + 3.9544$	$-0.392\ln(\tan\beta) + 0.1754$	0.9656
50	$0.9585\ln\left(\frac{\tan\beta}{\tan\phi}\right) + 4.0927$	$-0.423\ln(\tan\beta) + 0.2559$	0.9730

For slopes greater than 45° and the HB criteria, the variables used were: the geological strength index GSI, the material constant m_i, the unconfined compressive strength σ_{ci}, and the slope angle ß. The results of the parametric study were sorted for a combination of GSI - m_i. The a_c is computed based on the following equation:

$$a_c = C1 \times \ln\frac{\sigma_{ci}}{\gamma H} + C2$$

where C1 and C2 are the coefficients of the proposed equation varied in function of the slope angle ß and a_c is the value of critical acceleration.

Table 13 List of equations for coefficients C1 and C2 (β > 450).

GSI	m_i	Coefficient $C1_{(HB)}$	Coefficient $C2_{(HB)}$	$R^2_{adjusted}$
20	5	$0.006\tan\beta^2 + 0.0371\tan\beta + 0.1971$	$0.0381\tan\beta^2 - 0.5061\tan\beta + 0.0724$	0.99
	10	$0.0067\tan\beta^2 - 0.0042\tan\beta + 0.2046$	$0.0539\tan\beta^2 - 0.439\tan\beta + 0.2153$	0.99
	15	$0.0144\tan\beta^2 - 0.0489\tan\beta + 0.2245$	$0.0384\tan\beta^2 - 0.3437\tan\beta + 0.2529$	0.99
	20	$0.0147\tan\beta^2 - 0.0618\tan\beta + 0.2277$	$0.0531\tan\beta^2 - 0.3681\tan\beta + 0.3347$	0.99
	25	$0.0212\tan\beta^2 - 0.0902\tan\beta + 0.2421$	$0.0386\tan\beta^2 - 0.3106\tan\beta + 0.3459$	0.99
	5	$0.0007\tan\beta^2 + 0.0625\tan\beta + 0.2202$	$0.0588\tan\beta^2 - 0.5682\tan\beta + 0.1935$	0.99
	10	$-0.0055\tan\beta^2 + 0.0449\tan\beta + 0.1938$	$0.0988\tan\beta^2 - 0.6073\tan\beta + 0.4377$	0.99
30	15	$0.0163\tan\beta^2 - 0.05\tan\beta + 0.2455$	$0.0384\tan\beta^2 - 0.3535\tan\beta + 0.3544$	0.99
	20	$0.0212\tan\beta^2 - 0.0773\tan\beta + 0.2543$	$0.031\tan\beta^2 - 0.3089\tan\beta + 0.3879$	0.99
	25	$0.0176\tan\beta^2 - 0.0727\tan\beta + 0.2431$	$0.0543\tan\beta^2 - 0.3784\tan\beta + 0.4844$	0.99
	5	$-0.039\tan\beta^2 + 0.2088\tan\beta + 0.1739$	$0.1827\tan\beta^2 - 1.0009\tan\beta + 0.5576$	0.99
	10	$0.0122\tan\beta^2 - 0.0069\tan\beta + 0.2723$	$0.0413\tan\beta^2 - 0.4247\tan\beta + 0.3742$	0.99
40	15	$0.013\tan\beta^2 - 0.0312\tan\beta + 0.2598$	$0.0547\tan\beta^2 - 0.4251\tan\beta + 0.4907$	0.99
	20	$0.0166\tan\beta^2 - 0.0506\tan\beta + 0.2557$	$0.0516\tan\beta^2 - 0.4066\tan\beta + 0.5449$	0.99
	25	$0.0202\tan\beta^2 - 0.0703\tan\beta + 0.2583$	$0.0484\tan\beta^2 - 0.3868\tan\beta + 0.578$	0.99
	5	$-0.0334\tan\beta^2 + 0.2509\tan\beta + 0.1019$	$0.0823\tan\beta^2 - 0.7175\tan\beta + 0.5618$	0.91
	10	$-0.0003\tan\beta^2 + 0.0409\tan\beta + 0.2973$	$0.0729\tan\beta^2 - 0.5325\tan\beta + 0.5258$	0.98
50	15	$0.0079\tan\beta^2 + 0.002\tan\beta + 0.2824$	$0.0631\tan\beta^2 - 0.4883\tan\beta + 0.6154$	0.98
	20	$0.0209\tan\beta^2 - 0.068\tan\beta + 0.3175$	$0.0423\tan\beta^2 - 0.3603\tan\beta + 0.568$	0.98
	25	$0.0128\tan\beta^2 - 0.0456\tan\beta + 0.2824$	$0.074\tan\beta^2 - 0.458\tan\beta + 0.686$	0.98

In the following flow chart the steps of the proposed method that should be followed in order to compute the critical acceleration are presented.

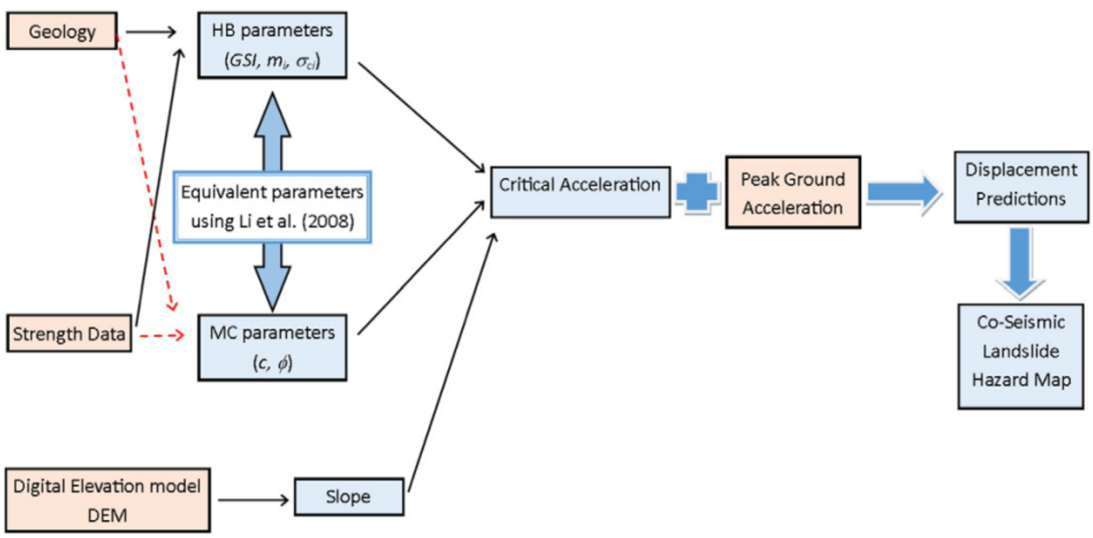

Figure 14 Flow chart for steps involved in the proposed approach to obtain the displacement predictions (boxes in light red signify available data) (Saade et al., 2016)

Physically based methods

Natural hazard is defined as the probability of occurrence of potentially damaging phenomena within a specified period of time and within a given area (Varnes, 1984). Zonation refers to the division of the land in homogeneous areas or domains according to the degree of actual or potential hazard (Varnes, 1984). Hence, the proposed models are able to predict landslide prone areas without any clear indication when those are likely to take place. So, in this framework, hazard is used as a quantitative estimation of landslide occurrence over a given region, whilst the time period is not defined in the model, since parameters such as lithology, slope inclination, structure, mechanical properties and geomorphology are time independent parameters and can be calculated in a deterministic way, by means of a safety factor.

Those models are hybrid models and can be applied at regional or local scales; in physical based models (or else, geotechnical landslide hazard models), the probability of occurrence of a landslide is based on the respective triggering the failure, factor (i.e. rainfall, earthquake induced ground motion) and expressed throughout F_S values.

Physically based landslide hazard assessment methods are based on the modelling of slope failure processes. They can be applicable over large areas (regional scale), if geological and geomorphological conditions are fairly homogeneous and landslide types relatively simple. They also apply to areas with incomplete or inexistent landslide inventories; this is considered as a major advantage for countries with incomplete landslide inventories.

Most of physically based landslide hazard assessment methods use the infinite slope model, therefore they are suitable for shallow landslides and this is one of the reasons why they have been used extensively in Greece and also in other countries. The above models account for different triggering parameters, such as: rainfall and transient groundwater response or effects of earthquake excitation (Corominas et al., 2014).

The main advantages and drawbacks of physically based methods for landslide hazard assessment are presented as follows:

Main advantages

a) they can be easily implemented in GIS environment;
b) outputs are more consistent and better conceived by engineers, compared to other approaches;
c) they present higher predictive capability and appear to be more suitable to quantify the influence of individual parameters contributing to shallow landslide initiation;
d) based on slope stability models, they allow the calculation of quantitative values of stability (safety factor, probability of failure).

Main drawbacks

a) parameterization can be a difficult task, as well as access to critical parameters, such as: regolith depth, transient slope hydrological processes, temporal changes in hydraulic properties;
b) there is a risk of over simplification, since a large amount of reliable input data is often necessary;

c) noticeable heterogeneities in geological, geomorphological and geotechnical conditions over large areas, might be misleading.

As it appears, the physically based methods for landslide hazard assessment, albeit they can provide relatively reliable results, their accuracy is dependent on the quality (ie. reliability, accuracy, completeness etc) of the available input data and information. However, their use is rather well conceived, by engineers and non-expert scientific personnel with a minimum of training.

In physically based methods, predisposing factors play an important role in landslide hazard analysis, under static or seismic conditions. Therefore, the following points are highlighted as being crucial for a reliable assessment, given the detail dictated by the scale used:

- Topographic information and its derivatives (need for high-resolution DEMs).
- Geological maps focusing traditionally in lithological and stratigraphical subdivision need to be converted into an engineering geological / geotechnical classification with emphasis on Quaternary sediments and rockmass structure, as well as shear strength characteristics.
- Structural information is important for landslide hazard assessment; information regarding dip and dip direction can improve reliability of output, but also depends strongly on the number of measurements and complexity of structure. Rock fracturing and faulting is also an important parameter since it defines at large, the mechanical properties of rock formations.
- Soil properties in the use of physically based slope stability models for LHA are key parameters, especially for shallow depth failures. Soil depth, defined as the depth from free surface down to a consolidated material (also known as regolith depth) is a crucial parameter.
- Spatial variability is also a crucial parameter, often ignored in landslide modeling due to lack of adequate data.
- Soil thickness can be estimated throughout physical based methods that model rates of weathering, denudation and accumulation.

The factor of safety landslide hazard assessment method can be calculated according to the assumed failure mechanism (static conditions):

- Infinite slope model: $$F_S = \frac{c'}{\gamma * \mathrm{t} * \sin\beta} + \frac{\tan\phi'}{\tan\beta} + \frac{\mathrm{m} * \gamma_\mathrm{w} * \tan\phi'}{\gamma * \tan\beta} \quad (1)$$

  where
  φ’: effective angle of friction of geomaterial (deg)
  c’ : effective cohesion of geomaterial (kPa)
  γ : specific weight of geomaterial (kN/m^3)
  β : slope angle (deg)

γ_w: specific weight of the water (kN/m^3)
t : normal thickness of failure slab (m)
m : percentage of the water saturated failure slab (%)
r_u = pore pressure ratio ($r_u = \gamma_w/\gamma$)

- Deterministic model for plane landslides: $F_S = \tan\varphi' / \tan\beta$ (2)

  where
  φ’: effective angle of friction of geomaterial (deg)
  ß : slope angle (deg)

- Deterministic model for circular landslides (Ferentinou et al., 2006):

$$F_S = 4.32 * \left[\frac{c'}{\gamma * \mathrm{H} * \sin\beta} \right] + 1.22 * (1 - r_u) * \frac{\tan\phi'}{\tan\beta} + 0.005 \qquad (3)$$

  where
  φ’: effective angle of friction of geomaterial (deg)
  c’: effective cohesion of geomaterial (kPa)
  H: height of the slope
  γ : specific weight of geomaterial (kN/m^3)
  γ_w: specific weight of the water (kN/m^3)
  ß : slope angle (deg)
  r_u: pore pressure ratio ($r_u = \gamma_w/\gamma$)

In the above geotechnical landslide hazard models two basic advantages are added to the already widely used physically based methods (deterministic methods):

1. The proposed tool is a dynamic tool which enables the user to modify as necessary the values of the geotechnical parameters, optimizing accordingly the landslide hazard model and producing landslide hazard maps referring to the temporal variability of geotechnical and hydrological or even seismological parameters.

2. Using the determinist model, the user can estimate F_S, assuming circular, planar or infinite slope failure mechanisms.

In case of seismic conditions, the driving equation of the infinite slope model turns into:

$$\mathrm{F} = \frac{c' + (z\gamma\cos^2\beta - z\rho\alpha\cos\beta\sin\beta - \gamma_w z_w \cos^2\beta)\tan\phi}{z\gamma\sin\beta\cos\beta + z\rho\alpha\cos^2\beta} \qquad (4)$$

where

φ': effective angle of friction of geomaterial (deg)
c': effective cohesion of geomaterial (kPa)
H: height of the slope (m)
γ : specific weight of geomaterial (kN/m^3)
γ_w: specific weight of the water (kN/m^3)
ρ: density (Mg/m^3)
ß : slope angle (deg)
r_u: pore pressure ratio ($r_u = \gamma_w/\gamma$)
a: seismic acceleration (g)
z: depth of sliding zone or failure surface (m)
z_w: height of water table (m)
m: percentage (%) of the water saturated failure slab ($m = z_w/z$)

The aforementioned physically based models have been tested successfully in pilot implementation areas in Greece and other partners countries both in regional scale or in local scale in the framework of the project SciNetNatHaz (2014).

3.4 Damage estimation methodologies for buildings

A brief discussion on existing vulnerability assessment methodologies, focusing mainly on fragility curves, will be presented in this section, since several extensive state-of-the-art reviews are already available in the literature and the reader is referred to them for further information. A JRC technical report for the seismic fragility curves for the European building stock has been published by Maio & Tsionis (2015) emphasizing on analytical fragility curves, “A beginner’s guide to fragility, vulnerability and risk” is under continuous development by Porter (2020), a book chapter by Rossetto et al. (2014) included in a publication presenting fragility functions for elements at risk, as a part of the SYNER-G research project (Pitilakis et al., 2014), to name just a few. Vulnerability functions are typically classified into four general approaches: empirical, expert judgement, analytical and hybrid.

Empirical approaches

Empirical methodologies are based on the study of statistical results of actual observed damages of elements at risk (i.e. buildings, bridges, lifelines etc.) exposed to past earthquakes. Vulnerability functions can be expressed in the form of damage probability matrices or tables of mean values and standard deviations of loss for each level of excitation. When reliable extensive damage data are available, empirical vulnerability functions are considered highly credible since they are derived from observations of the actual performance of assets in real seismic events. On the other hand, empirical approaches can have some important drawbacks (Porter, 2020):

- Several building types may have not yet experienced strong motion (especially new buildings)

- Extensive damage data are not available for high levels of excitation, where high losses are most likely, due to the rarity of such events

- Available data can be heterogenous, the sample may not be representative of the building stock, inadequate inspections of buildings may have not revealed the actual damage

- Actual loss data (in economic terms) can be hard to collect either from construction permits or insurers

- It is difficult to estimate the ground shaking level at the observations (macroseismic intensity values are sometimes being used which also involve damage in their definition)

- Small or poor-quality databases can lead to misleading results.

Expert judgement

In cases where no empirical data are available or the assets are difficult to model, the opinion of experts is asked to provide estimates on vulnerability quantities (e.g. mean loss, damage probability etc.). Expert opinion can be very efficient, capable of producing a new vulnerability function at the cost of a few person-hours each and of estimating the performance of buildings that have not yet experienced strong motion. Expert approaches can be grouped in two main categories, mathematical and behavioral. The first mathematically combines the answers of several experts that have no interaction with each other, while the latter aim at producing some type of group consensus among experts, who are typically encouraged to interact with one another and share their assessments (Maio & Tsionis, 2015). The major disadvantages of expert judgement approaches relate to the subjectivity of their opinions, the influence of dominant personalities and the tendency to reach speedy conclusions.

Analytical methods

Analytical methods are based on the estimation of damage distributions through the simulation of an element's structural response subjected to seismic action. They are widely used to provide insight where empirical methods cannot (new buildings, high intensities, effects of special building properties such as soft storey conditions, the infill panels configuration etc.). Seismic input can be represented by a response spectrum (static methods) or an acceleration time-history (dynamic methods). Numerical models need to be developed and a compromise has to be made between the accuracy of the representation of the nonlinear behavior and the robustness and cost-efficiency of the model (Rossetto et al., 2014).

The major problems of analytical methodologies are the computational cost (especially in the case of time-consuming inelastic dynamic time-history analyses) and the lack of validation by earthquake experience and/or experimental tests.

Apart from the analysis method distinctions between analytical approaches can relate to the modelling of structural (i.e. distributed plasticity or concentrated plastic hinges) and non-structural elements (e.g. infill panels), the choice between more realistic 3D models or less time-consuming 2D representations (or even single degree of freedom oscillators in some cases), the selection of the intensity measure (PGA, S_d, $S_a(T)$, etc.), the selection of appropriate damage index models, the probability distribution model and the associated uncertainties, etc. An extensive review of analytical approaches for the derivation of fragility curves has been presented by Maio & Tsionis (2015).

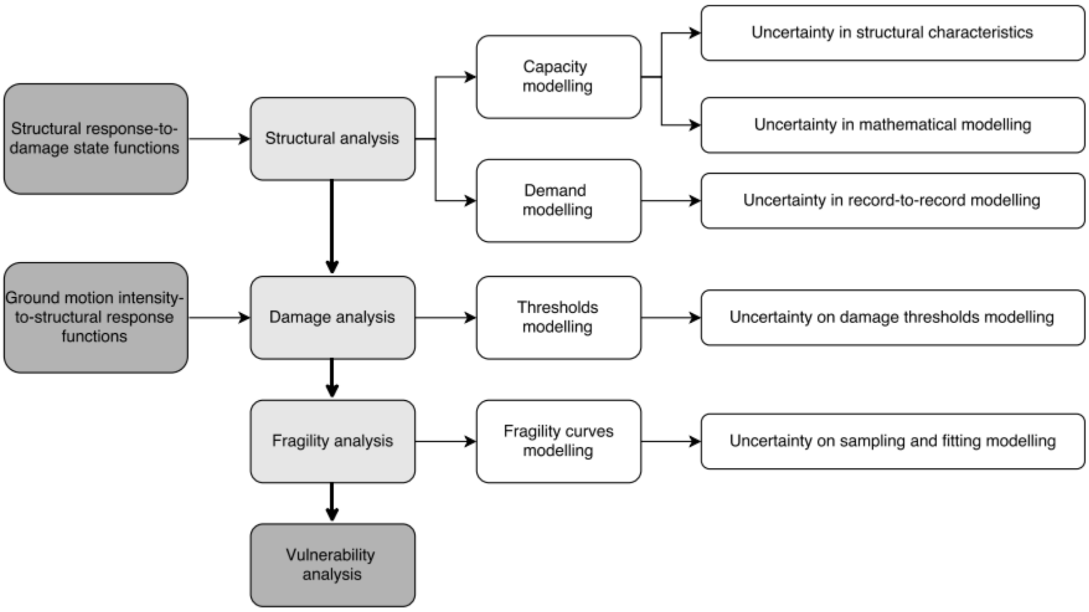

Figure 15. Main components and phases considered in analytical fragility assessment methodologies and associated uncertainties Maio & Tsionis (2015)

Some of the available mechanics-based vulnerability assessment methods are DBELA (Displacement-Based Earthquake Loss Assessment) and SP-BELA (simplified displacement-based method) – both considering that the nonlinear response of a reinforced concrete structure can be obtained from a nonlinear static analysis of the structure.

DBELA method (Crowley et al. 2004; Bal et al. 2008a) relies on the principles of direct displacement-based design method of Priestley (1997, 2003). DBELA method compares the displacement capacities of the substitute SDOF models of the buildings are compared with the seismic demand at their effective periods of vibration at different levels of damage. Buildings are classified on the basis of their response mechanisms: beam-sway or column-sway and the displacement capacities and periods of vibration for each damage state computed. Structural displacements are used to define the limit states of damage.

This methodology is used additional to HAZUS methodology to get more sophisticated structural loss estimates where applicable due to structural element knowledge of the building inventories at the region in interest. DBELA methodology is also written as an open source (Python or Matlab) code on GitHub platform.

SP-BELA stands for a simplified displacement-based method; it can be considered as an alternative to DBELA (Crowley et al., 2008) and is included along with DBELA and many other analytical methods (such as SPO2IDA of Vamvatsikos and Cornell, 2006; Dolsek and Fajfar, 2004; Ruiz Garcia and Miranda, 2007; Vidic, Fajfar and Fischinger, 1994; Lin and Miranda, 2008; N2 from EC8 or Capacity Spectrum Method from FEMA, 2005 but also DBELA) in the GEM's Integrated Risk Modeller's Toolkit (https://github.com/GEMScienceTools/rmtk).

Hybrid approaches

It is possible to combine two (or more) of the aforementioned techniques for the derivation of vulnerability models, an approach that is usually referred as hybrid. The need to develop such methodologies rises from limitations of each of previous approaches, for example the lack of empirical damage data for several building typologies or for high levels of input motions, or the lack of validation for analytically estimated results. In Deliverable T1.1.1, a hybrid approach developed at the Laboratory of Reinforced Concrete and Masonry Structures in the Aristotle University of Thessaloniki (Greece) has been presented, that combines the results of inelastic time-history analysis of 2D models of typical RC structures, with available (empirical) damage data from previous seismic events. A combination between analytical, empirical and expert opinion was presented by the EERI-WHE group within the PAGER project (Jaiswal and Wald, 2010), attempting to define the proportion of collapses for building typologies given a shaking intensity expressed in EMS-98 Intensity for several nations worldwide. A comparative analysis of building types has been carried out and then comparison of analytically or empirically derived curves by national studies (Pomonis et al., 2009).

New trends in fragility curves derivation - Soil-structure interaction

The common practice in seismic risk assessment of structures in urban scale is to derive fragility curves that were developed for fixed base structures. The soil properties are not taken into account with respect to their effect on the foundation stiffness and the resulting dynamic characteristics of the examined structures. Yet, soil-structure interaction (SSI) effects have been extensively investigated and their importance in the dynamic response of structures has been proved to be quite significant in several cases (e.g. Veletsos and Meek 1974, Stewart et al. 1999).

Since soil-structure interaction results in an elongation of the structural period and in increased system damping due to the radiation of seismic waves, it is common belief that it leads to reduced response in most cases and is often neglected in modern Seismic Codes, as being on the safe side of the calculations. Indeed, consideration of SSI is mandatory during the study of a new structure only when it leads to unfavorable response. On the other hand, since the purpose of seismic risk assessment studies is not to be on the safe side of the design but to estimate the actual building response as closely as possible, the interaction phenomena should be properly introduced even when the expected result is favorable for the examined structure. Therefore, along with possible detrimental effects of SSI, the cases of reduced response compared to the fixed-base structure should also be identified, in order to provide an accurate feedback to the involved stakeholders and to facilitate proper decision making during the post-earthquake crisis management.

Recent studies have been reported considering the soil-structure interaction effects on the seismic vulnerability of structures, by developing fragility curves for flexibly based structures (Ulrich et al 2011, Saez et al. 2011, Rajeev and Tesfamariam 2012, Fotopoulou et al. 2012, Pitilakis et al. 2014, Karapetrou et al. 2015, Cavalieri et al. 2020). Comparisons with fragility curves of fixed base structures reveals that soil structure interaction seem often - but not always - result in a reduction of the structural fragility due to the combined effect of radiation damping, modification of vibrating modes and hysteretic soil dissipation considering its non-linear behavior (Saez et al. 2011, Rajeev and Tesfamariam 2012). Yet, there are several combinations of structures and soil deposit properties where SSI may yield increased vulnerability, especially when nonlinear soil response is appropriately accounted for (Karapetrou et al. 2015). Especially, when the comparison takes place between the fixed base structural response for type A earthquake motion (outcrop) and the SSI response for modified earthquake motion that considers the site effects, there are several cases that SSI effects are detrimental, depending also on the combination of the examined soil deposit properties and structural features (Fotopoulou et al. 2012, Pitilakis et al. 2014 etc). It should be mentioned that research in this field is ongoing and most of the aforementioned studies are not conclusive, considering the dependence of the investigated effects on the specific selection of the examined structures and foundation soil properties in each study.

On the other hand, Rovithis et al. (2017) proposed a simplified approach to consider SSI effects in the framework of seismic risk assessment at urban scale, employing a methodology based on FEMA 440. This approach, which was initially presented for the case of Kalochori, N. Greece (Rovithis et al.

2017) and later applied for the city of Thessaloniki (Karatzetzou et al. 2018), comprises of the following stages:

1. modification of the imposed seismic motion at the base of the structure due to increased damping (kinematic interaction may also be included if considered significant for the examined foundation type);

2. modification of the dynamic characteristics of the SSI system due to foundation soil compliance.

Despite the approximate nature of the aforementioned pilot studies, the estimation may drastically improve in cases where more refined data are available for the structural properties of the examined building stock (i.e. foundation type, structural system, response period etc). Of course, this approach does not offer an exact estimation of the SSI effect on the structural fragility, yet, it can provide insight of its potential effect in urban scale for a specific set of building features and foundation soil characteristics.

Apart from soil structure interaction, recent studies also investigate the effect of additional parameters on the structural fragility, such as aging of buildings (Pitilakis et al. 2014), building foundation near slopes (Fotopoulou et al. 2013, Mavrouli et al. 2014), soil liquefaction, tsunamis etc. Furthermore, machine learning techniques have recently been proposed to derive seismic fragility curves (Kiani et al., 2019). Research on those topics is still ongoing.

Fragility curves conversion into different intensity measures

In seismic risk assessment studies, the choice of appropriate ground motion intensity measures IM (scalar, vector etc) is of crucial importance. This is especially true for the development of fragility curves conditional on an intensity measure, in order to perform seismic scenario-based risk assessment. Given that fragility curves are, in general, structure and site specific, a comparison among them, is complicated. The same is true when hazard at a site of interest is not available for the IM originally considered in the fragility assessment. Therefore, the need of development of methodologies to convert fragilities into a target IM is now well recognized and various relevant studies have been published in recent years (e.g. Ohtori and Hirata, 2006; Weatherill et al., 2015; Michel et al, 2018; Suzuki and Iervolino, 2020).

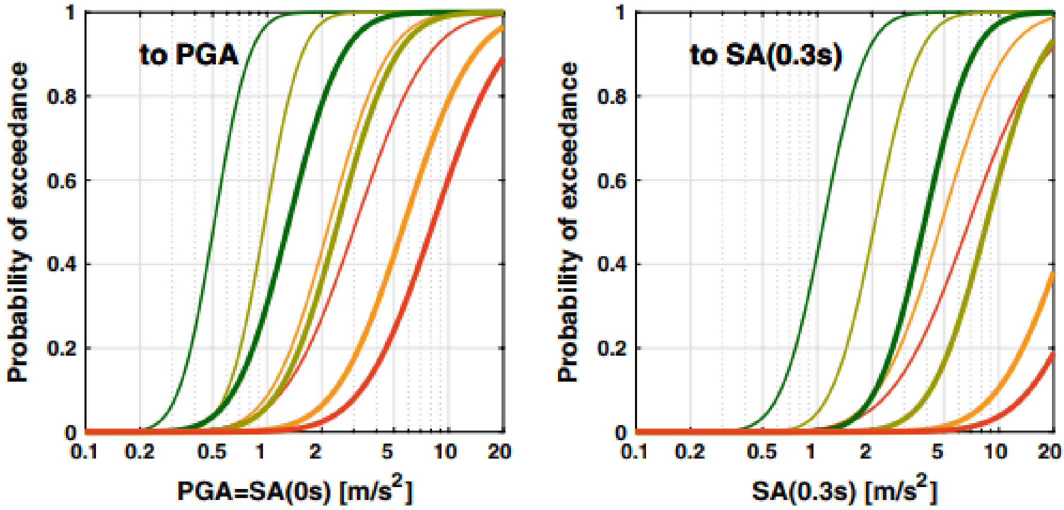

Figure 16. Fragility curves for masonry (thin lines) and reinforced concrete (thick lines) building typologies converted to PGA (left) and Sa(0.3s) (right) (Michel et al., 2018)

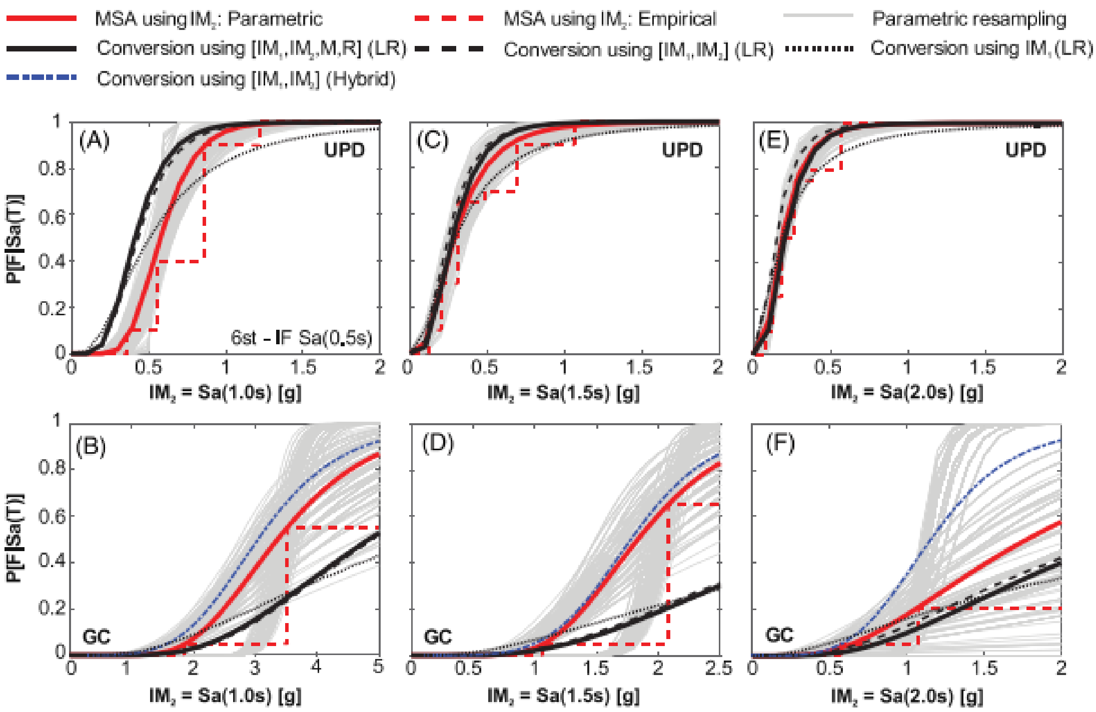

Figure 17. Comparison of converted and reference fragility curves to spectral acceleration at a larger period (from Sa(0.5s) to Sa(T>0.5 s)) (Suzuki and Iervolino, 2020)

3.5 INFRASTRUCTURE LOSS ESTIMATION METHODS

3.5.1 FRAGILITY FUNCTIONS FOR TYPICAL BRIDGE STRUCTURES

The numerous studies in literature focus on the main issues in vulnerability of bridges structures, such as classification of bridges, methods for deriving fragility functions, selecting proper intensity measures, damage states and damage measures in order to estimate the seismic loss accurately. The methodology for the production of fragility curves is a crucial step of this complex process. There are various methods to develop fragility curves for bridge structures such as empirical, expert opinion, numerical (nonlinear static and dynamic analyses), and parameterised methods. Empirical and opinion-based curves are the first introduced and limited ones in the literature, while most previous studies use numerical analysis The advantage of implementing the numerical (analytical) method is that it can take into account all uncertainties successfully. However, the analysis is time-consuming, very sensitive to modeling and computational inefficient. The aformentioned methods and the other issues as constracting the fragility curves are summarized in the following and detailed literature review is presented in **Error! Unknown switch argument.**.

Empirical Methods

Empirical fragility curves for bridges are rather limited in comparison to those for buildings. Basöz et al. (1999) used damage data from the 1994 Northridge earthquake to produce damage probabilities and fragility curves for as-built or retrofitted bridges with continuous or simply-supported deck. Shinozuka et al. (2000a) and Tanaka et al. (2000) proposed fragility curves based on the damage observed on the bridges of the Hanshin Expressway and those managed by the Japan Highway Public Corporation (Yamazaki et al. 2000) after the 1995 Kobe earthquake. Elnashai et al. (2004) derived fragility curves using damage data from the Northridge and Kobe earthqaukes.

Expert Opinion

Fragility assessment based on expert opinion was developed for bridges and other facilities in California by ATC (1985). Earthquake engineering experts were asked to suggest estimates of the probability of a bridge being in one of seven damage states and of the expected repair time. They were also asked to rate their experience to reduce the uncertainty due to the subjective nature of the estimates. The results were first presented in the form of damage probabilities, later converted to vulnerability functions and restoration curves. Vulnerability functions describe the expected damage of bridges as a function of the Modified Mercalli Intensity, whereas restoration curves define the fraction of pre-earthquake capacity or usability as function of time after the earthquake.

Numerical Methods: Nonlinear Static Analysis

This method was first presented in FEMA 273 where the ‘‘Coefficient Method” has been used to define the target displacement and then it was updated in FEMA 356. The non-linear static analysis refers to the pushover analysis that will result in a well-known curve identified as ‘‘Capacity Curve”. The ultimate goal of this approach is to obtain the structure’s dynamic properties such as stiffness, strength, and ductility under seismic loading.

The capacity spectrum method (CSM) makes use of an equivalent single-degree-of-freedom (SDOF) system which is characterised by the capacity curve of the full multi-degree-of-freedom (MDOF) structure obtained by nonlinear static (pushover) analysis. The force-displacement capacity curve is converted to the acceleration-displacement format (Fajfar and Gašperšič 1996). Damage states are defined on the capacity curve and the corresponding median value of the intensity measure is either read directly for spectral displacement, or it is adopted from the damped acceleration-displacement response spectrum that intersects the capacity curve at that point for PGA. The damping ratio of the spectrum should match the displacement of the SDOF system at each performance level.

The primary application of the CSM for the development of bridge fragility curves was in HAZUS and its updates (FEMA 2010), where a uniform value of standard deviation β = 0.6 was adopted on the basis of observed data. HAZUS also provides the median values of fragility curves for reference bridges together with modification factors that account for the skew, period and arch action of the deck of specific bridges. The fragility curves of HAZUS were adapted by Azevedo et al. (2010) for the bridges in the Lisbon area, based on the requirements of the applicable seismic design code for the performance objectives and the material properties.

Moschonas et al. (2009) used the CSM for the development of fragility curves for modern highway bridges in Greece. The analysis was performed for the earthquake acting separately in the longitudinal and the transverse direction of the bridge and considering the closure of the gap between the deck and the abutments. The pushover curve of each bridge was estimated by means of pushover analysis. A default value for the lognormal standard deviation β = 0.6 was used throughout. For existing multi-span simply-supported highway bridges in Italy, Cardone et al. (2011) performed adaptive pushover analysis, where the modal properties at each step were used to estimate the shape of the displacement increment vector, as well as for the conversion of the capacity curve to the acceleration displacement response spectrum format. Again, a uniform value, β = 0.6, was used for the standard deviation.

Numerical Methods: Nonlinear Dynamic Analysis

Nonlinear time-history analysis is more time-consuming than the CSM but makes it possible to account for the variability of the ground motion by running analyses for a set of recorded or artificial ground motion data. The analysis is normally performed for a complete three-dimensional (3D) model of the bridge that properly accounts for the nonlinear behaviour of all key components such as the piers, bearings, joints, soil, etc. According to literature review, refinements in modeling of the soil body reveals more accurate results than modeling superstructure. However, the computational time increases due to detailed soil body model.

In order to reduce the computation time, Marano et al. (2006) performed pushover analysis of the complete bridge in order to define the properties of an equivalent SDOF system that was subsequently used in the time-history analyses. Shinozuka et al. (2000b) compared fragility curves for a four-span regular bridge obtained with the CSM and nonlinear dynamic analysis. The fragility curves were in excellent agreement for minor damage state whereas for the high PGA, the capacity spectrum method underestimated the response parameters by almost 50 % and the agreement was not as good for the major damage state.

Moschonas et al. (2009) obtained similar fragility curves for a three-span regular bridge with monolithic deck-pier connection that were produced based on nonlinear dynamic analysis and on the CSM. Banerjee and Shinozuka (2008) compared empirical fragility curves and numerical ones that were based on nonlinear dynamic analyses of three reinforced concrete (RC) bridges with different configurations of geometry, using a set of 60 artificial accelerograms.

It's been found that the analytical curves were more conservative than the empirical ones. An iterative optimisation procedure was then developed so that the limit values of damage measures were calibrated and a better agreement was obtained between empirical and numerical fragility curves.

Parameterized Fragility Curves

It is well-known that bridges with different structural configuration will have different fragility curves (e.g. Zhang et al. 2008). On the other hand, bridges belonging to the same class may have different fragilities because of their specific geometric characteristics (e.g. Moschonas et al. 2009). To avoid time-consuming calculations for individual bridges, parameterized fragility curves were proposed in literature.

Karim and Yamazaki (2003) constructed fragility curves for idealised bridges with fixed or sliding bearings based on nonlinear dynamic analyses of 30 bridge models for a suite of 250 accelerograms and found a strong correlation between the mean and standard deviation of the fragility curves.

Mackie and Stojadinovič (2007) derived fragility curves based on time-history analysis of 22 two-span bridges with monolithic deck-pier connection, considering different values of the span length, pier height, material properties, amount of longitudinal and transverse reinforcement and soil stiffness. Instead of using the same damage fragility curve for all within a class of bridges in the bridge inventory, such as those provided by HAZUS, the proposed damage fragility curves account for the structural characteristics of each particular bridge through the use of the bridge force reduction factor parameter.

Regarding to intensity measures, the criteria for the selection of the most appropriate one is mainly the correlation with damage and the effort required for its computation. In addition, there is a concern about the uncertainty related to the modelling, to the seismic action, the geometry and the material properties. Refinements in vulnerability analysis of bridges relate to the effects of skew and cumulative seismic damage after the main shock and provoking a reduction of their structural capacity. As regards the seismic action, the effect of spatial variability is included in the analysis and the hazard is related not only to ground shaking but also to ground failure such as liquefaction. Also, according to significant number of studies, fragility curves should be developed for the whole lifetime of a bridge in order to account for corrosion and flood scour.

Intensity Measures

Peak ground acceleration (PGA) is the most common seismic intensity measure in the literature because it has been demonstrated to have high correlation with damage. Other intensity measures used in existing fragility studies for bridges are the peak ground velocity (PGV) and the acceleration or velocity spectrum intensity (SI).

In a comprehensive study, Avşar and Yakut (2010) investigated the correlation between different intensity measures and damage of ordinary modern highway bridges in Turkey. Nonlinear dynamic analysis was performed for 52 prototype bridges (constructed after the 1990s in different parts of Turkey) with 25 recorded accelerograms and accounted for the variability of geometry and material parameters. The damage parameters, in terms of deck displacement and column curvature, was correlated to PGA, PGV, the ratio PGA/PGV and also to acceleration spectrum intensity (ASI). ASI was defined as the area under the 5 %-damped elastic response spectrum within the periods T_i and T_f. The values T_i = 0.40 s and T_f = 1.10 s were selected in order to reflect the period range for the ordinary highway bridges in Turkey. Both damage measures had higher coefficients of determination with ASI and PGV than with PGA and PGA/PGV.

Damage States, Damage Measures, Functionality

Fragility curves of bridges involve several damage states. The most studies in the literature adapted of five damage states, namely: no damage, slight, moderate, extensive or complete damage. Although different wording is used, the definitions originate from the first version of HAZUS. Intermediate, i.e. moderate or extensive, damage states are not examined in some of the studies available in literature. Moreover, as the shortcomings of several studies consider only collapse or loss of load-bearing capacity.

Damage measures refer to specific components of the bridge, in particular piers, cap beams, bearings, abutments, deck and gaps. Drift ratio, curvature, rotation and displacement are the pier response quantities normally used as damage measures. The values of drift limits are taken from literature or from experimental data (Li J et al. 2012). As regards curvature ductility, similar values are adopted. However, the higher values used by Nielson and DesRoches (2007) relate to steel-jacketed columns. Divergence in the threshold values for the rotation of the pier end is due to the fact that they originate from experimental data in Qi'ang et al. (2012) and Saxena et al. (2000), while they have been calculated for a specific bridge by Yi et al. (2007).

Bearings are often the critical elements in bridges and are therefore included in the model used for the development of fragility curves. There is no consensus on the limit states; the choice depends on the available data from manufacturers, guidance from design codes and engineering judgement, resulting in different values for the shear deformation of elastomeric bearings and the two extreme damage states. Divergence is also observed for fixed and expansion bearings when the limit values are based on experimental data only (Choi et al. 2004) or a combination with expert opinion (Ghosh and Padgett 2010). The friction force, horizontal strength and the displacement that lead to unseating of the deck have also been used as damage measures for the bearings. Other damage measures used in previous studies include concrete and steel strain at the component level, as well as the Park and Ang (1985) Damage Index and the bridge displacement ductility, calculated from the capacity curve.

Damage states may be further associated to the functionality of the bridge. Functionality levels were defined by the loss of vertical and lateral load-capacity. Among the approaches examined for relating the vertical load-carrying capacity and the intensity measure, detailed analysis of the bridge to establish a relation between the residual horizontal capacity and the maximum horizontal displacement showed the lowest model error. Monti and Nisticò (2002) proposed three levels of functionality: full for light damage, emergency traffic for high damage, and closure for collapse. Lehman et al. (2004) also defined three service levels, each associated to a description of physical damage and the required repair. Mackie and

Stojadinovič (2006) identified five levels of traffic capacity, ranging from immediate access to closure, related to the remaining traffic capacity of the bridge.

Padgett and DesRoches (2007a) used data collected from experts to relate damage states and bridge functionality. Results were presented as functionality probabilities that provide the probability that the bridge functionality will be 0,50 or 100 % in a number of days after an earthquake that causes a certain level of damage on abutments, bearings, columns and footings. Based on HAZUS (FEMA 2010) provided restoration curves for highway bridges. They give the percentage of functionality of a bridge that suffered a given damage level as a function of time following the seismic event.

The uncertainties regarding the seismic action, geometry, material properties and modelling are also mentioned in the recent existing studies as well as the special issues refer to damaged and retrofitted bridges, the effects of corrosion, skew angle, soil-structure interaction, and liquefaction. For instance, regarding to skew angle, Avşar et al. (2011) confirmed the increased mean value and the negligible influence on the fragility curves for ordinary highway bridges with the deck supported on bearings and a skew angle higher than 30^{o} . Skew did not change the fragility curves for the lower damage level, corresponding to yielding.

Table 14 Literature review; references, bridge types, methodology, intensity measure, damage parameters, damage states (reproduced and updated from Tsionis and Fardis 2014 in SYNER-G project)

Reference	**Bridge type**	**Methodology**	**Intensity measure**	**Damage parameter/index**	**Damage state**
Agrawal et al. (2012)	Multi-span continuous steel	Nonlinear dynamic	PGA	Curvature demand	Slight, moderate, extensive, complete
Akbari et al. (2012)	RC Continuous span bridges (irregular configuration)	Nonlinear dynamic	PGA	Curvature demand	none, minor, moderate, major, collapse
Amirihormozaki (2015)	Horizontally curved steel	Nonlinear dynamic	PGA	Curvature, displacement	Slight, Moderate, extensive,

	bridge, I-girder	and static			collapse
ATC (1985)	Continuous, simply-supported; monolithic, bearings	Expert opinion	Mercalli Intensity	Observed Damage	Seven damage states considered.
Avşar et al. (2011)	Continuous; elastomeric bearings	Nonlinear dynamic	PGA, PGV, ASI	Curvature	Slight and complete
Aygün et al. (2011)	Continuous; fixed bearings	Nonlinear dynamic	PGA	Displacement, bearing deformation	Slight, moderate, extensive, collapse
Azevedo et al (2010)	-	Adapted from FEMA (2010)	Sa	Observed Damage	none, slight, moderate, extensive, complete
Banerjee and Shinozuka (2008)	Continuous w/joint(s); monolithic	Nonlinear dynamic	PGA	Rotational ductility demand	none, slight, moderate, extensive, complete
Basöz et al. (1999)	Continuous, simply-sup., retrofitted	Empirical	PGA	Observed Damage	none, minor, moderate, major, collapse
Billah (2020)	Multi-span continuous concrete girder		PGA	Column displacement ductility, deformation of elastomeric bearing, abutment wing wall, back wall	Slight, moderate, extensive, complete
Cardone et al. (2011)	Simply-sup.; fixed,	Nonlinear static	PGA	Curvature	Slight, moderate and

	sliding, elastomeric bearings				complete
Ceresa et al. (2012)	Continuous, simply-sup.; elastomeric bearings	Nonlinear dynamic	PGA	Rotational ductility, demand, shear	None, slight, moderate, extensive and complete
Chen et al (2019)	Tall-pier highway bridges	Nonlinear dynamic	PGV	Shear deformation (rubber bearings), curvature ductility (pier columns)	Slight, moderate, extensive, complete
Choe et al. (2009)	Continuous; monolithic; new code	Nonlinear static	Sa	Shear demand	-
Choi et al. (2004)	Cont., simply-sup.; fixed, sliding, elast. bearings	Nonlinear dynamic	PGA	Column curvature ductility; deformation	none, minor, moderate, major, collapse
De Felice and Giannini (2010)	Simply-supported; bearings; old code	Nonlinear dynamic	Sa	Curvature, shear capacity	collapse
Elnashai et al. (2004)	-	Empirical	PGA	Displacement	none, minor, moderate, major, collapse
Elnashai et al. (2004)	Continuous; monolithic	Nonlinear dynamic	PGA	Displacement	none, minor, moderate, major, collapse

FEMA (2010)	Cont., simply-sup.; fixed, sliding, elast. Bearings	Nonlinear static	Sa	Observed data	none, slight, moderate, extensive, complete
Franchin et al. (2006)	Simply-supported	Nonlinear dynamic	Sa	Displacement ductility demand at each pier	Collapse
Gardoni et al. (2003)	Continuous w/ joint(s)	Nonlinear static	Sa	Drift Demand; Normalised shear demand	-
Gardoni and Rosowsky (2009)	Continuous ; monolithic	Nonlinear static	Sa	Deformation demand; shear demand	-
Jeong and Elnashai (2007)	Continuous w/ or w/o joints, simply-supported	Nonlinear dynamic	PGA	Curvature	Slight and complete
Karim and Yamazaki (2001)	Bridge piers (only component -based)	Nonlinear dynamic	PGA, PGV	Park and Ang Damage Index	None, slight, moderate, extensive, complete
Karim and Yamazaki (2001)	Continuous ; monolithic , elastomeric bearings	Nonlinear dynamic	PGA, PGV, SI	Park and Ang Damage Index	None, slight, moderate, extensive and complete).
Karim and Yamazaki (2003)	Continuous ; monolithic	Nonlinear dynamic	PGA, PGV, SI	Displacement and ultimate ductility	slight, moderate, extensive and complete

Kibboua et al. (2011)	Bridge piers (only component -based)	Nonlinear dynamic	PGA	Displacement and ultimate ductility	none, slight, moderate, extensive, complete
Kim and Shinozuka (2004)	Continuous w/or w/o joints; monolithic , retrofitted	Nonlinear dynamic	PGA	Ductility Demand	none, slight, moderate, extensive, complete
Kurian et al. (2006)	Simply-supported; bearings	Nonlinear dynamic	PGA	Ultimate displacement ductility	none, minor, moderate, extensive, complete
Kwon and Elnashai (2009)	Continuous ; fixed and expansion bearings	Nonlinear dynamic	PGA	Displacement	Serviceability, damage control, collapse prevention
Kwon et al. (2009)	Continuous ; monolithic	Nonlinear dynamic	PGA	foundation displacement, rotation and pile top displacement	No damage, repairable, irrepairable, collapse
Li et al. (2012)	Continuous ; monolithic	Nonlinear dynamic	PGA	Drift ratio	None, slight, moderate, extensive, complete
Liu et al (2020)	Continuous	Nonlinear dynamic	PGA, Sa	Displacement ductility (piers)	No damage, slight, moderate, extensive, complete
Lupoi et al. (2004)	Continuous	Nonlinear dynamic	PGA	Curvature demand	-

Lupoi et al. (2005)	Continuous	Nonlinear dynamic	PGA	Curvature Ductility	-
Mackie and Stojadinovic (2004)	Continuous	Nonlinear dynamic	Sa	Drift ratio	Slight, extensive and complete
Mackie and Stojadinovic´ (2007)	Continuous; monolithic	Nonlinear dynamic	Sa	The drift ratio of the bridge column	Concrete cover spalling, longitudinal bar buckling, and column failure
Marano et al. (2006)	Continuous	Nonlinear dynamic	PGA	Drift ratio	none, minor, moderate, extensive, complete).
Monti and Nistico` (2002)	Simply-supported	Nonlinear static	PGA	Displacement (piers)	Slight, extensive and complete
Moschonas et al. (2009)	Continuous; monolithic, elastomeric bearings;	Nonlinear static	PGA	Bridge-deck displacement; bearing shear deformation	none, minor, moderate, extensive, complete
Nateghi and Shahsavar (2004)	Continuous; elastomeric bearings	Nonlinear dynamic	PGA, PGV	Inelastic Displacement Ductility Ratio; Park and Ang damage index	none, slight, moderate, extensive and complete
Nielson and DesRoches (2007)	Simply-sup.; elastomeric bearings and steel	Nonlinear dynamic	PGA	Column ductility	slight, moderate, extensive and complete

	dowels;				
Noori et al. (2019)	Simply-supported reinforced concrete girder bridges with skewed superstructure	Nonlinear dynamic	PGV	Column curvature ductility, shear key and bearing deformation, abutment unseating	Aesthetic damage, minor and major functional damage
Padgett and DesRoches (2009)	Simply sup.; fixed, movable, elastomeric bearings; retrofitted	Nonlinear dynamic	PGA	Column curvature,ductility; bearing deformation; abutment deformation	slight, moderate, extensive and complete
Ramadan (2020)	Continuous box girder bridge	Nonlinear dynamic	PGV	Deck Drift	Operational, Life Safety, Collapse
Park and Choi (2011)	Simply-supported; fixed, expansion bearings; no seismic design	Nonlinear dynamic	PGA, Sa	Displacement, curvature, shear, base shear	slight, moderate, extensive and complete
Prasad and Banerjee (2013)	Continuous; monolithic	Nonlinear dynamic	PGA	Displacement ductility	Minor, moderate, major, complete
Qi'ang et al. (2012)	Continuous; monolithic	Nonlinear dynamic	PGA	Rotational ductility, demand	none, slight, moderate, extensive, and complete
Saxena et	Continuous	Nonlinear	PGA	Rotational ductility	none, slight,

al. (2000)		dynamic		demand	moderate, extensive, and complete
Shinozuka et al. (2000a)	Continuous	Empirical	PGA	Observed damage	Minor, Moderate, Major
Shinozuka et al. (2000a)	Continuous	Nonlinear dynamic	PGA	Ductility demand	Minor, Moderate, Major
Shinozuka et al. (2000b)	Continuous	Nonlinear static	PGA	Rotational ductility demand	Slight and extensive
Shirazian et al. (2011)	Simply-supported; fixed bearings	Nonlinear dynamic	PGA	Column, Displacement ductility	Slight and complete
Soleimani (2020)	Single frame, two span, box-girder	Nonlinear dynamic	Sa	Displacement, Curvature ductility	Slight, moderate, extensive, complete
Soltanieh (2019)	RC Continuous span bridges (irregular configuration)	Nonlinear dynamic	PGV	Curvature ductility, Displacement, rotation	Minor, moderate, extensive, complete
Sullivan (2010)	Simply-supported; fixed, movable bearings;	Nonlinear dynamic	PGA	-	Slight, moderate, extensive, and complete
Tanaka et al. (2000)	-	Empirical	PGA	Observed Damage	Collapse and major
Yamazaki et al. (2000)	-	Empirical	PGA, PGV, JMAI	Damage Rank	none, slight, moderate, extensive, and

					complete
Y. Xie and R. DesRoches (2019)	Two-span RC box-girder bridge	Nonlinear dynamic	Sa	Displacement ductility, Passive displacement, Active displacement, Transverse abutment pile displacement, Translation, Displacement, Deck unseating displacement, Bearing deformation, Shear key displacement	None, slight, moderate, extensive and complete)
Yi et al. (2007)	Continuous	Nonlinear dynamic	Return period	Drift ratio	slight, moderate, extensive and complete
Zhang et al. (2008)	Cont., simply-sup., joint; monolithic, elast. bearings;	Static analysis	PGD	Section ductility, shear strain	slight, moderate, extensive and complete
Zhang et al. (2008)	Cont., simply-sup., joint; monolithic, elast. bearings;	Nonlinear dynamic	PGA	Section ductility, shear strain	slight, moderate, extensive and complete
Zhong et al. (2012)	Continuous; monolithic	Nonlinear static	Sa	Deformation demand; shear demand	Only one damage state is considered (failure)

3.5.2 FRAGILITY FUNCTIONS FOR BURRIED PIPELINES

Fragility Functions

From last few years, it has been seen that for post-earthquake analysis, empirical based fragility relations are developed by many researchers. Fragility is a conditional probability state of a system or its component to reach or exceed the limit damage states at a provided damage measuring scale.

$$Fragility = P\,[D\ \geq C\,|IM]$$

P, D, C, and IM represents conditional probability, seismic demand, capacity of a system or its component and intensity measuring scale. Many relations are based on repairs rate (RR) i.e. leaks or breaks per unit length of pipelines and intensity of earthquake measure. American Lifelines Alliance (ALA) presented a relation for buried pipelines as,

$$RR = a.\ IM^{b}$$

a and b parameters are found by regression analysis of post-earthquake. Later, Gehl et al. presented a Poisson Distribution formula for estimation of probability of n damages as,

$$P\,(N = n) = \frac{(RR \times L)^{n}}{n!} \times e^{-RR \times L}$$

L is the total length of pipelines under consideration. Pipe under consideration may fail due to any damage to its length and probability of failure may be evaluated as,

$$P_f = 1 - P(N = 0) = 1 - \ e^{-RR \times L}$$

Most commonly used seismic intensity parameters are peak ground acceleration (PGA), modified mercalli scale (MMI), peak ground velocity (PGV), peak ground displacement (PGD), ground strain (ε_g) and composite parameter developed by Pineda Pornas and Ordaz as PGV^2/PGA. Lanzano et al. presented a pie chart for intensity parameters used by various researchers. Raja et al. explained that almost 80% leaks and 20% breaks in BCPs are due to TWP hazards and 80% breaks and 20% leaks are due to PGD hazards.

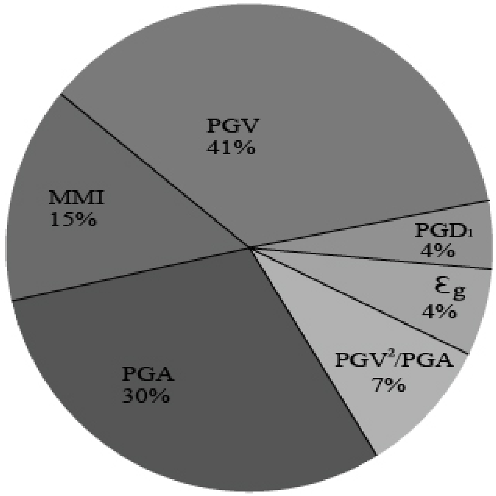

Figure 18 Percentage of various seismic intensity parameters used for development of fragility relationships.

Fragility equations developed by various researchers are enlisted in **Error! Unknown switch argument.**.

Table 15 Fragility equations developed by various researchers

Fragility relation	Researchers	Year
$RR = 10^{b+6.39\log PGA}$	Katayama et al.	1975
$RR = 1.698 \times 10^{-16} \times PGA^{6.06}$	R. Isoyama and T. Katayama	1982
$RR = 0.0001PGV^{2.25}$	O'Rourke and G. Ayala	1993
$RR = K_1\ 0.0001658PGV^{1.98}$	J. Eidinger et al.	1995
$RR = 10^{1.25\times\log PGA-0.63}$	O'Rourke et al.	1998
$RR = (V_{max}/266)^{1.22}$	O'Rourke and S.S. Jeon	1999
$RR = 3.11 \times 10^{-3}\ (PGV - 15)^{1.30}$	R. Isoyama et al.	2000
$RR = 0.00187PGV$	ALA 2001	2001
$RR = \begin{cases} 0 & \text{If } 0 < PGV < 5.35 \\ 0.1172 + 0.7281\varphi\,(PGV{:}\,51.7964, 19.7811) & \text{If } 5.35 \le PGV < 95 \\ 0.00137PGV + 0.70458 & \text{If } PGV \ge 95 \end{cases}$ Where, $\varphi\,(PGV;\mu,\sigma) = \int_{-\infty}^{PGV} \frac{1}{\sqrt{2\pi\sigma}}\, e^{-\left(\frac{1}{2}\right)\left[\frac{v-\mu}{\sigma}\right]^2} dv$	P. Porras and M. Ordaz	2003
$RR = 0.034PGV^{0.92}$	O'Rourke and E. Deyoe	2004
$RR = 0.035PGV^{0.92}$	O'Rourke and E. Deyoe	2004
$RR = 513{\epsilon_g}^{0.89}$	O'Rourke and E. Deyoe	2004
$RR = 724{\epsilon_g}^{0.92}$	O'Rourke and E. Deyoe	2004
$RR = 1905{\epsilon_g}^{1.12}$	M. O'Rourke	2009
$RR = 10^{-4.52}\ GMPGV^{2.38}$	O'Rourke et al.	2014
$RR = 0.0839\epsilon_g + 0.41$	O'Rourke et al.	2014
$RR = 2951{\epsilon_g}^{1.16}$	O'Rourke, E. Filipov. E. Uckan	2015

A comparison of fragility curves (RR in kms vs. PGV in cm/sec) developed by various researchers have been made. It can be observed that results of O'Rourke and Ayala (1993) and O. Rourke and Deyoe (2004) R Wave, are overestimated. Edinger et al,. 1995 curve have limited range as it is applicable only for small diameter segmented pipes. O'Rourke and Jeon (1999) curve is based only on one earthquake i.e. Northridge earthquake. Isoyama et al.,2000 used 6 earthquakes records but the curve is only valid for specific region of Japan as it is based on data collected from 1995 Kobe, Japan Earthquake. ALA 2001 have exceptionally low values as compared to other researchers and does not include the pipe and soil properties. Fragility relations developed by O'Rourke and Deyoe (2004) for R-wave (surface waves) and S-wave (body waves) are based on damage data from five earthquakes. O'Rourke et al., 2014 developed a new fragility relation for WP hazards of buried segmented pipes.

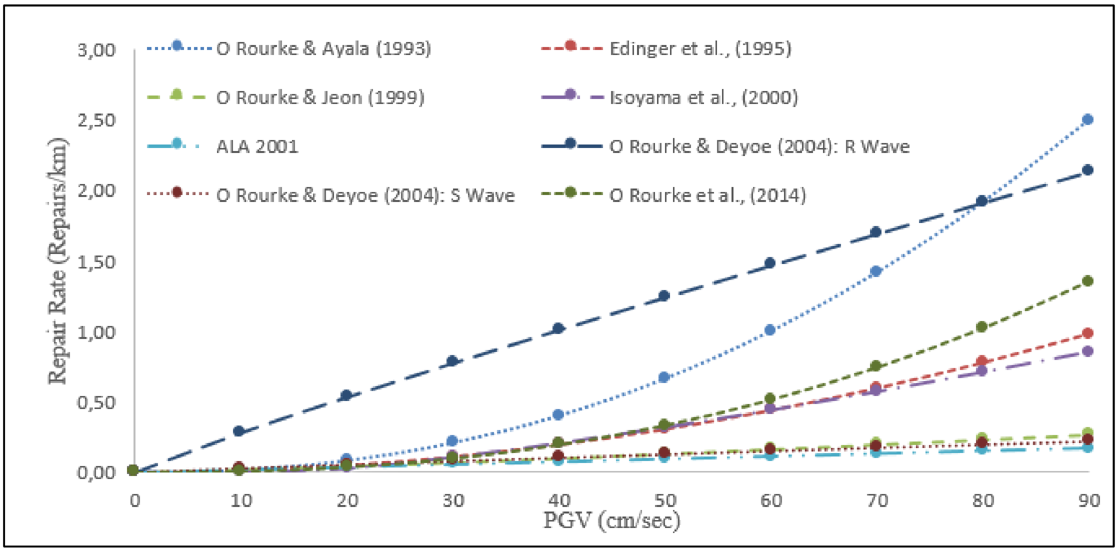

Figure 19 Comparison of fragility curves developed by various researchers (RR against PGV)

It is noted that most of fragility curves are developed only for segmented pipes. Similarly, most of the available curves have considered wave propagation hazards. Limited curves have been observed related to PGD hazards. It is also noticed that most of equation are developed on empirical basis.

ALA equation for PGV is updated by adding a multiplier factor that adds the properties of pipe material, their connection types, soil conditions and various diameters of buried pipes. Modification factor values are given in below **Error! Unknown switch argument.**.

$$RR = K1 \times 0.00187\ PGV$$

Table 16 Modification factor values for different soil-pipe conditions

Identity	Material	Connection	Soil condition	Diameter	Multiplier (K_1)
A1	CI	C	All soils	Small	1.00
A2	CI	C	Corrosive soils	Small	1.40
A3	CI	C	Non-Corrosive soils	Small	0.70
A4	CI	RG	All soils	Small	0.80
A5	WS	LAW	All soils	Small	0.60
A6	WS	LAW	Corrosive soils	Small	0.90
A7	WS	LAW	Non-Corrosive soils	Small	0.30
A8	WS	LAW	All soils	Large	0.15
A9	WS	RG	All soils	Small	0.70
A10	WS	S_C	All soils	Small	1.30
A11	WS	R_V	All soils	Small	1.30
A12	AC	RG	All soils	Small	0.50
A13	AC	C	All soils	Small	1.00
A14	CS	LAW	All soils	Large	0.70
A15	CS	C	All soils	Large	1.00
A16	CS	RG	All soils	Large	0.80
A17	PVC	RG	All soils	Small	0.50
A18	DI	RG	All soils	Small	0.50

CI = Cast Iron, WS= welded steel, AC= Asbestos cement, CS= Concrete with cylinder, PVC= Polyvinyl chloride, DI= Ductile iron, C= Cement, RG= Rubber gasketed, S_c=Screwed, R_v= Riveted, LAW= Lap arc welded, Small diameter= 0.1-0.3m, Large = 0.4m or more

Below figure presents the comparison of PGV vs. their repair rates for different categories of pipes based on modification factor K_1.

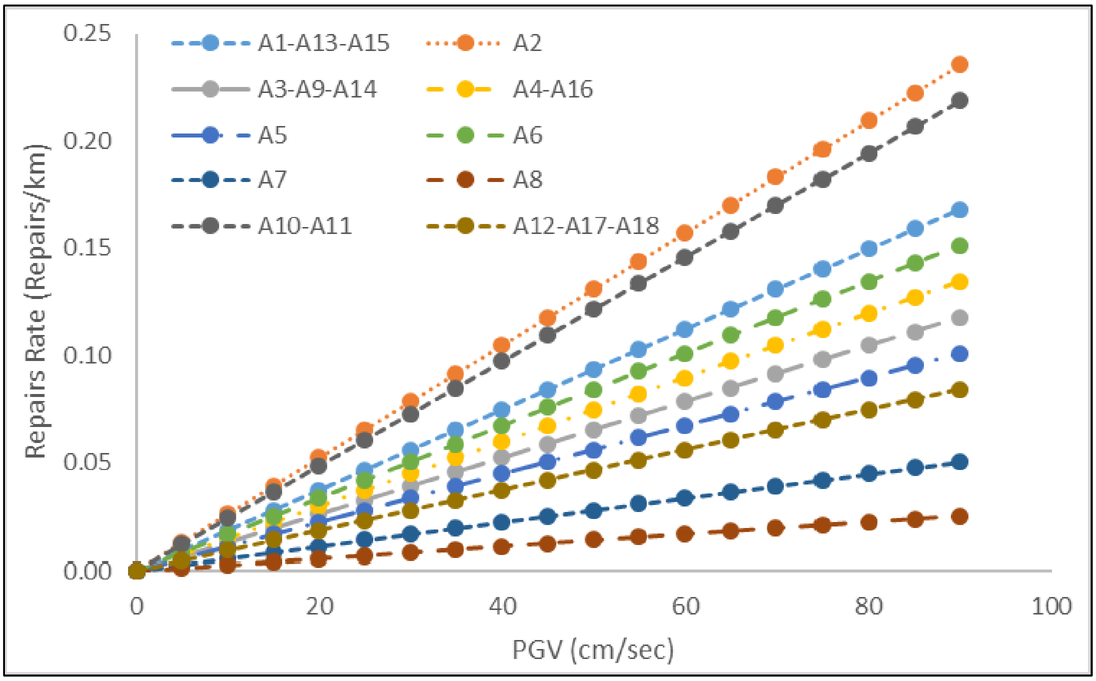

Figure 20 Comparison of repairs rate vs. PGV based on K1

From above graph, it is observed that geometric, physical, and mechanical properties of both pipelines and soil can influence their fragility. Cast iron pipes of small diameters with cement- based connection perform poorly under corrosive soil condition than all other combinations. Similarly, welded steel pipes of small diameters with screwed and riveted connection also perform poorly in all soil conditions. However, welded steel pipes of large diameter with lap arc welded connection perform very well among all other combination.

Table 17 Damage states for pipelines

State	Damage	Patterns
DS0	Slight	No damage; pipe buckling without losses; damage to the supports of aboveground pipelines without damage to the pipeline.
DS1	Significant	Pipe buckling with material losses; longitudinal and circumferential cracks; compression joint break.
DS2	Severe	Tension cracks for continuous pipelines; joint loosening in the segmented pipelines.

Fragility functions are convoluted with the hazard to obtain the risk of the system. In particular, for each scenario simulation, i.e., for each PGA and PGV simulated in the hazard module for the specific pipeline segment, it is possible to calculate the probability of reaching DS0, DS1, and DS2 for both strong ground shaking (SGS) and ground failure GF. The simulations provide the frequency of damage for each segment of pipeline, and the modal value among all the simulations identifies the expected DS for the specific segment, resulting in a map of the expected damage states on the infrastructure that can be used as tool to prioritize the inspections in the aftermath of an earthquake.

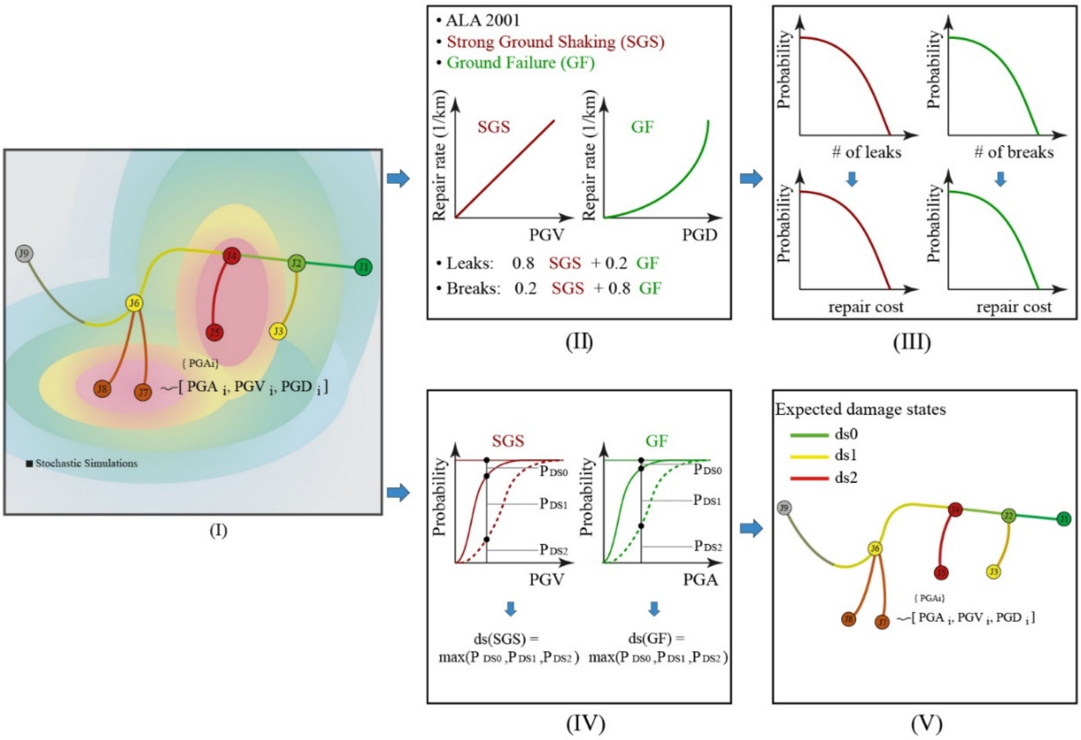

Figure 21 Scenario-based seismic risk assessment in terms of loss curves and damage maps: (I) hazard simulation in terms of PGA, PGV, and PGD; (II) vulnerability functions; (III) loss curves; (IV) fragility functions; and (V) damage maps.

3.6 SOCIO-ECONOMIC CONSEQUENCE ESTIMATION

For computing casualty estimates, occupancy criteria are needed, especially if building damage estimates have been computed. These criteria can refer to use (residential, etc.) and sometimes occupancy rate (day/night).

The most common output of seismic risk assessment and loss estimation scenarios in urban areas is the assignment of the buildings in appropriate damage states (the ones adopted by the fragility curves) that can sometimes correspond to post-earthquake tagging (e.g. Kappos et al. 2008, 2010). It should be noted though that the tagging scheme is not common in all countries (Karakostas et al., 2012). When the fragility curves' damage states are associated with economic loss (i.e. cost of repair / cost of reconstruction, Kappos & Panagopoulos, 2010, Martins & Silva, 2020), the output can be presented in monetary terms, as well.

Further extensions of the seismic risk scenario results can refer to socio-economic consequences such as the restoration time required for the buildings to be fully operational again. The most common way to plot restoration curves is by having as abscissa the restoration time and as ordinate the percentage of restoration. The information that the conventional restoration curve gives is the time needed for restoring a certain percentage of damage of a building if it has been found in a particular damage level. Another way to construct restoration curves (which we call here as post-earthquake restoration curves) is having as abscissa a seismic variable (peak ground acceleration, intensity etc.) and as ordinate the time needed for an actual percentage to be restored. Restoration curves have been proposed by Kappos et al. (2009, 2010) for the Grevena (Greece) and Düzce (Turkey) scenarios within the framework of the SRM-DGC project (**Error! Unknown switch argument.**). A more recent approach has been developed by UCLA (Burton et al., 2015) and integrated it into the QGIS framework as part of the OpenQuake IRMT plugin (Tormane 2019, **Error! Unknown switch argument.**).

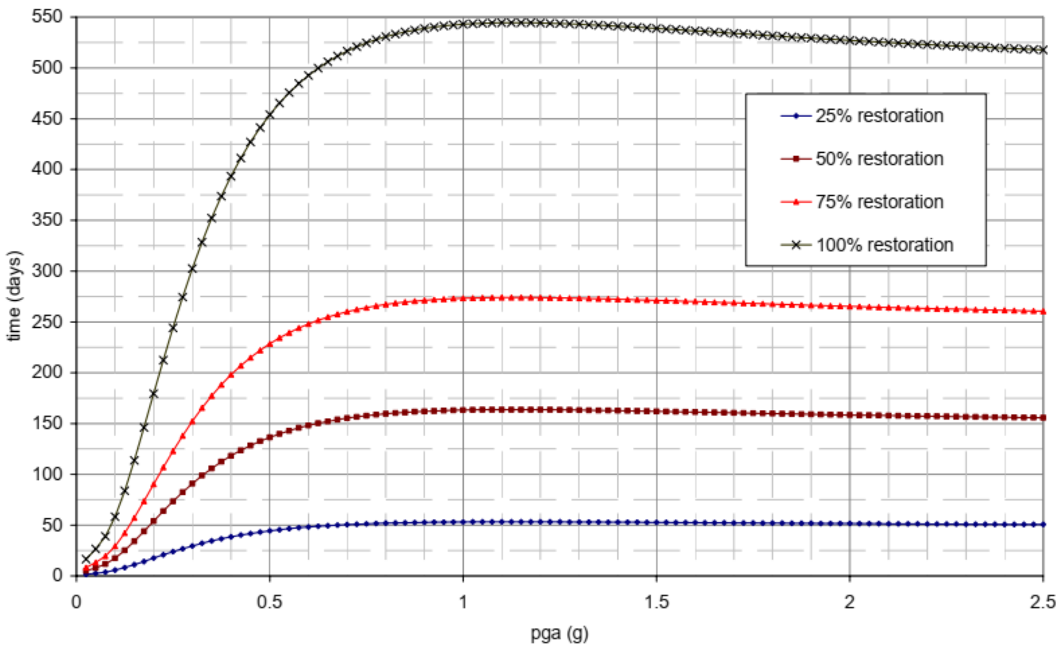

Figure 22. Post-earthquake restoration curves for various restoration levels for moment frame reinforced concrete buildings designed according to the old Greek codes (Kappos et al., 2009)

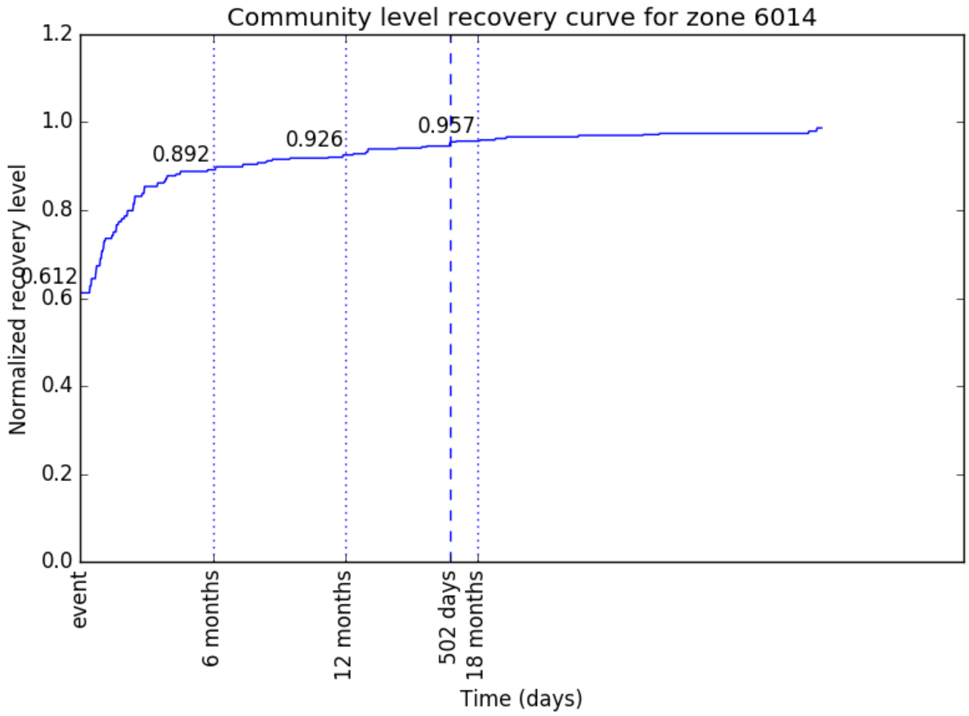

Figure 23. The community-level recovery function for one of the zones under analysis, showing how the normalized recovery level evolves with time after the earthquake (OpenQuake Integrated Risk Modelling Toolkit documentation)

Additional results obtained implicitly from seismic risk scenarios can include the number of casualties (deaths or injuries) during an earthquake event, taking into account the occurrence time of the earthquake. An application of the model proposed by Coburn and Spence (2002) has been carried out in the city of Thessaloniki, within the framework of the RiskUE project (**Error! Unknown switch argument.**, Pitilakis et al., 2006). Furthermore, collapse probabilities of buildings can be taken into account to test the transportation network under uncontrolled evacuation scenarios; a case study has been carried out at the MASSIVE research project (**Error! Unknown switch argument.**, Kontoes et al., 2012)

Table 18. Expected number of casualties in the Thessaloniki, RiskUE scenario (Pitilakis et al., 2006)

	Level I		Level II	
Time of earthquake	12:00	24:00	12:00	24:00
Dead or unsavable	246	360	216	291
Life threatening cases needing immediate medical attention	216	310	210	287
Injury requiring hospital treatment	261	371	241	323
Light injury not necessitating hospitalization	234	319	237	323

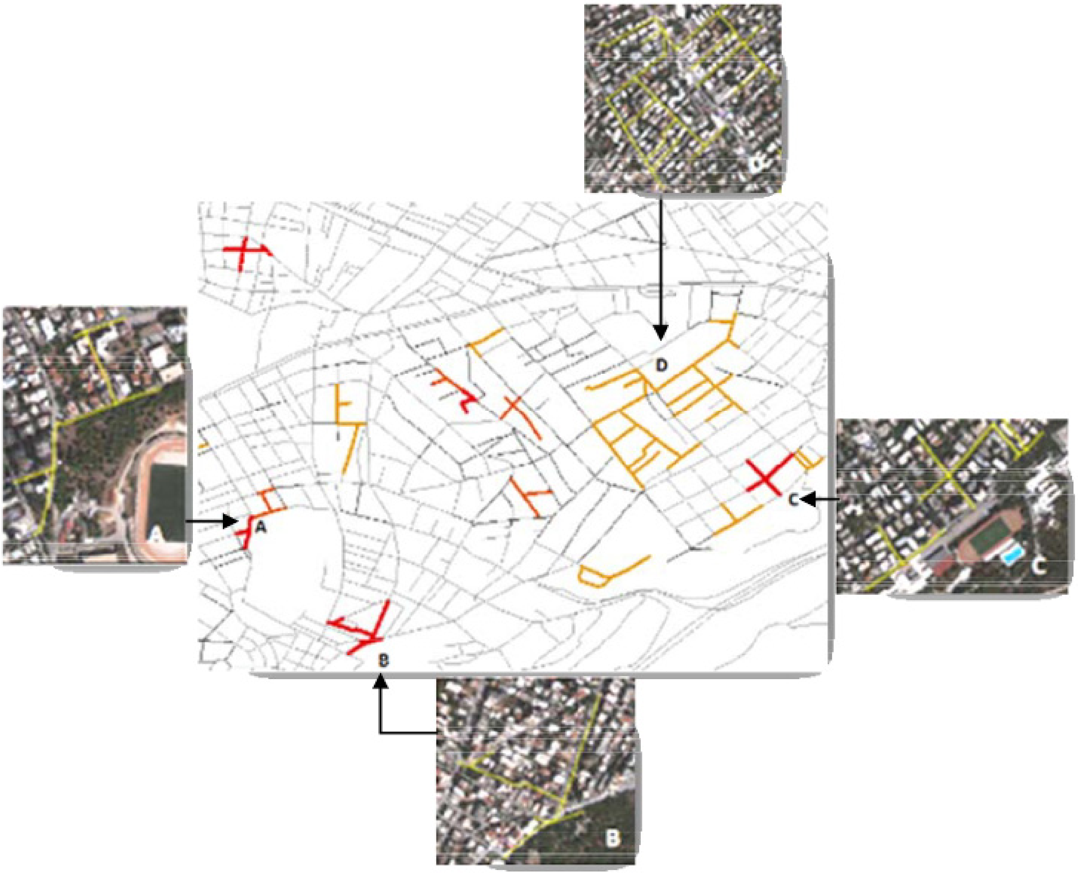

Figure 24. An evacuation vulnerability example for the municipality of Aghia Paraskevi (Athens, Greece). The color corresponds to the ratio of population evacuated to the BLD (bulk lane demand). Orange color represents a value of 300 persons per lane while red of more than 500 (Kontoes et al., 2012)

4 AVAILABLE REDA SOFTWARE

4.1 REDA SOFTWARE OR SYSTEMS

Table 19. Comparison of software capable of REDA implementation

REDA Software or system name and last version	Owner or operator	Licensing type / modifiable	Methods	Hazard input	Exposure and vulnerability input	Outputs and their format	Areas where it was applied and at which scale	Website and reference
AFAD-RED	AFAD (Turkey)	Not open source, written in VB-Net, C# environment and Arc-	Its methodology is mostly similar to HAZUS; it relies on fragility functions for various types of structures.	Preliminary results are automatically generated after receiving earthquake source parameters (epicenter, depth, magnitude) using attenuation relationships at	Loss estimations are computed using building fragility functions and consequence models. A HAZUS-based damage to Loss Model for development of Vulnerability Model can be used for determining loss		Turkey	

		Object		Vs30=760 m/s then applied soil amplification according to the Vs30 database. The output is as PGA, PGV and Intensity maps. Different GMPEs can be selected as a weighted average. Moderate results include Fault type, length and azimuth parameters into the calculation of expected hazard level. Advanced Results include recorded ground motion analysis where first calibration is applied to estimate the recorded ground motion at Vs30 = 760 m/s, then the calibration of ground motion parameter maps	ratio. It also provides a rapid and brief representation of seismic damage and loss evaluation for bridges. The vulnerability of transportation systems can be performed by choosing seven different intensity measure parameters: PGA, PGV, PGD, Sd, Intensity, S1 and SS, and defining a specific fragility functions.			

				is performed, and the soil amplification is applied to get the resulting final PGA, PGV, spectral acceleration (SA @ 0.2 sec, SA @ 1 sec), spectral displacement (SD) and Intensity maps.				
Armagedom	BRGM		Structural damage estimation: - Level 1: empirical method (namely LM1 in RISK-UE), derived from the work of Giovinazzi and Lagomarsino - - Level 2: analytical method similar to HAZUS 99 where each building class is assigned a capacity curve and the capacity	ShakeMap or scenarios	Building typology is inspired by the EMS-98 classes and refined with sub-typologies.	Collapsed dwellings and injuries	France (used in the SEISAID system)	Sedan et al (2013)

			spectrum method is used. Socio-economic losses: - consequence models					
CAPRA software collection	ERN-AL Consortium for the World Bank, the Inter-American Development Bank and the UN-ISDR, Universitad de los Andes (Colombia), CIMOC (Resear	Open Source Apache 2.0 License Programming language: Visual Basic, Requirements: MS .NET Framework	Probabilistic loss assessment algorithm: expected loss and variance calculation based on hazard analysis and vulnerability functions.	Probabilistic (using CAPRA-EQ or CRISIS2007, capable also of tsunami hazard assessment), accounting also for local site effects using SEISMIC HAZARD INTEGRATION or SOIL EFFECTS CAPRA modules	- *.shp files with certain formatting requirements for exposure; - estimation of direct losses by means of vulnerability functions (can be defined using FUNVUL Simplified, ERN Vulnerability or FUNVUL Components CAPRA modules); can be provided in *.ASCII or *.xml format.	- Expected Loss and variance calculation, Loss probability distribution function calculation for the event and Loss exceedance rate calculation using the loss PDF associated to each event and its occurrence frequency. Output format: - Text file *.res containing for each scenario analyzed the expected loss (EP), the variance of the loss	Central and South America and in some countries of Europe, Africa and Asia.	https://ecapra.org/

	ch Center on Materials and Civil Infrastructre)					(VarP), • Excepted annual damage per building, annual human loss per building in *.shp file and viewed as a map		
ELER (3.1, launched in 2010)	NERIES Project	Free download, written in Matlab but code not shared	- Level 0: similar to PAGER system of USGS - Level 1: intensity based empirical vulnerability relationship is employed to find number of damaged buildings. The casualty estimation is done through number of damaged buildings. - Level 2: spectral acceleration-displacement-based vulnerability assessment methodology is utilized for the building	- Level 0 and 1: intensity distribution (ShakeMap or included IPE) - Level 2: ShakeMaps or custom ShakeMap module with different GMPEs included	- Level 0: population distribution (Landscan data included); - Level 1: EMS98 Intensity based building vulnerability with uncertainties and casualty distribution; - Level 2: capacity and fragility functions, distribution of population per building typologies, replacement cost and loss ratio related to damage states and pipeline location and typologies	- Level 0: estimates the number and distribution of casualties; - Level 1: calculates number of damaged buildings and associated casualty; - Level 2: also calculates number of damaged buildings and associated casualty.	Turkey (especially Istanbul)	https://eqe.boun.edu.tr/en/eler-tool

			damage estimation. The casualty estimation is done through number of damaged buildings using HAZUS99 and HAZUS-MH (2003) methodologies					
HAZUS (4.2)	FEMA, USA	Free but runs with ESRI ArcGIS 10.5.1 +	Hazus is designed to support two general types of analysis (Basic and Advanced) split into three levels of data updates: - Levels 1: default hazard, inventory and damage information. The effects of possible liquefaction and landslide hazards are ignored. - Level 2: combination of local and default hazard, inventory and damage data. - Level 3: input	Probabilistic or deterministic (includes GMPEs mostly specific to US). Hazard module account for soil characteristics, including site classification according to the National Earthquake Hazard Reduction Program (NEHRP). Can also perform induced liquefaction, landslide and tsunami analysis (Potential Earthquake Hazards). For the	The Hazus Earthquake Model comes with a large library of baseline nationwide inventory data, which can be updated with local data to increase the accuracy of the model. For most elements, capacity and fragility functions are used, as well as consequence or vulnerability functions for loss estimation purposes. Hazus integrates local inventory data including essential	- Ground Motion Descriptions/Maps - Direct Physical Damage - General Building Stock: Structural and nonstructural damage state probabilities; cost of repair or replacement; Loss of contents; Business inventory loss; Relocation costs; Business income loss; Employee wage loss; Loss of rental income. - Direct Physical Damage - Essential facilities: Structural damage state probabilities by facility; Expected functionality	USA, Cairo (Egypt)	https://www.fema.gov/hazus-software

			detailed engineering data. For the evaluation of damage to buildings and essential facilities, a standardized response spectrum shape is used, relying on PGA and SA values, as well as capacity, fragility or vulnerability functions. All details can be found in the Hazus Earthquake Model Technical Manual.	analysis of building damage, three ground motion parameters are used: PGA, SA at 0.3 seconds, and SA at 1.0 second. PGV is used in the analysis of pipeline damage.	facilities, system, general building stock, user-defined facilities, or Advanced Engineering Building Model (AEBM) structures.	at Day 1, 3, 7, 14, 30 and 90 by facility. - High Potential Loss Facilities: Structural damage state probabilities and expected functionality for military facilities; - Direct Physical Damage – User-Defined Facilities - Direct Physical Damage – Advanced Engineering Building Model: Damage state probabilities; casualties; losses - Direct Physical Damage: For components of the 13 transportation and utility systems, damage state probabilities, cost of repair or replacement, and expected functionality for various times following earthquake by facility; For potable water, wastewater and natural gas pipeline		

						distribution systems, the estimated number of leaks and breaks; For potable water and electric power systems: estimate of service outages at Day 1, 3, 7, 30 and 90. - Induced Physical Damage - Inundated Areas, Fire Following Earthquake and Debris. - Social Losses: Number of displaced households per census tract; Number of people requiring temporary shelter per census tract. Casualties per census tract in four categories of severity based on three different times of day (2 am, 2 pm and 5 pm). Aggregate estimates of casualties by time of day, injury severity, and general occupancy class.		
MAEviz	MAE Center through the	Open source platform:	It implements Consequence-Based Risk Management (CRM) to estimate	MAEviz can take into account liquefaction hazard in	The MAEviz tool provides as default some inventories stored in tables and	Output table, maps of economics losses, social losses, fiscal impact.	Mid-America	http://mae.cee.illinois.edu/software/software_maeviz.ht

	Earthquake Engineering Research Centers Program of the National Science Foundation under NSF Award No. EEC-9701785.	Eclipse RCP Programming language: JAVA	the damage and the losses for buildings, bridges and lifeline (gas, water, electric facilities). For buildings, it estimates structural and nonstructural damage, economic losses and liquefaction damage. For bridges, it computes damage, loss of functionality and repair cost analysis. For lifelines it calculates the network damage and the repair rate analysis. Finally, it computes socio-economic losses such as shelter needs, fiscal and business interruption. The hazard used when evaluating these fragilities is obtained by	addition to ground shaking. The hazard is response spectral based and local site effects are taken into account. There are some default scenarios and probabilistic hazard maps in the catalog box however the user can upload their own hazard following a graphical interface. The user can also choose to create the scenario using an analysis. The user has to provide the spectrum type, the earthquake location, the coordinates of the region of interest and some advanced parameters such as the fault type, the dip angle,	shapefiles. The inventory buildings contain information about the construction type, number of storeys, occupancy level, year of construction and building area. The user can upload their own inventory in the 'catalog box' and also can upload data about bridges and lifelines. The vulnerability functions were derived by structural analysis which considering the aleatory structural features uncertainty and the excitation uncertainty. The fragility curves have been developed for construction typical of the Mid America region and provide the conditional probability of being in, or exceeding a particular damage state given by the	Detailed or summary report for structural damage		ml

			performing a transformation from elastic spectral acceleration to elastic spectral displacement without regard for inelasticity in building response. Based on analyzes for structural damage and optional nonstructural damage, MAEViz compute the direct economic losses. More additional economic and socioeconomic analyses are available: the building repair cost based on the structural damage and building type, the building retrofit cost estimation, the number of casualties and the fiscal impact.	etc.	seismic demand parameter. Three fragility curves are provided and four damage states are obtained by difference between adjacent curves.			
OpenQ	Global	Open	Can be used for	Classical PSHA	Inputs for the	- asset-specific loss	Worldwide,	https://www.g

uake (3.10)	Earthquake Model Foundation (GEM)	source	various types of analyses (providing logic tree support), combining input from the hazard module (or user provided), exposure and vulnerability input consisting mainly of fragility or vulnerability functions: - Scenario Damage Assessment - Scenario Risk Assessment - Classical Probabilistic Seismic Damage Analysis - Classical Probabilistic Seismic Risk Analysis - Stochastic Event Based Probabilistic Seismic Damage Analysis - Stochastic Event	(hazard curves, hazard maps, uniform hazard spectra, disaggregation), Event-based hazard (stochastic earthquake event sets and ground motion fields, hazard curves, hazard maps), Scenario hazard (single event - stochastically generated ground motion fields). 5 typologies for modeling seismic sources, 100+ GMPEs implemented and tested.	damage assessment step consist in exposure models (i.e., GEM building taxonomy) in terms of built areas or single assets. Fragility models are then applied in order to estimate damage distribution and consequence functions for loss estimation, or directly vulnerability functions.	exceedance curves, average annual loss, loss maps, building typology disaggregation - event loss tables, loss exceedance curves - asset specific and aggregated, average annual loss, loss maps, loss disaggregation - loss statistics, loss maps - collapse maps, damage distribution per asset and building typology	with major contributions to Australia, Arabia, Canada, Caribbean and Central America, Europe, Indonesia, South America, Southeast Asia, Taiwan and South Africa but also Global Hazard and Risk Earthquake Models.	lobalquakemodel.org/openquake

			Based Probabilistic Seismic Risk Analysis - Retrofit Benefit-Cost Ratio Analysis					
PAGER	USGS (United States Geological Survey)	Open source	Loss estimates are only based on empirical models (linking intensity with casualty probability) while other estimates such as the distribution of impacted buildings make use of the other methods. PAGER generates estimates of the ranges of potential fatalities and economic losses based on country-specific loss models that account for differences in	Updated ground-motions maps are provided by the USGS ShakeMap® system		The number of people exposed to various levels of shaking is then calculated by combining the maps of predicted ground shaking with Oak Ridge National Laboratory's Landscan global population database. Pager report contain: • Summary of the basic earthquake parameters; • Impact scale alert level for fatalities and economic losses • Table showing population exposed to different MMI levels • Map of MMI contours	World-wide	https://earthquake.usgs.gov/data/pager

			construction practices and building vulnerabilities around the globe. In addition, the PAGER system estimates potential for earthquake-induced landslides.			• Region specific structures and general description of vulnerability of the buildings in the region		
QLARM	ICES Foundation		Parameters introduced in the QLARM database are the following: 1) soil amplification factors; 2) distributions of building stock and population into vulnerability classes; and 3) the most recent population numbers by settlement or district. The building and population distributions are constructed using	Approaches to estimate soil amplification: (a) local approach based on the existing data regarding soil properties, microzonation, and geological maps to derive the amplification factor for each discrete city model; (b) global approach based on Vs30 values derived from topographic slopes	Vulnerability classes are assigned to different building types considering the vulnerability table given by the European Macroseismic Scale EMS-98.	QLARM provides estimates on the number of fatalities and average damage on buildings on global scale. It is used daily: a) in real-time to distribute alert messages in case of large earthquake worldwide daily and b) in scenario mode to estimates losses to be expected in future events in high-risk seismic zones of the globe.	World-wide	http://www.icesfoundation.org/Pages/CustomPage.aspx?ID=122; Trendafilosky et al (2009)

			the percentage of the number of buildings and population belonging to a particular vulnerability class. The building damage in QLARM is calculated using the European Macroseismic Method (Giovinazzi, 2005). The human losses are estimated using the casualty event-tree model proposed by Stojanovski and Dong (1994). Simplified daily population dynamics as suggested by Coburn and Spence (2002) are integrated.					
SELENA (6.6)	NORSAR, Universidad de Alicante	Open-source (Matlab or others)	SELENA is an adaptation of the HAZUS-MH Methodology, but with additions such as integration of	Has modules for probabilistic, deterministic or Real-time input analysis.	The user has to supply built area or number of buildings in different model building types, capacity curves and	SELENA will compute the probability of damage in each one of the four damage states (slight, moderate, extensive, and	Norway, Romania, Haiti, India, Cuba	https://personal.ua.es/en/sergio-molina/selena-rise-en.html

			other demand spectrums (EC8, Indian IS 1983 and Cuba NC 46-2013, beside IBC 2006). CSM, MADRS or IDCM methods are used for determining the building performance points. A logic tree approach is used.	The user has to supply (depending on chosen method) earthquake sources, (empirical) GMPEs (some included), soil maps and corresponding ground-motion amplification factors. It can account for topographic amplification of ground motion (ICMS 2008 Italy and EC8 methods included).	fragility curves corresponding to each of the model building types and finally cost models for building repair or replacement.	complete) for the given building types, fatalities, people in need of shelter, reconstruction costs, the amount of debris, the total number of uninhabitable buildings and displaced households. Outputs are supplied as text files or maps, using the RISE additional software (which provides .kml output for Google Earth).		

4.2 AFAD-RED

The operational parameters of AFAD-RED allow the users to define analysis of hazard, building damage, casualty loss, economic loss, critical facilities, lifeline systems, transportation systems and fast risk assessment in terms of town/village, district, county or user defined grids for scenario or real event. Custom-developed graphical user interfaces are used throughout to insert parameters and monitor results. The code is developed for AFAD users only and is closed source in VB-Net and C# environment; Arc-Object is used for mapping and GIS visualization.

Preliminary results are automatically generated after receiving earthquake source parameters (epicenter, depth, magnitude) using attenuation relationships at Vs30=760 m/s then applied soil amplification according to the Vs30 database. The output is as PGA, PGV and Intensity maps. Different attenuation relationships can be selected as a weighted average.

Moderate results include Fault type, length and azimuth parameters into the calculation of expected hazard level.

Advanced Results include recorded ground motion analysis where first calibration is applied to estimate the recorded ground motion at Vs30 = 760 m/s, then the calibration of ground motion parameter maps is performed, and the soil amplification is applied to get the resulting final PGA, PGV, spectral acceleration (SA @ 0.2 sec, SA @ 1 sec), spectral displacement (SD) and Intensity maps.

It provides estimates of (%) of the lifelines and critical facilities structural damage rates and forecasts of direct economic losses in tabular form.

Building loss estimation is performed by AFAD-RED by considering consequence model from HAZUS together with fragility functions. Vulnerability functions were derived from damage ratios defined at **Error! Unknown switch argument.**.

Table 20. Damage to Loss Model for development of Vulnerability Model (HAZUS)

Damage States	Loss Ratio
Slight	0.02
Moderate	0.10
Extensive	0.50
Complete	1.00

TYPICAL BRIDGE STRUCTURES DAMAGE ASSESSMENT IN AFAD-RED

AFAD-RED provides a rapid and brief representation of seismic damage and loss evaluation for highway bridges. The software offers eight different analyses options in the operational parameters module including seismic hazard and risk assessment for transportation systems (**Error! Unknown switch argument.**). Damage and loss results can be reported in five different modules, such as grid, county, district, town/ village, intensity levels. Soil amplification, Topography elevation, and station record data (in case real ground motion data parameters would be included into the analyses) can be taken into account by "include" module.

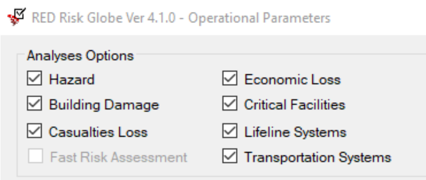

Figure 25. Analysis option for transportation system

In the vulnerability module represents six different sub-modules including bridges in the transportation system (**Error! Unknown switch argument.**). The vulnerability of transportation systems can be performed by choosing seven different intensity measure parameters: PGA, PGV, PGD, Sd, Intensity, S1 and SS.

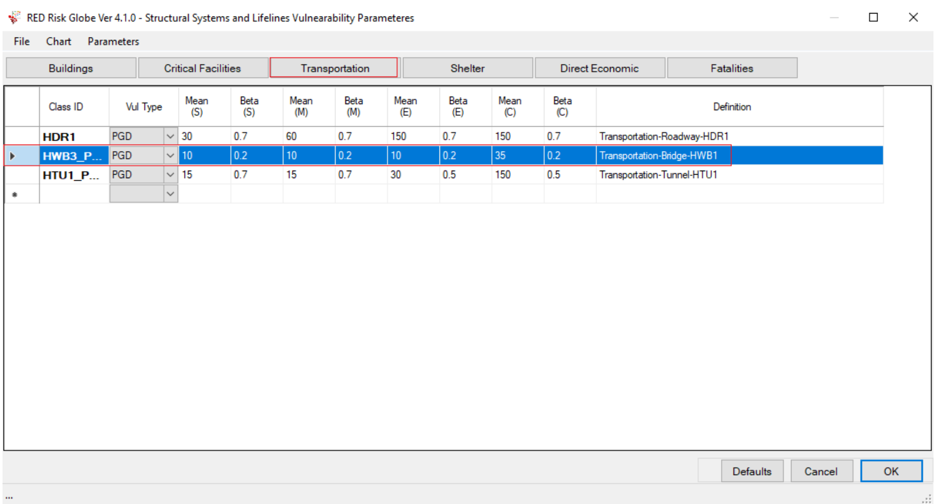

Figure 26. Vulnerability for bridge structures

The damage probability curves calculate the probability of the cumulative damage that is equal or greater than a certain damage level (slight, moderate, extensive, complete), taking into account the log-normal distribution of the damages. For bridge vulnerability assessment, log-normal distribution parameters such as Mean and Beta (standard deviation) can be embedded for each damage level (**Error! Unknown switch argument.**).

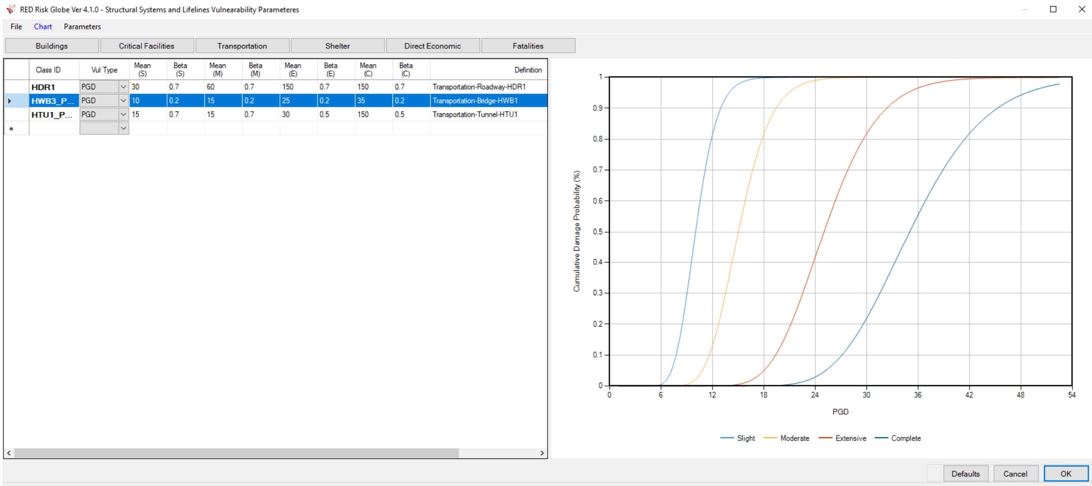

Figure 27. Vulnerability types for bridge structures. (log-normal distribution parameters)

The majority of the fragility functions were relied on the methodology and data that were presented in ATC-13 (ATC 1985) and ATC-25 (ATC 1991) reports following an expert judgement approach. Loss estimation method for transportation systems is adopted from Applied Technology Council, ATC-25 (1991) – see **Error! Unknown switch argument.**. Different methods can be improved after comprehensive literature review.

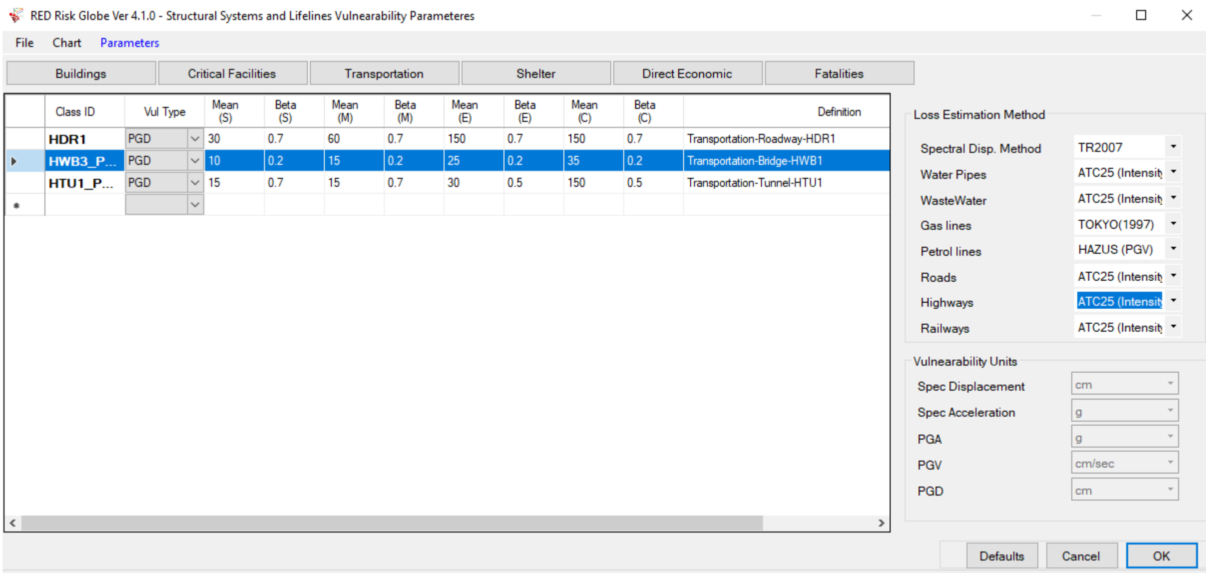

Figure 28. Loss estimation method for transportation system

In the database parameters, transportation input files can be uploaded (**Error! Unknown switch argument.**)

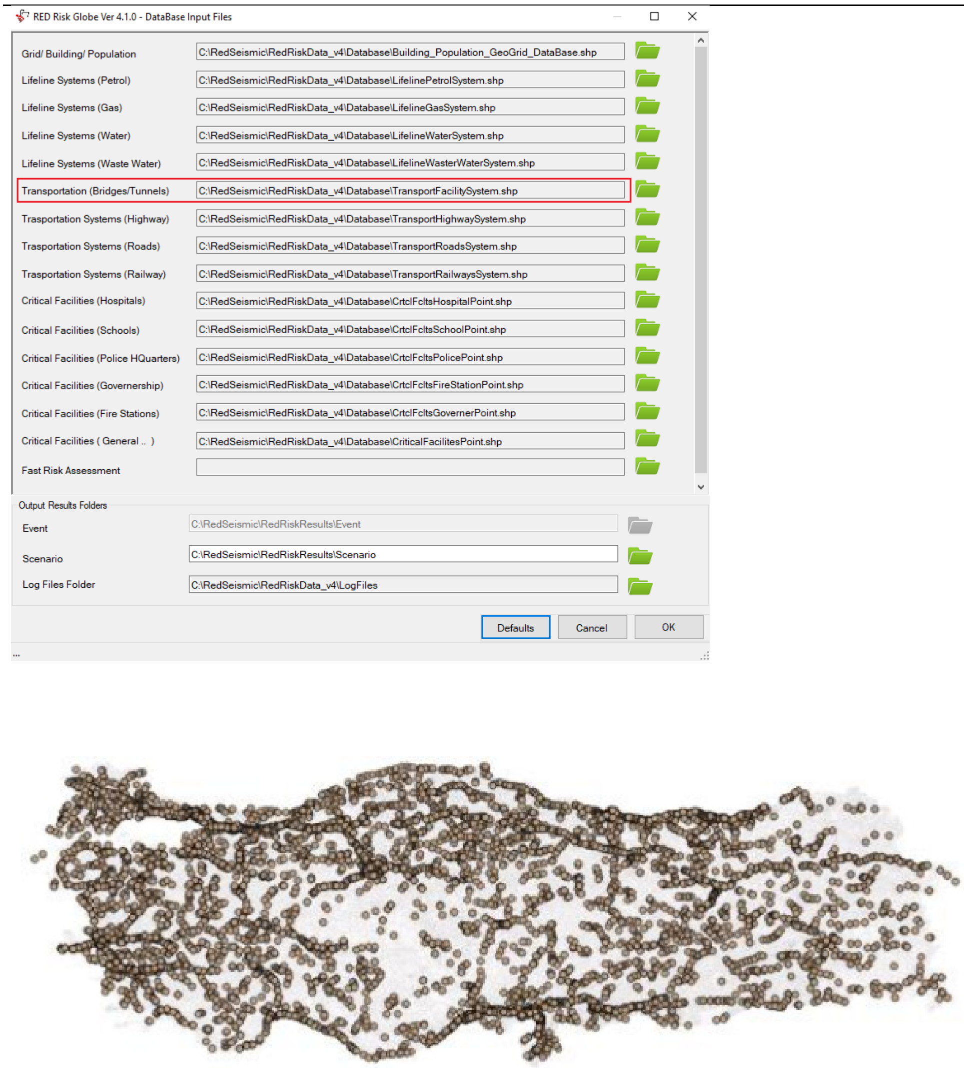

Figure 29. Uploading the shape file and Bridge and Tunnels inventory

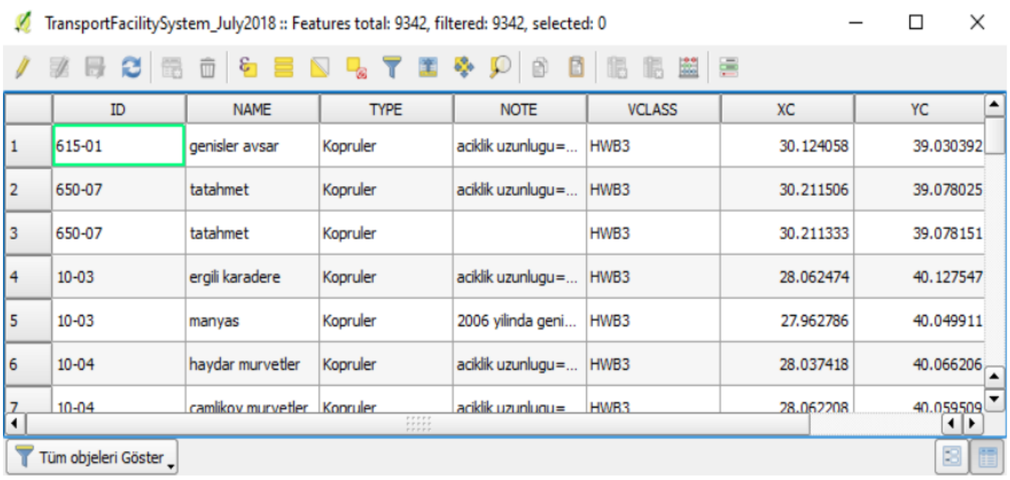

	ID	NAME	TYPE	NOTE	VCLASS	XC	YC
1	615-01	genisler avsar	Kopruler	aciklik uzunlugu=...	HWB3	30.124058	39.030392
2	650-07	tatahmet	Kopruler	aciklik uzunlugu=...	HWB3	30.211506	39.078025
3	650-07	tatahmet	Kopruler		HWB3	30.211333	39.078151
4	10-03	ergili karadere	Kopruler	aciklik uzunlugu=...	HWB3	28.062474	40.127547
5	10-03	manyas	Kopruler	2006 yilinda geni...	HWB3	27.962786	40.049911
6	10-04	haydar murvetler	Kopruler	aciklik uzunlugu=...	HWB3	28.037418	40.066206
7	10-04	camlikoy murvetler	Kopruler	aciklik uzunlugu=	HWB3	28.062208	40.059509

Figure 30. Shape file for the bridges in Turkey

Regarding to analyses methodology, NEHRP 1997 is being used. Regarding "minimum Intensity for Lifeline Losses": the lowest intensity of earthquake that damages in lifeline systems will be included in the analysis is entered in this box. As a standard, this value is taken as 7, life vein damage is not included in the analysis in less severe earthquakes. These values are used in accordance with the purpose. In order to predict ground motions empirically, various numbers of attenuation relationships are introduced in the attenuation relationships module for parameters such as PGA, PGV, PGD, SA, and intensity. The weight of chosen attenuation relationships can be adjusted. The PGD-based attenuation relationships can be used to obtain more sensitive results for transportation systems (**Error! Unknown switch argument.**).

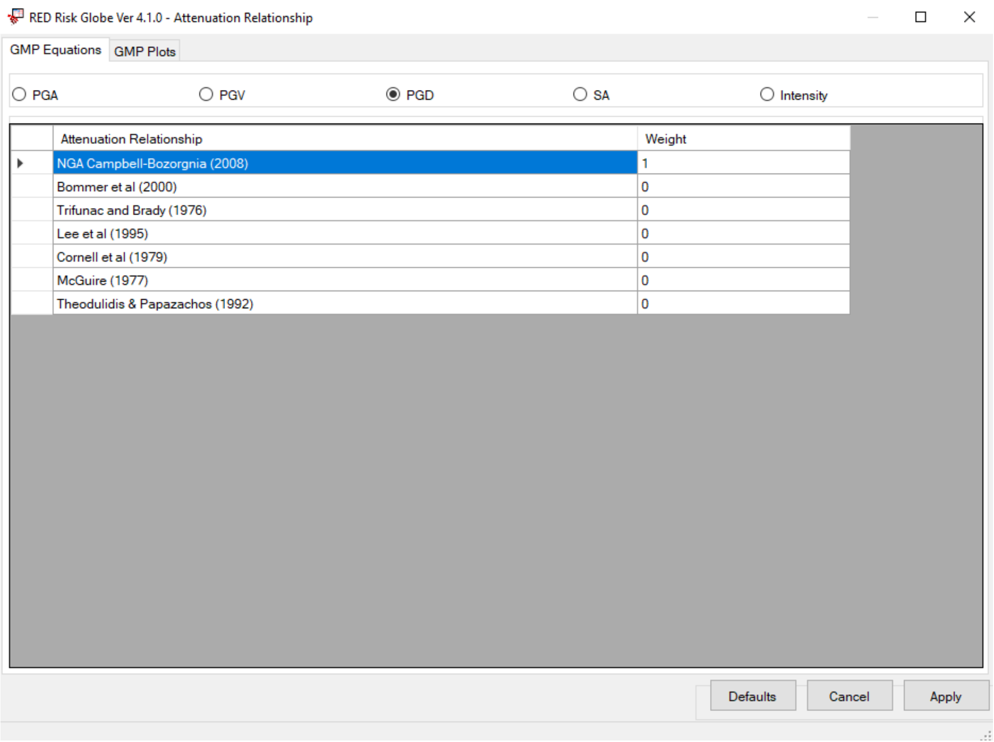

Figure 31. Attenuation Relationship Equations

The GMP can be plotted by taking account of some parameters such as fault type (unknown, strike slip, normal, reverse), average dip, rupture width, rupture depth, shear wave velocity (**Error! Unknown switch argument.**).

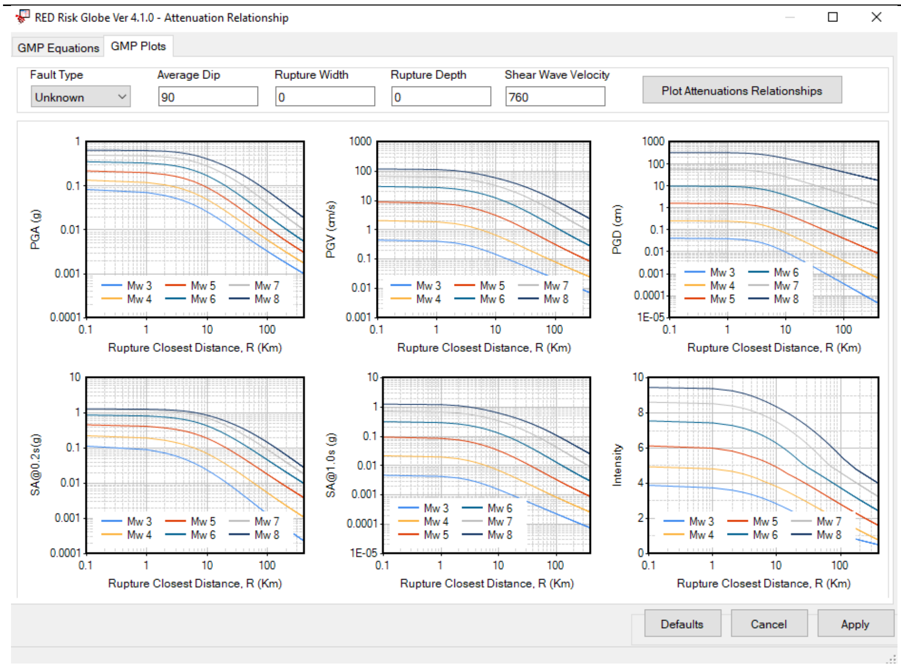

Figure 32. Attenuation Relationships module in AFAD-RED

After running the analysis for hazard and risk assessment, the output can be present in a report choosing risk type, class, table header, and color bar type. The output can be presented in map or table. As **Error! Unknown switch argument.** illustrates, a reference point from a transportation network chosen. The value of 0.0276 shown in the red frame in the figure means that the related transportation facility has a probability of completely collapse with a ratio of 27.6/1000.

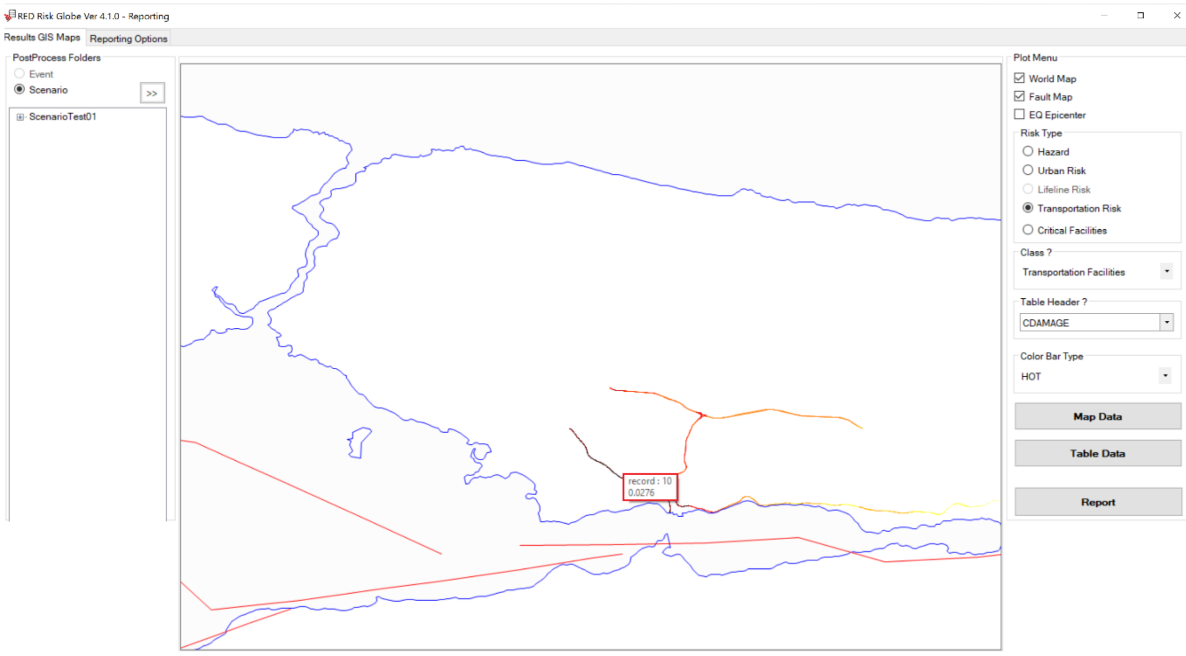

Figure 33. Results, in the form of GIS Maps

Serviceability ratios of bridges can be adjusted in the reporting options (**Error! Unknown switch argument.**).

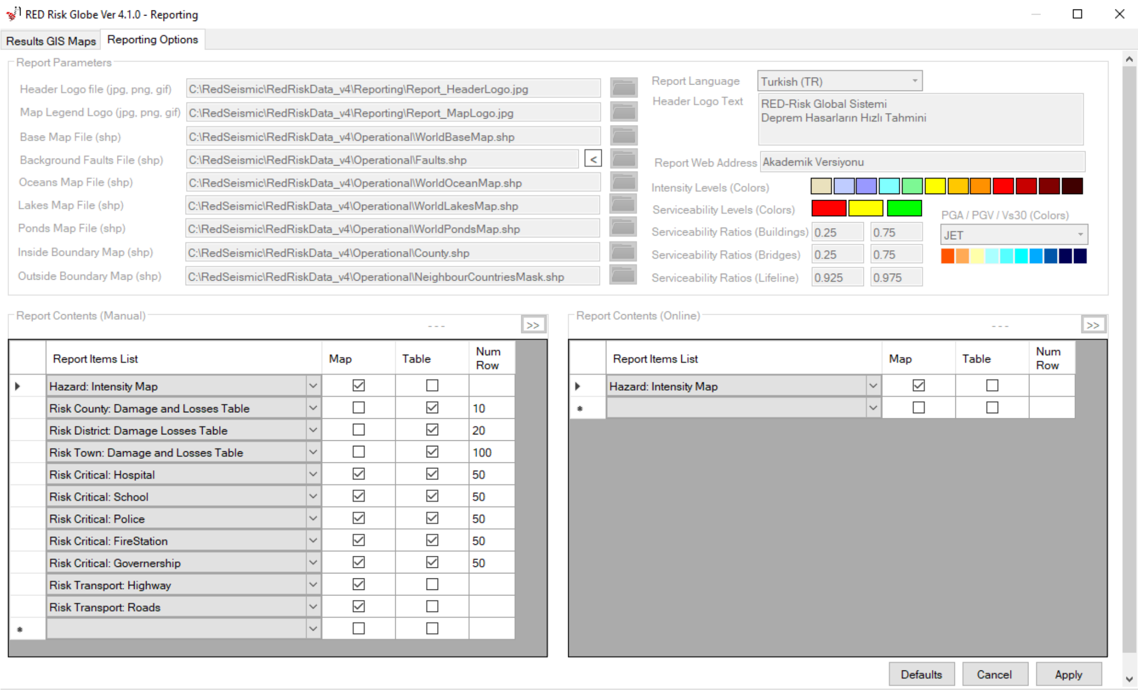

Figure 34. Results: reporting options

The fragility curves can be constructed by various methods in the literature (empirical methods, expert opinion, numerical methods, parameterized fragility curves). AFAD-RED utilizes proper methods for transportation systems and is able to estimate the damage probabilities at certain damage state.

4.3 CAPRA SOFTWARE COLLECTION

CAPRA (Central American Probabilistic Risk Assessment) is a techno-scientific methodology and information platform, composed of multi-hazards software for computing loss estimates.

The platform CAPRA (Comprehensive Approach to Probabilistic Risk Assessment) has been developed by the ERN-AL Consortium for the World Bank, the Inter-American Development Bank and the UN-ISDR, Universitad de los Andes (Colombia), CIMOC (Research Center on Materials and Civil Infrastructure); ERN-LA consortium is composed by the following companies and institutions: ERN Ingenieros Consultores (México), ITEC (Colombia), INGENIAR (Colombia) and CIMNE (Spain).

The main software is CAPRA GIS and this needs three main sets of files in order to run: one file related to the hazard provided by CRISIS module, in *.ame format; one file related to the vulnerability can be obtained using

ERN-Vulnerability, or this can be user-defined with any methodology chosen by the user, provided they are input in the *.dat required standard format; one file related to exposure data base in *.shp format.

CRISIS 2007 is the CAPRA seismic and tsunami hazard module is available for download at (https://ecapra.org/topics/crisis-2007). It provides the probable maximum value of the parameter characterizing the seismic intensity for different exceedance rates or return periods. An .ame file type is created in this module, which includes multiple grids on the area of study, for the different possible intensity parameters of the seismic hazard. Hazard is calculated combining the following: sources geometry (which will influence on the probability distribution of the hypocentral distances), sources seismicity (defined by a Poisson seismicity model, which will provide the probability distribution of the occurrence of a particular magnitude within the source) and attenuation functions (which provides the probability distribution of strong motion, given the magnitude and hypocentral distance).

The ERN-Vulnerabilidad_v2 module is available for download at (https://ecapra.org/topics/ern-vulnerability) and includes a vulnerability curves data base, proposed by different authors and ERN-AL, and allows their edition depending on the main characteristic of the structural types under analysis, and on formats compatible with CAPRA-GIS.

The vulnerability module quantifies the damage caused to each asset class by the intensity of a given event at a site. The classification of the assets, for buildings of an urban area, is based on a combination of structural characteristics like construction material, construction type, building use, number of levels, age, etc. Damage is estimated in terms of the Mean Damage Ratio (MDR) that is defined as the ratio of the expected repair cost to the economic value of the structure. A vulnerability curve is defined relating the damage to the earthquake intensity, expressed, at each location, in terms of the maximum acceleration or spectral acceleration, velocity, interstory drift or displacement.

The exposure is mainly related to the infrastructure components or to the exposed population that can be affected by a particular event. Characterization of exposure requires identification of individual components, including variables such as location, physical, geometric and engineering characteristics, economic value and level of human occupancy.

The precision degree of the results depends on the level of resolution and on the details of the information. Each building is characterized by the geographic location, the economic value, the year of construction, the number of levels, the structural type and the human occupancy.

CAPRA Data Entry is a new CAPRA software oriented to support building inspection processes. This software is the technical solution developed to enhance collection and administration of field information of exposed structures, required in the refinement of the exposure model integrated in seismic risk assessment projects. CAPRA Data Entry offers various tools for managing evaluation forms of diverse projects, consolidating work teams, field work assistance, data analysis, and generation of various formats to visualize results such as reports, maps, tables and statistical graphs, among others. This software will be available online and for mobile devices (https://ecapra.org/topics/capra-data-entry) (not available for free download).

The main output of CAPRA-GIS is the expected annual damage ratio (the ratio of repair cost to the real monetary value of the structure) of each structure that is geo-referenced. When it is multiplied by the exposed value yields the total economic loss for that specific structure. Another result that CAPRA delivers is an aggregate loss exceedance curve for the whole building portfolio.

The results per building are appended to the *.shp file, which are the total annual loss value per building, and the corresponding normalized ratio of annual loss per building or expected annual damage, as well as the annual human loss per building.

The main results of CAPRA-GIS are provided in a *.res file that can be opened using any text editor

and contains, for each scenario analyzed, the expected loss (EP), the variance of the loss (VarP), and parameters a and b that fully define the beta distribution of the loss for a given scenario.

CAPRA's risk assessment tools can be used for rapid post-event damage and loss assessments at different scales depending on information availability, having been tested with events in Asia, Europe (i.e. Spain, Italy) and Latin America.

4.4 ELER

ELER software uses a proxy procedure that relies on land use cover and population distributions to develop regional scale building inventories (Demircioglu et al. 2009).

ELER is designed as open-source software to allow for community-based maintenance and further development of the database and earthquake loss estimating procedures. The software provides for the estimation of losses in three levels of analysis. These levels of analysis are designed to commensurate with the quality of the available building inventory and demographic data. The first two levels are in Intensity based whereas the third level is more sophisticated and based on the event parameters the distribution of PGA, PGV, SA (T=0.2 s) and SA (T=1 s). The spectral values are estimated depending on a choice of ground motion prediction models. Local site effects are incorporated either with the Borcherdt (1994) methodology or, if available, with the use of Vs30 based amplification functions within GMPEs. If strong ground motion recordings are also available, the prediction distributions are bias corrected using the peak values obtained from these recordings. The loss estimation of buildings is estimated using HAZUS methodology, and the lifeline (pipeline, transportation, etc.) losses are estimated from PGV based hazard calculated via PGV related GMPEs.

ELER is structured in such a way that a building inventory can be classified in terms of any classification system as long as the empirical and/or mechanical fragility relationships associated with each building type is defined by the user.

Pipeline Damage Assessment in ELER

The pipeline damage module in ELER v3.0 can be used to estimate damages to urban pipeline systems such as potable water, wastewater and natural gas. Observations acquired from past urban earthquakes supplemented by the worldwide experience are used as a guide to assess the physical vulnerabilities of pipelines. ATC 25 (1991) provides an extensive compilation of lifeline vulnerability functions and estimates of required time to restore the facilities. A number of empirical correlations relating expected pipeline damage to PGV are available in the literature. O'Rourke and Ayala (1993), Eidinger and Avila (1999) and O'Rourke and Deyoeto (2004) can be cited among them. These correlations may be used to estimate repair rate and number of repairs in the pipeline system due to wave propagation. ELER uses the HAZUS-MH (FEMA, 2003) methodology, which is based on O'Rourke and Ayala (1993), to estimate pipeline damages. The O'Rourke and Ayala (1993) model correlates the repair rate with PGV and material type as given in the equation below.

$$\text{Repair Rate} \cong 0.0001*[\text{PGV}]^{(2.25)} \quad \text{(for brittle type material)}$$

$$\text{Repair Rate} \cong 0.00003*[\text{PGV}]^{(2.25)} \quad \text{(for ductile type material)}$$

where repair rate is the number of repairs per a km of pipeline and PGV is in cm/sec. In this methodology, damages due to seismic waves are expected to consist of 80% leaks and 20% breaks.

The pipeline inventory is a grid-based distribution of pipe length for each cell. The damage results are given in the form of repair numbers per kilometer, due to leaks and breaks. Numbers of expected repairs at each cell are calculated as the product of repair rate and total pipeline length.

4.5 HAZUS

HAZUS (version 4.2) estimate physical, economic, and social impacts of disasters, such as earthquake, hurricane, flood and tsunami (since 2017) in USA. It's main dependency is of ESRI ArcGIS commercial software.

The software is not open source but a very detailed documentation is available for modifiable reproduction. Many regional or country based loss estimation tools uses the HAZUS methodology. Beside multiple implementations in its design area (United States of America territory), HAZUS was also directly used for Egypt.

HAZUS can use seismic hazard input maps from USGS, in which the soil effects are already implemented. For methodology users, an important input methodology for hazard calculations is the weighted GMPE usage which is explained in detail in the Open file report of USGS 2014-1091 ("Documentation for the 2014 Update of the United States National Seismic Hazard Maps"). HAZUS uses Capacity Spectrum Method based on the analytical fragility relationships for building damage assessment.

HAZUS output is spatially given in terms of potential loss estimates of physical damage to residential and commercial buildings, schools, critical facilities, and infrastructure; economic loss including lost jobs, business interruptions, repair, and reconstruction costs; and social impacts, including estimates of shelter requirements, displaced households, and population exposed to scenario floods, earthquakes, and hurricanes, and tsunamis (https://www.fema.gov/flood-maps/tools-resources/flood-map-products/hazus).

US nationwide databases include the following groups and could give good insight to check if the same type of inventory data is available at the Black Sea Programme area as well as their distribution (total count in city, district, etc. level) or exact location:

- Demographics: Population, Employment, Housing
- Building Stock: Residential, Commercial, Industrial
- Essential Facilities: Hospitals, Schools, Police Stations, Fire Stations
- Transportation: Highways, Bridges, Railways, Tunnels, Airports, Ports and Harbors, Ferry Facilities
- Utilities: Waste Water, Potable Water, Oil, Gas, Electric Power, Communication Facilities
- High Potential Loss Facilities: Dams and Levees, Nuclear Facilities, Hazardous Material Sites, Military Installations

Building damage functions are in terms of capacity response spectrum curves for structural, non-structural acceleration, non-structural drift fragility curves with possibility of combination of damage assessment due to both ground shaking and ground failure together as well as separately.

4.6 MAEVIZ

MAEviz, developed in the Mid-America Earthquake Center in University of Illinois, integrates spatial information, data, and visual information to perform seismic risk assessment and analysis (http://mae.cee.illinois.edu/software/software_maeviz.html). It can perform earthquake risk assessment for buildings (structural and non-structural damage), bridges and gas networks with a built-in library of fragility relationships. In addition to applications in USA and important application of the software has been conducted for the Zeytinburnu District of Istanbul (Elnashai et al., 2007).

MAEViz is a seismic risk assessment software developed by the Mid-America Earthquake (MAE) Center and the National Center for Supercomputing Applications (NCSA).

MAEviz implements Consequence-Based Risk Management (CRM) to estimate the damage and the losses for buildings, bridges and lifeline (gas, water, electric facilities). For buildings, it estimates structural and nonstructural damage, economic losses and liquefaction damage. For bridges, it computes damage, loss of functionality and repair cost analysis. For lifelines it calculates the network damage and the repair rate analysis. Finally, it computes socio-economic losses such as shelter needs, fiscal and business interruption. To achieve these results the following are required: hazard, inventory and fragility models.

Regarding the hazard module MAEviz can take into account liquefaction hazard in addition to ground shaking. The hazard is response spectral based and local site effects are taken into account. There are some default scenarios and probabilistic hazard maps in the catalog box however the user can upload their own hazard following a graphical interface. The user can also choose to create the scenario using an analysis. The user has to provide the spectrum type, the earthquake location, the coordinates of the region of interest and some advanced parameters such as the fault type, the dip angle, etc.

The MAEviz tool provides as default some inventories stored in tables and shapefiles. The inventory buildings contain information about the construction type, number of storeys, occupancy level, year of construction and building area. The user can upload their own inventory in the 'catalog box' and also can upload data about bridges and lifelines. This data stored in shapefiles allows a direct visualization.

The vulnerability functions were derived by structural analysis which considering the aleatory structural features uncertainty and the excitation uncertainty. The fragility curves have been developed for construction typical of the Mid America region and provide the conditional probability of being in, or exceeding a particular damage state given by the seismic demand parameter. Three fragility curves are provided and four damage states are obtained by difference between adjacent curves. The hazard used when evaluating these fragilities is obtained by performing a transformation from elastic spectral acceleration to elastic spectral displacement without regard for inelasticity in building response.

Based on analyzes for structural damage and optional nonstructural damage, MAEViz compute the direct economic losses. More additional economic and socioeconomic analyses are available: the building repair cost based on the structural damage and building type, the building retrofit cost estimation, the number of casualties and the fiscal impact.

4.7 OPENQUAKE

OpenQuake is an open-source multi-purpose tool developed and being updated by Global Earthquake Model (GEM) Foundation based in Pavia, Italy (https://www.globalquakemodel.org/).

The hazard component of the OpenQuake-engine can compute seismic hazard using various approaches. Three types of analysis are currently supported:

- Classical Probabilistic Seismic Hazard Analysis (PSHA), allowing calculation of hazard curves and hazard maps following the classical integration procedure (Cornell, 1968, McGuire (1976)) as formulated by Field et al., 2003.
- Event-Based Probabilistic Seismic Hazard Analysis, allowing calculation of ground motion fields from stochastic event sets. Traditional results - such as hazard curves - can be obtained by post-processing the set of computed ground-motion fields.
- Scenario Based Seismic Hazard Analysis (SSHA), allowing the calculation of ground motion fields from a single earthquake rupture scenario taking into account ground motion aleatory variability.

The seismic risk results are calculated using the OpenQuake risk library (oq-risklib), an opensource suite of tools for seismic risk assessment and loss estimation. This library is written in the Python programming language and available in the form of a “developers” release at the following location: https://github.com/gem/oq-engine/tree/master/openquake/risklib.

The risk component of the OpenQuake-engine can compute both scenario-based and probabilistic seismic damage and risk using various approaches. The following types of analysis are currently supported:

- Scenario Damage Assessment, for the calculation of damage distribution statistics for a portfolio of buildings from a single earthquake rupture scenario taking into account aleatory and epistemic ground-motion variability.

- Scenario Risk Assessment, for the calculation of individual asset and portfolio loss statistics due to a single earthquake rupture scenario taking into account aleatory and epistemic ground-motion variability. Correlation in the vulnerability of different assets of the same typology can also be taken into consideration.
- Classical Probabilistic Seismic Damage Analysis, for the calculation of damage state probabilities over a specified time period, and probabilistic collapse maps, starting from the hazard curves computed following the classical integration procedure (Cornell, 1968, McGuire (1976)) as formulated by Field et al., 2003.
- Classical Probabilistic Seismic Risk Analysis, for the calculation of loss curves and loss maps, starting from the hazard curves computed following the classical integration procedure (Cornell, 1968, McGuire (1976)) as formulated by Field et al., 2003.
- Stochastic Event Based Probabilistic Seismic Damage Analysis, for the calculation of event damage tables starting from stochastic event sets. Other results such as damage state-exceedance curves, probabilistic damage maps, and average annual damages or collapses can be obtained by post-processing the event damage tables.
- Stochastic Event Based Probabilistic Seismic Risk Analysis, for the calculation of event loss tables starting from stochastic event sets. Other results such as loss exceedance curves, probabilistic loss maps, and average annual losses can be obtained by post-processing the event loss tables.
- Retrofit Benefit-Cost Ratio Analysis, which is useful in estimating the net-present value of the potential benefits of performing retrofitting for a portfolio of assets (in terms of decreased losses in seismic events), measured relative to the upfront cost of retrofitting.

Each calculation workflow has a modular structure, so that intermediate results can be saved and analysed. Moreover, each calculator can be extended independently of the others so that additional calculation options and methodologies can be easily introduced, without affecting the overall calculation workflow.

The OpenQuake-engine calculators (e.g. Classical PSHA, Event Based PSHA, Disaggregation, UHS) produce a set of hazard results (i.e. hazard curves, hazard maps, ground motion fields, disaggregation matrices, UHS, for each logic-tree realization) which reflects epistemic uncertainties introduced in the PSHA input model. For each logic tree sample, results are computed and stored. Calculation of results statistics (mean, standard deviation, quantiles) are supported by all the calculators.

The OpenQuake-engine is used in many national and regional seismic hazard mapping programs. The use in projects at regional level allowed to develop a global fragility/vulnerability database. Globally the risk evaluations can be done country based on monetary loss values based on industrial, commercial and residential building types instead of proxy (population). In Europe while defining the vulnerability functions, an extra expression is added to define the quality of same type of structures, such as low-code, moderate-code buildings, etc. (i.e. Turkey is considered to have low-code building types). Global vulnerability implemented models are more than 500. (23.09.2020 – Willis & GEM Webinar: "Earthquake science for (re)insurance decision-makers: bridging the gap between academia (GEM) and industry (Willis Tower Watson)). Calibration and testing are usually done by the damage data when available (i.e. via PAGER system in USGS for USA events).

The next step would be to use OpenQuake for real-time assessment. This opportunity will be explored in the near future.

4.8 PAGER

PAGER (Prompt Assessment of Global Earthquakes for Response) is an automated system that assesses the impact of significant earthquakes around the world, informing emergency responders, government and aid agencies, and the media of the scope of the potential disaster.

PAGER development and maintenance are supported by the USGS under the Advanced National Seismic System (ANSS), with additional funding from the Global Earthquake Model (GEM) project, and a grant from the U.S. Agency for International Development/Office of Foreign Disaster Assistance (USAID/OFDA). Landscan population data from Oak Ridge National Laboratory, and data from Munich Reinsurance, EM-DAT, and NOAA were vital for developing and calibrating PAGER loss models.

The shaking-related impact assessed by system PAGER is controlled by the distribution and severity of shaking, the population exposed to each shaking intensity level, and population vulnerability correlated with the degree of seismic resistance of the local building stock.

PAGER uses earthquake parameters to calculate estimates of ground shaking by using the methodology and software developed for ShakeMap (http://earthquake.usgs.gov/shakemap/). The number of people exposed to each shaking intensity level is then calculated by combining the maps of estimated ground shaking with a comprehensive worldwide population database (Landscan, from Oak Ridge National Laboratory).

Next, based on the population exposed to each intensity level of shaking, the PAGER system estimates total losses based on country specific models developed from economic and casualty data collected from past earthquakes. Finally, the alert levels are produced, determined by estimated ranges of fatalities and economic loss, with the higher of the two setting the overall alert level. The alert level determines which users are actively notified, and, at the same time, all PAGER content is automatically distributed to the Web on the USGS Earthquake Hazards Program Web pages, as part of the earthquake summary information, for immediate consumption.

PAGER uses a new Earthquake Impact Scale (EIS) that is based on two complementary criteria. The first criterion is the estimated cost of damage; this is most suitable for domestic events and those in earthquake-resistant communities. The second criterion, representing estimated ranges of fatalities, is generally more appropriate for global events, particularly in developing countries.

Alert level and color	Estimated fatalities	Estimated losses (U.S. $$)
Red	1,000+	$1 billion+
Orange	100 – 999	$100 million – $1 billion
Yellow	1 – 99	$1 million – $100 million
Green	0	< $1 million

Earthquake Impact Scale with Alert Level thresholds.

PAGER provides shaking and loss estimates following significant earthquakes anywhere in the world. These estimates are generally available within 30 minutes and are updated as more information becomes available. Rapid estimates include the number of people and names of cities exposed to each shaking intensity level as well as the likely ranges of fatalities and economic losses.

Information on the extent of shaking will be uncertain in the minutes and hours following an earthquake and typically improves as additional sensor data and reported intensities are acquired and incorporated into models of the earthquake's source. Users of PAGER need to account for uncertainty and always seek the most current PAGER release for any earthquake.

The PAGER report contains the following information:

- **summary of the basic earthquake parameters**, including origin time, local time, magnitude, hypocenter, and the name of the region where the earthquake took place.
- **earthquake Impact Scale alert levels** for fatalities (left) and economic losses (right).
- **table showing population exposed** to different estimated Modifed Mercalli Intensity (MMI) levels and the possible damage at dfferent intensity levels for resistant and vulnerable structures.
- **map of MMI contours** plotted over the Landscan (Oak Ridge National Laboratory) population base map.
- The total population exposure to a given MMI value is obtained by summing the population between the contour lines. This total is shown in the population exposure table (E).
- **region-specific structure and earthquake commentary**. The Structures comment may contain the most vulnerable building type(s) in the region or a general description of the vulnerability of the buildings in the region. The

- Historical Earthquakes section includes a table of population exposure and fatalities for three previous nearby earthquakes, and, in some cases, the potential for _res, landslides, liquefaction, or other hazards, based on past earthquakes in the region, will be noted
- **table of MMI estimates for selected settlements**.A maximum of 11 settlements that fall within the map boundary are included in the table. The table contains country capitals and the six settlements with the highest estimated intensity. The remaining settlements listed are selected by population. Settlement name, location, and population are obtained from the freely-available GeoNames geographical database (GeoNames.org).

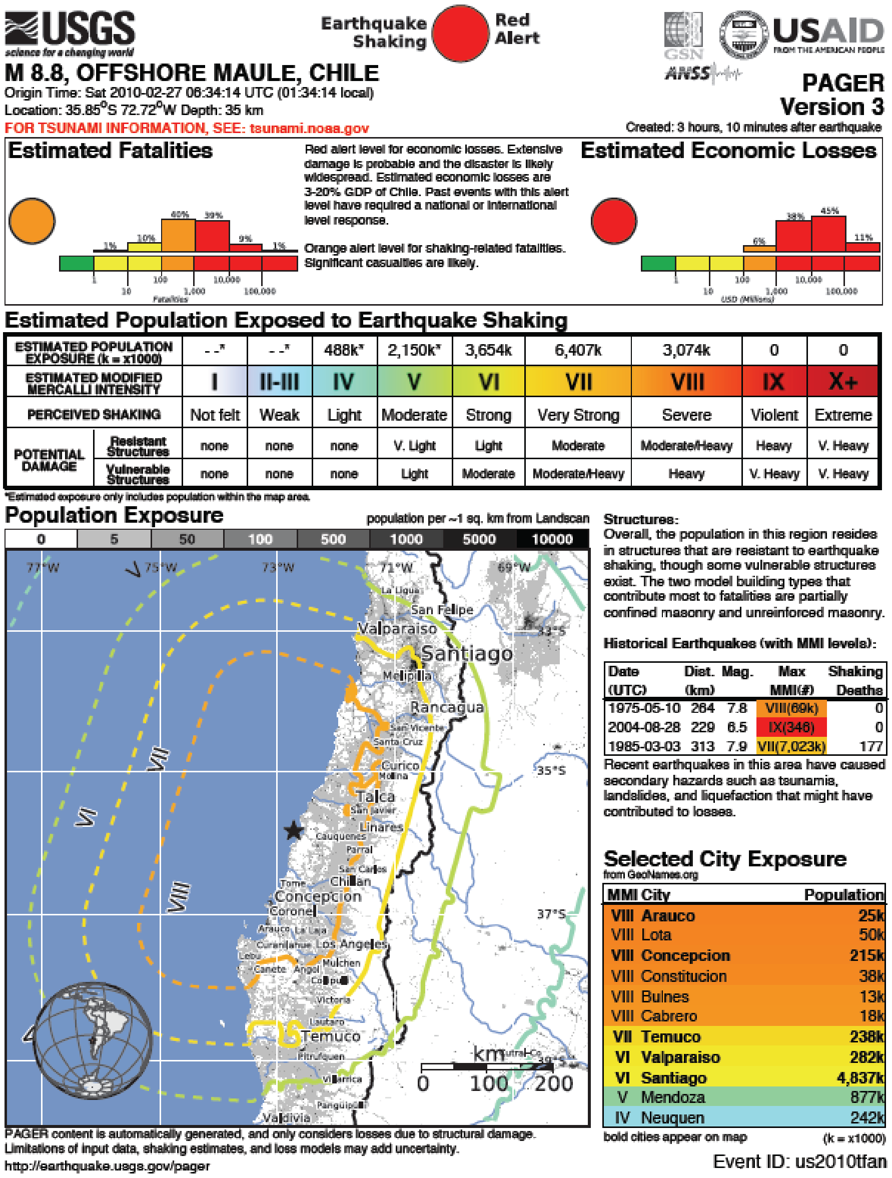

PAGER report on damaging earthquake in Chile

Archive information on the Black Sea area is available:

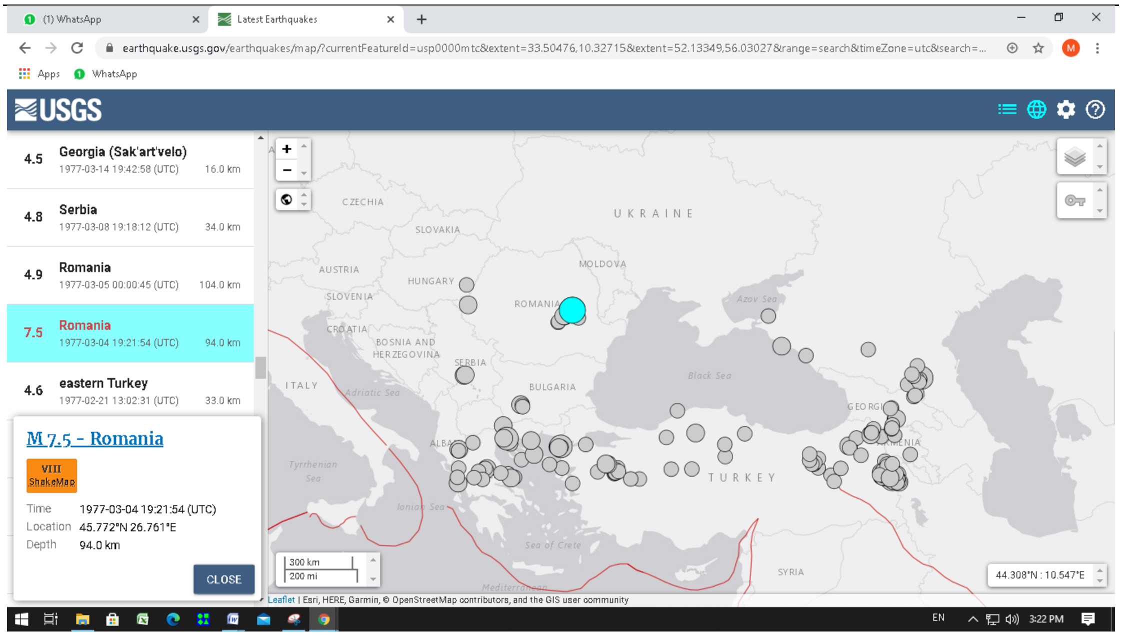

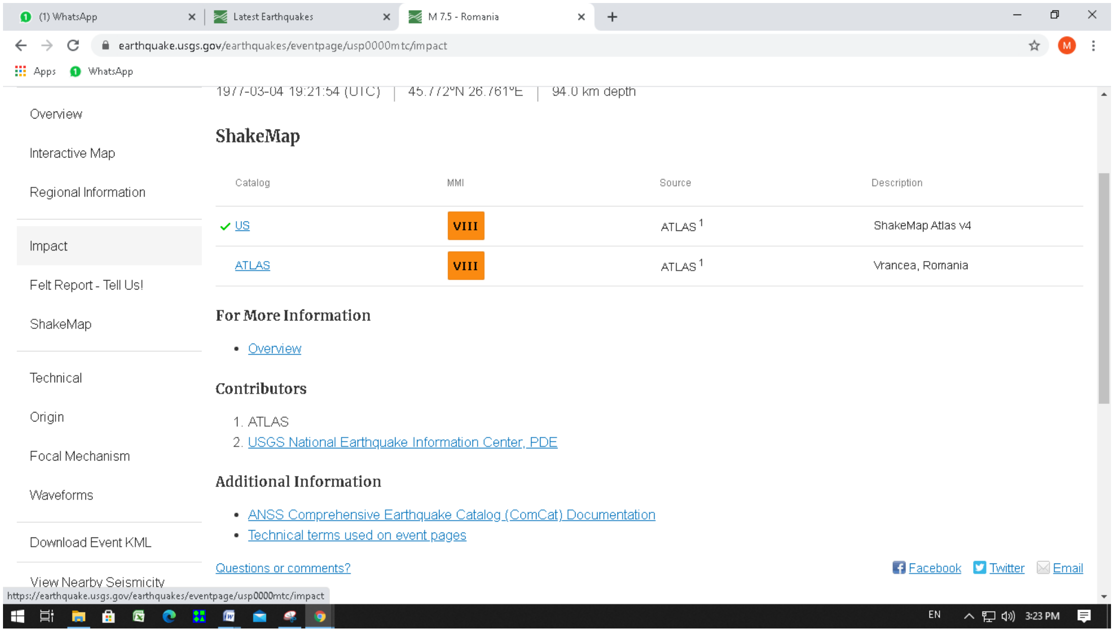

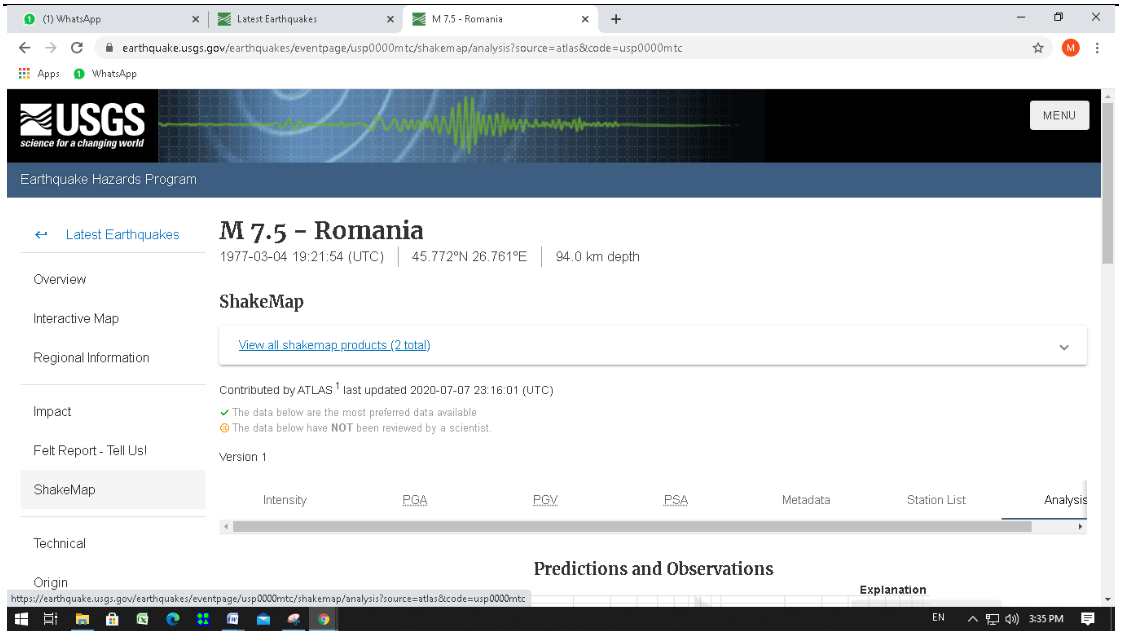

PAGER rapidly assesses earthquake impacts by comparing the population exposed to each level of shaking intensity (ShakeMaps) with models of economic and fatality losses based on past earthquakes in each country or region of the world (Earle et al. 2009a, b). The ShakeMaps are constrained, if available, by measurements from strong-motion seismometers in the region surrounding the ruptured fault. In case ground motion recordings are insufficient, ShakeMaps are constrained using empirical ground motion prediction equations based on magnitude, site amplification, and distance to the fault. Soil/rock site-specific ground-motion amplification map is based on topographic slope and then the estimated ground motions are converted to a map of seismic intensities. Based on the population exposed to each shaking intensity level, the PAGER system estimates total shaking-related losses based on country-specific models developed from economic and casualty data collected from past earthquakes.

PAGER products are generated for all earthquakes of magnitude 5.5 and greater globally and for lower magnitudes of about 3.5-4.0 within the US. In the hours following significant earthquakes, as more information becomes available, PAGER's content is modified.

The code is not open source, but consecutive number of libraries of data as well as documentation is available. It also allows to define datasets used within.

4.9 SELENA

SELENA (SEimic Loss EstimatioN using a logic tree Approach) (version 6.6) is an open source (MATLAB and C#) tool and utilizes the capacity-spectrum method with a logic tree-based weighting of input parameters and follows the same loss estimation approach of HAZUS. GIS software can be utilized at multiple levels of resolution to display predicted losses graphically.

The user has to supply a number of input files that contain the necessary input data (e.g., building inventory data, demographic data, definition of seismic scenario etc.) in a simple pre-defined ASCII format. SELENA computes ground shaking maps for various spectral periods (PGA, Sa(0.3 s) and Sa(1.0 s), damage probabilities, absolute damage estimates (including Mean Damage Ratios MDR) as well as economic losses and numbers of casualties.

Earthquake ground shaking estimates can be calculated based on the following approaches:

- Deterministic
- Probabilistic
- Real Time

For real time analysis, data from strong motion stations (at least PGA values) can also be used with certain limitations. Based on these ground motion parameters SELENA generates site-specific response spectra based on IBC-2006 (International Code Council 2006), Eurocode 8 (CEN 2003) and Indian seismic building code IS 1893.

SELENA uses analytical approach for obtaining building damage with different user-selectable methodologies:

- the traditional capacity spectrum method (CSM) as proposed by ATC-40 (ATC 1996)
- the Modified Acceleration Displacement Response Spectra (MADRS) method according to FEMA 440 (FEMA 2005)
- the Improved Displacement Coefficient Method (I-DCM) as given by FEMA 440 (FEMA 2005).

SELENA needs the GNU Scientific library (GSL) and the Qt cross-platform application and UI framework (for the SELENA GUI). For RISe (Risk Illustrator for SELENA) the .NET framework (Windows) or the mono framework (Linux/Unix) need to be installed.

Starting with version 5 of SELENA, the MATLAB m-code has been translated into C-code which allows SELENA to run without using MATLAB; it is, however, still possible to use SELENA from MATLAB. Furthermore, the m-code has been changed in such way that it now can run without any special MATLAB Toolboxes (which was required before) and it now also now runs using the free (open source) MATLAB clone Octave (http://www.gnu.org/software/octave/).

4.10 OTHER SOFTWARE

Lu Xinzheng et al. published a new paper in Earthquake Spectra (2020),36(2):806 with the title "An open-source framework for regional earthquake loss estimation using the city-scale nonlinear time history analysis". Other software and systems can be visualized in the table of the 4.1 subchapter. In the last years, multiple rapid earthquake loss estimation systems started to arise. However, in the Black Sea area, beside national systems such as Seisdaro (in Romania) and AFAD-RED (in Turkey) or regional and international systems (such as PAGER, QLARM or soon to come EMSC estimates beside crowd-sourced processed Did you feel it? Feedback), there are no other operational systems at the moment.

5 METHODOLOGY SELECTION FOR REDA

In order to show preferences for some of the multiple available REDA methods and software also presented in the previous chapters, we think that is suitable to start with mentioning our selection criteria, considering the expectations and goals for a REDA system in the Black Sea Area along with data availability, as reflected by D.T1.1.1. In order for the REDACt system to be efficient, we expect that it will need to:

- be capable of receiving and using either near real-time output from seismic network systems in partner countries or critical parameters of the time histories (e.g., PGA, PGV, Spectral Acceleration etc.) as well as input parameters from other European or world-wide seismic institutions such as EMSC-CSEM or USGS or initiatives such as ORFEUS EIDA (e.g., real-time earthquake source parameters);
- produce rapid results (in less than 30 minutes after a moderate or large magnitude earthquake in the Black Sea Area), primarily in terms of estimated percentage of damaged buildings and fatalities; allow for a re-run of the scenario, with updated data but also, for example, with ShakeMaps from other institutions;
- evaluate liquefaction and landslide potential and also their effects in terms of damage and socio-economic loss - provide a geotechnical failure module;
- be written using a programing environment flexible, stable, without a tendency of depreciation, preferably non-commercial software dependency and with multiple connectivity potential also toward GIS platforms and webGIS services;
- be capable of presenting results at different scales (whether methodologically imposed but also resulting from aggregation) – in order to serve multiple type of stakeholder needs (at national, regional or local level);
- quantify and express uncertainties of the results;
- be capable of integrating regionally-specific exposure and vulnerability models;

- account for various building typologies and be capable of showing them (along with fragility functions) properly;
- be capable of integrating aspects referring to other types of structure vulnerability, beside buildings (such as bridges, tunnels, lifelines, other fragility or vulnerability functions for specific structures);
- provide a module for the estimation of seismic and co-seismic losses on lifeline networks (such as natural gas pipelines);
- consider the integration of and with important well-acknowledged works at national, European and world-wide level (such as CAPRA, OpenQuake, PAGER), providing regional improvements and updated methods. Also, allow for direct comparison of results with output from other works, both for operational and scientific purposes.

Under these aspects, we foresee as suitable for the development of the REDA system in the following framework:

- The system will work on two modes:
  - on scenario-based mode (a priori);
  - on real-time data provided by seismic networks.
- It will comprise of multiple levels of analysis (modules):
  - Seismic hazard module:
    - include output from seismic networks and services, consisting of:
      - earthquake parameters (first of all: latitude, longitude, depth, magnitude, magnitude type, but also if available: focal mechanism, fault geometry and errors in parameter determination etc.);
      - seismic station parameters for the specific earthquake: PGA, SA at periods such as 0.3, 1 and 3 s., PGV (and also, if possible, quality of the data and relevant soil characteristics for the station site);
      - crowd-sourced intensities or other data useful in validation and methodology parameter adjustments.
    - be capable of using ShakeMap-like hazard input, as a reference methodology at world-wide and European level, keeping in mind that ShakeMap systems are already in place in Romania, Greece or Turkey, are publicly available from USGS and at European scale (http://shakemapeu.ingv.it/);
    - capable of running single-scenarios (but check with stakeholders if probabilistic approaches would be important at this moment to integrate);
    - be flexible enough and easy configurable, allowing the integration of multiple rupture models, seismic source

definitions, GMPEs (also using the xml format of the OpenQuake hazardlib) and weighting schemes.

- Geotechnical failure module, enabling:
  - evaluation of liquefaction susceptibility, based on geological and geomorphological maps;
  - evaluation of liquefaction potential (hazard) based on a
  - logistic regression model to predict the probability of liquefaction occurrence as a function of simple and globally available geospatial features (derived from digital elevation models), standard ground motion parameters (e.g. peak ground acceleration) and spatially continuous data as a proxy for important subsurface parameters;
  - evaluation of landslide hazard assessment, based on: a) an empirical landslide probability model, b) hybrid statistical model combined with failure criteria and c) physically based models;
- Level 1 loss estimation module, using a Macroseismic damage estimation tool consisting of the EMS98 intensity based empirical vulnerability relationships and casualty vulnerability models; further refinements, at least in exposure data, to other systems in place such as PAGER or QLARM, needs to be further discussed.
- Level 2 loss estimation module, performing building damage estimation using fragility functions and consequence models for socio-economic determination of direct losses. Many REDA software relies on fragility functions nowadays from a methodological point of view. In our case, multiple accounting for different design spectra – with multiple differences among country's specifications in design codes, will need to be considered. Beside improvements in the software implementation of this methodology and interface enhancements in the new REDA, new considerations regarding the inclusion of a method of accounting for main-shock impact and/or include validated vulnerability data quickly could be added, and also a new approach to quantifying and tracing uncertainties.
- Module for the estimation of seismic and co-seismic losses on lifeline networks (such as natural gas pipelines), using an adaptation of methodologies in HAZUS or AFAD-RED but also extended the focus toward economic consequence modelling and repairing time and costs, for a Decision Support System suitable for stakeholders.

- It is highly recommended to include both in both loss estimation modules a local-specific model accounting distribution of population considering the hour but also the day (work day, weekend or holiday) of the earthquake.

- Among the recommendations of programming environment for REDA are Python (general tendency to use it in the scientific community – for example in ShakeMap 4, OpenQuake, Seiscomp3, Obspy, Geopsy etc.) or Java; the REDA code could be open-source, shared on platforms such as GitHub and promoted for use and development in the world-wide community. However, it is to be considered that limitations of stand-alone Python scripts in providing Graphical User Interface and a friendly user experience could make it a less favorable choice (compared to alternatives such as Visual Basic .NET.) if the REDA system is going to be used not only by the scientific community, but also by non-experienced stakeholders – which is partially the goal of our project. A consensus is yet to be reached, also following stakeholder meetings for understanding their needs more specifically.
- The REDA will provide outputs in the form of maps, graphs (those two contributing to automatic reports useful for stakeholder reporting needs and bureaucratic procedures) and data which will be easily integrated in a webGIS platform but also in the REDACt Smartphone app.

6 CONCLUSIONS

In this deliverable we analyzed the main methodologies and software used for rapid earthquake loss estimation world-wide. This allows us to discriminate between approaches significantly different, more or less detailed from a modeling point of view:

- based on seismic intensity values and direct correlations with potential of casualties and economic losses (PAGER approach; ELER Level 0);
- based on seismic intensity values and vulnerability functions for buildings (Giovinazzi, 2005; used in QLARM and in ELER Level 1) and casualty models;
- based on seismic PGA, PGV and SA values, capacity and fragility functions or directly vulnerability functions for structures (used in HAZUS or EU-RISK and most of the recent REDA software and more recommended even though harder to provide input for);
- more empirical approaches (but generally less used) can be found, relying on GIS multi-criteria decision analysis.

In most REDA systems, an initial effort is put in quantifying the expected damage of buildings and structures such as bridges and later using these estimates in computing socio-economic direct and indirect impact, generally with empirical models. At a systemic level (for transportation networks or lifelines), the models are generally observational and highly uncertain in applying to other case study areas. The scale of the analysis (which in many situations shouldn't be at individual structure level but at a broader more generic level, depending on the way fragility or vulnerability functions are tied to very detailed structural typologies) has a significant impact on the analysis, as well as regional and national differences.

In order for REDACt Project to develop a successful REDA system in the Black Sea area we believe that it is suitable for it to contain a combination of the above-mentioned methodologies for earthquake loss estimations, along with harmonized hazard and exposure datasets as detailed as possible and at comparable resolutions from country to country. One of the methods should provide very rapidly a first general casualty estimation, enabling a prompt activation of emergency management procedures. However, tests will be required to examine if the discrepancies between different methodologies, using different intensity measurements and datasets, are significant enough that may lead to misleading results.

Compared to existing world-wide systems, the opportunity of the REDACt platform to provide improved loss estimations in the Black Sea area is great. In its design, new concepts such as rapid loss validation, dynamic adjustment of vulnerability models but also regional specific data integration (in terms of hazard, with important specific effects of intermediate-depth Vrancea earthquakes; in terms of building typologies and socio-economic vulnerability) should be considered. Also, adding a cascading-hazard module to the REDA, which with available methods can assess the susceptibility and the regional hazard for landslides and liquefaction, would render it as an important example in the field. Designing the platform in order to be easily adjustable elsewhere and modifiable would be a significant goal toward the sustainability of this initiative.

REFERENCES

Abrahamson, N. A. and J. J. Bommer (2005). Probability and uncertainty in seismic hazard analysis. Earthquake spectra 21(2), 603–607.

A Scientific Network for Earthquake, Landslide and Flood Hazard Prevention: Deliverable No. D.01.01 "Current Status Assessment (Legislation and bibliography review)". BSB JOP 2007-13 Project SciNetNatHaz, 2014 [http://scinetnathaz.net/wp-content/uploads/2016/11/D_03_01_Vol_2_landslides_HA.pdf]

Agrawal, A. K., Ghosn, M., Alampalli, S., & Pan, Y. (2012). Seismic fragility of retrofitted multispan continuous steel bridges in New York. Journal of Bridge Engineering, 17(4), 562-575.

Akbari, R. (2012). Seismic fragility analysis of reinforced concrete continuous span bridges with irregular configuration. Structure and Infrastructure Engineering, 8(9), 873-889.

American Lifelines Alliance, "Guideline for the Design of Buried Steel Pipe," USA, 2001,2005.

AmiriHormozaki, E., Pekcan, G., & Itani, A. (2015). Analytical fragility functions for horizontally curved steel I-girder highway bridges. Earthquake Spectra, 31(4), 2235-2254.

Andrews, D.C., Martin, G.R., 2000. Criteria for liquefaction of silty sands, Proceedings of the 12th World Conference on Earthquake Engineering, Auckland, New Zealand.

Applied Technology Council, ATC (1985) Earthquake damage evaluation data for California. Report No. ATC-13, Applied Technology Council, Redwood City, CA

Applied Technology Council, ATC (1991) Seismic vulnerability and impact of disruption of life lines in the conterminous United States. Report No. ATC-25, Applied Technology Council, Redwood City, CA

ATC (Applied Technology Council) (1985) Earthquake damage evaluation data for California, Redwood

Avşar Ö, Yakut A (2010) Evaluation of ground motion intensity measures for the fragility curves of ordinary highway bridges in Turkey. In: Proceedings of the 9th US national & 10th Canadian conference on earthquake engineering, Toronto

Avşar Ö, Yakut A, Caner A (2011) Analytical fragility curves for ordinary highway bridges in Turkey. Earthq Spectra 27(4):971–996

Aygün B, Duenas-Osorio L, Padgett JE, DesRoches R (2011) Efficient longitudinal seismic fragility assessment of a multispan continuous steel bridge on liquefiable soils. ASCE J Bridge Eng 16(1):93–107

Azevedo J, Guerreiro L, Bento R, Lopes M, Proenc¸a J (2010) Seismic vulnerability of lifelines in the greater Lisbon area. Bull Earthq Eng 8(1):157–180

Baker, J. W. (2008). An introduction to probabilistic seismic hazard analy sis (psha). https://web.stanford.edu/~bakerjw/Publications/Baker_(2008)_Intro_to_PSHA_v1_3.pdf.

Bardakis VG, Fardis MN (2011) Nonlinear dynamic v elastic analysis for seismic deformation demands in concrete bridges having deck integral with the piers. Bull Earthq Eng 9(2):519–536

Basöz N, Kiremidjian AS (1996) Risk assessment for highway transportation systems. The John A. Blume Earthquake Engineering Center, Stanford Basöz NI, Kiremidjian AS, King SA, Law KH (1999) Statistical analysis of bridge damage data from the 1994 Northridge, CA, earthquake. Earthq Spectra 15(1):25-54

Bastin S, Quigley M, Bassett K (2015) Paleoliquefaction in easter Christchurch. N Z Geol Soc Am Bull 127:1348–1365

Bastin S, Stringer M, Green R, Wotherspoon L, van Ballegooy S, Cox B, Osuchowski A (2018) Geomorphological controls on the distribution of liquefaction in Blenheim, New Zealand, during the 2016 Mw7.8 Kaikoura Earthquake. Geotechnical Earthquake Engineering and Soil Dynamics V GSP 290

Bastin S, van Ballegooy S, Mellsop N, Wotherspoon L. 2020. Liquefaction case histories from the 1987 Edgecumbe earthquake, New Zealand-Insights from an extensive CPT dataset and paleo-liquefaction trenching. Engineering Geology 271, 105404

Bastin, S., van Ballegooy, S., Mellsop, N., Wotherspoon, L., (2017). Liquefaction case histories from Whakatane, New Zealand as a result of the 1987 Edgecumbe Earthquake - Insights from an extensive CPT dataset and paleo-liquefaction trenching, 3rd International Conference on Performance-based Design in Earthquake Geotechnical Engineering (PBD-III) Vancouver, BC, Canada, July 16-19

Billah, A. M., & Alam, M. S. (2020). Seismic Fragility Assessment of Multi-Span Concrete Highway Bridges in British Columbia Considering Soil-Structure Interaction. Canadian Journal of Civil Engineering, (ja).

Borcherdt RD (1994) Estimates of site-dependent response spectra for design (method and justification). Earthq Spectra 10:617–654

Boulanger, R.W., & Idriss, I.M. 2006. Liquefaction susceptibility criteria for silts and clays. Journal of Geotechnical and Geoenvironmental Engineering. 132 (11): 1413–1426.

Bray JD, Sancio RB (2006) Assessment of the liquefaction susceptibility of fine-grained soils. J Geotech Geoenviron Eng 132:1165–1177

Burton, H.V., Deierlein, G., Lallemant, D., Lin, T., 2016. Framework for Incorporating Probabilistic Building Performance in the Assessment of Community Seismic Resilience. J. Struct. Eng. 142. https://doi.org/10.1061/(ASCE)ST.1943-541X.0001321

Cardone D, Perrone G, Sofia S (2011) A performance-based adaptive methodology for the seismic evaluation of multi-span simply supported deck bridges. Bull Earthq Eng 9(5):1463–1498 Casciati F,

Cavalieri F., Correia A.A., Crowley H., Pinho R. (2020), "Dynamic soil-structure interaction models for fragility characterisation of buildings with shallow foundations", Soil Dynamics and Earthquake Engineering, vol. 132, pp. 106004, https://doi.org/10.1016/j.soildyn.2019.106004

CDMG, 1999. Guidelines for analyzing and mitigating liquefaction hazards in California, California Department of Conservation, Division of Mines and Geology, Special Publication 117, p. 63

Ceresa P, Borzi B, Noto F, Onida M (2012a) Application of a probabilistic mechanics-based methodology for the seismic risk assessment of the Italian RC bridges. In: 15th world conference on earthquake engineering, Lisbon

Cetin, K. O., Seed, R. B., Der Kiureghian A., Tokimatsu K., Kayen R. E., Bilge H. T., Ilgac M., Harder, L. H. Jr., Moss, R. E. S., and K. Chowdhury (2016-b), "SPT-Based Probabilistic and Deterministic Assessment of Seismic Soil Liquefaction Triggering Hazard", ASCE J. of Geotech. and Geoenvir.

Chen, X. (2020). System Fragility Assessment of Tall-Pier Bridges Subjected to Near-Fault Ground Motions. Journal of Bridge Engineering, 25(3), 04019143.

Choe D-E, Gardoni P, Rosowsky D, Haukaas T (2009) Seismic fragility estimates for reinforced concrete bridges subject to corrosion. Struct Saf 31:275–283

Choi E, DesRoches R, Nielson B (2004) Seismic fragility of typical bridges in moderate seismic zones. Eng Struct 26(2):187–199

Civico R, Brunori CA, De Martini PM, Pucci S, Cinti FR, Pantosti D (2015) Liquefaction susceptibility assessment in fluvial plains using airborne lidar: the case of the 2012 Emilia earthquake sequence area (Italy). Nat Hazards Earth Syst Sci 15:2473–2483

CNS 2001. Code for seismic design of buildings. National Standard GB 50011-2001. China Building Industry Press, Beijing.

Coburn, A., Spence, R., 2002. Earthquake Protection, 2nd ed, John Wiley & Sons. John Wiley & Sons, Ltd.

Cornell C. A. (1968). Engineering seismic risk analysis Bull Seism Soc Am, 58 (5), pp. 1583-1606Demircioglu MB, Erdik M, Hancilar U, Sesetyan K, Tuzun C, Yenidogan, Zulfikar AC (2009), Technical Manual – Earthquake Loss Estimation Routine ELER-v1.0, Bogazici University, Department of Earthquake Engineering, Istanbul, March 2009

Corominas j., Van Westen C., Frattini P., Cascini L., Malet J.-P., Fotopoulou S., Catani F., Van Den Eeckhaut M., Mavrouli O., Agliardi F., Pitilakis K., Winter M. G., Pastor M., Ferlisi S., Tofani V., Hervas J., Smith J. T., (2014), "Recommendations for the quantitative analysis of landslide risk", Bull Assoc Eng. Geol. Environ 10.1007/s10064-013-0538-8

Crowley H., Borzi B., Pinho R., Colombi M., Onida M. (2008) Comparison of Two Mechanics-Based Methods for Simplified Structural Analysis in Vulnerability Assessment, Advances in Civil Engineering, Article ID 438379

De Felice G, Giannini R (2010) An efficient approach for seismic fragility assessment with application to old reinforced concrete bridges. J Earthq Eng 14(2):231–251

Di Manna P, Guerrieri L, Piccardi L, Vittori E, Castaldini D, Berlusconi A, Bonadeo L, Comerci V, Ferrario F, Gambillara R, Livio F, Lucarini M, Michetti AM (2012) Ground effects induced by the 2012 seismic sequence in Emilia: implications for seismic hazard assessment in the Po Plain. Ann Geophys 55(4):697–703

Donahue, J.L., Bray, J.D., and Reimer, M.R.. "Liquefaction Testing of Fine-Grained Soil prepared Using Slurry Deposition", 08/01/2006-07/31/2007, , K. Pitilakis"Proc. 4th Inter. Conf. Earthquake Geotechnical Engineering", 2007, "Paper No. 1226, June 25-28".

Douglas, J. (2018). Ground motion prediction equations 1964–2018, report. Accessible on http://www. gmpe. org. uk/gmpereport2014. pdf .

Douglas J. (2007) Inferred ground motions on Guadeloupe during the 2004 Les Saintes earthquake, Bull. Earthq. Eng. 5 (3): 363-376.

Earle PS, Wald DJ, Allen TI, Jaiswal KS, Porter KA, Hearne MG (2009b) Rapid exposure and loss estimates for the May 12, 2008 MW 7.9 Wenchuan earthquake provided by the U.S. Geological Survey's PAGER system. In: Proceedings of the 14th world conference earthquake engineering Beijing, China, Paper, 8 pp

Earle PS, Wald DJ, Jaiswal KS, Allen TI, Marano KD, Hotovec AJ, Hearne MG, Fee JM (2009a) Prompt Assessment of Global Earthquakes for Response (PAGER): a system for rapidly determining the impact of global earthquakes worldwide. U.S. Geological Survey Open-File Report 2009-1131

Eidinger J., B. Maison, D. Lee and B. Lau, "East bay municipal district water distribution damage in 1989 Loma Prieta earthquake," in Conference of Lifeline Earthquake Engineering, Reston, 1995.

Elnashai AS, Borzi B, Vlachos S (2004) Deformation-based vulnerability functions for RC bridges. Struct Eng Mech 17(2):215–244

Elnashai,AS, Hampton S, Karaman H, Lee JS, Mclaren T, Myers J, Navarro C, Sahin M, Spencer B, Tolbert N (2007) Overview and applications of Maeviz-Hazturk 2007. J Earthq Eng 12(S2),:100–108

Erdik M., K. Sesetyan, M.B. Demircioglu, C. Zulfikar, U. Hancilar, C Tuzun, e Harmandar; A. Ansal (ed.), Perspectives on European Earthquake Engineering and Seismology, Geotechnical, Geological and Earthquake Engineering 34, DOI 10.1007/978-3-319-07118-3_2

FEMA (2010) Hazus MH MR5 technical manual. Federal Emergency Management Agency, Washington, DC

Ferentinou M. D., M. Sakellariou, V. Matziaris, and S. Charalambous, "An Introduced Methodology for Estimating Landslide Hazard for Seismic and Rainfall Induced Landslides in a Geographical Information System Environment" in "Geohazards", ECI Symposium Series, (2006). https://dc.engconfintl.org/geohazards/40

Fotopoulou S., Karapetrou S., Pitilakis K. (2012), "Seismic vulnerability of RC buildings considering SSI and aging effects", Proceedings of the Proceedings of the 15WCEE international conference, Lisboa

Fotopoulou S.D., Pitilakis K.D. (2013), "Fragility curves for reinforced concrete buildings to seismically triggered slow-moving slides", Soil Dynamics and Earthquake Engineering, vol. 48, pp. 143-161, https://doi.org/10.1016/j.soildyn.2013.01.004

Franchin P, Lupoi A, Pinto PE (2006) On the role of road networks in reducing human losses after earthquakes. J Earthq Eng 10(2):195–206

Gardoni P, Mosalam KM, Der Kiureghian A (2003) Probabilistic seismic models and fragility estimates for RC bridges. J Earthq Eng 7(1):79–106

Gardoni P, Rosowsky D (2009) Seismic fragility increment functions for deteriorating reinforced concrete bridges. Struct Infrastruct Eng 7(11):869–879

Gehl P., N. Desramaut, A. Réveillère and H. Modaressi, "Fragility Functions of Gas and Oil Networks," in Geotechnical, Geological and Earthquake Engineering, SYNER-G: Typology Definition and Fragility Functions for Physical Elements at Seismic Risk, 2014, pp. 187-220.

Guerin-Marthe S., Gehl P., Negulescu C., Auclair S., Fayjaloun R. (2020) Rapid earthquake response: The state-of-the art and recommendations with a focus on European systems, International Journal of Disaster Risk Reduction, doi:10.1016/j.ijdrr.2020.101958.

Gutenberg, B. and C. F. Richter (1944). Frequency of earthquakes in california. Bulletin of the Seismological Society of America 34 (4), 185–188.

Holzer TL, Noce TE, Bennett MJ 2011. Liquefaction probability curves for surficial geologic deposits. Environmental and Engineering Geoscience, XVII(1):1-21

Idriss IM, Boulanger RW. Examination of SPT-Based Liquefaction Triggering Correlations. Earthquake Spectra. 2012;28(3):989-1018. doi:10.1193/1.4000071

Idriss, I.M., Boulanger, R.W., 2008. Soil Liquefaction during Earthquakes. EERI Publication, 235 pp

Ishihara K., 1985. Stability of natural deposits during earthquakes. Proceedings of the 11th International Conference on Soil Mechanics and Foundation Engineering, vol. 1, A.A. Iwasaki et al. (1978

Isoyama R. and Katayama T., "Reliability evaluation of water supply system during earthquakes.," University of Tokyo, 1982.

Isoyama R., E. Ishida, K. Yune and T. Shirozu, "Seismic damage estimation procedure for water supply pipelines," in 12th World Conference on Earthquake Engineering, Auckland, 2000.

Iwasaki, T. Tokida, K., Tatsuoka, F., Watanabe, S., Yasuda, S., Sato, H., 1982. Microzonation for soil liquefaction potential using simplified methods, Proceedings of the 3rd International Conference on microzonation, Seattle, 3, pp. 1310-1330.

Jeong SH, Elnashai AS (2007) Probabilistic fragility analysis parameterized by fundamental response quantities. Eng Struct 29(6):1238–1251

Jessee, M. A., Hamburger M. W., Allstadt K., Wald D. J., Robeson S. M., Tanyas H., Hearne M., Thompson E. 2018. A global empirical model for near-real-time assessment of seismically induced landslides. Journal of Geophysical Research: Earth Surface, 123, 1835–1859. https://doi.org/10.1029/2017JF004494

Juang, C. Hsein, Liu, Chia-Nan, Chen, Chien-Hsun, Hwang, Jin-Hung, Lu, Chih-Chieh, 2008. Calibration of liquefaction potential index: a re-visit focusing on a new CPTU model. Eng. Geol. 102 (1), 19–30. http://dx.doi.org/10.1016/j.enggeo.2008.06.005

Kappos, A.J., Stylianidis, K.C., Sextos, A., Papanikolaou, V., Panagopoulos, G., Kouris, L., Goutzika, E., Panagiotopoulos, Ch. (2009) "SRM-DGC. Development and Proposition for Implementation of an Efficient Methodology and Appropriate Local Instruments for the Management, Prevention and Reduction of Seismic Risk in Düzce-Turkey, Grevena-Greece and Catania-Italy. D14: Vulnerability Analysis and Loss Estimation in Grevena", AUTh, Greece.

Kappos, A.J., Panagopoulos, G., 2010. Fragility curves for reinforced concrete buildings in Greece. Structure and Infrastructure Engineering 6, 39–53. https://doi.org/10.1080/15732470802663771

Kappos, A.J., Panagopoulos, G., Penelis, G.G., 2008. Development of a seismic damage and loss scenario for contemporary and historical buildings in Thessaloniki, Greece. Soil Dynamics and Earthquake Engineering 28, 836–850.

Kappos, A.J., Panagopoulos, G.K., Sextos, A.G., Papanikolaou, V.K., Stylianidis, K.C., 2010. Development of comprehensive earthquake loss scenarios for a Greek and a Turkish city - structural aspects. Earthquakes and Structures 1, 197–214.

Karakostas, C., Lekidis, V., Kappos, A.J., Panagopoulos, G.K., Keramitsoglou, I., Kontoes, Ch., 2012. Evaluation of seismic vulnerability of buildings in Athens and L'Aquila in the framework of the MASSIVE seismic mitigation system, in: 15 WCEE. Lisbon, Portugal.

Karapetrou S.T., Fotopoulou S.D., Pitilakis K.D. (2015), "Seismic vulnerability assessment of high-rise non-ductile RC buildings considering soil-structure interaction effects", Soil Dynamics and Earthquake Engineering, vol. 73, pp. 42-57, https://doi.org/10.1016/j.soildyn.2015.02.016

Karatzetzou A., Riga E., Pitilakis K. (2018), "Soil structure interaction effects at urban scale", Proceedings of the 16th European Conference on Earthquake Engineering (16ECEE), Thessaloniki, Greece

Karim KR, Yamazaki F (2001) Effect of earthquake ground motions on fragility curves of highway bridge piers based on numerical simulation. Earthq Eng Struct Dyn 30(12):1839–1856

Karim KR, Yamazaki F (2003) A simplified method of constructing fragility curves for highway bridges. Earthq Eng Struct Dyn 32(10):1603–1626

Katayama et al, “Earthquake damage to water and gas distribution systems,” in U.S. National Conference on Earthquake Engineering, Oakland, 1975.

Kiani, J., Camp, C., Pezeshk, S., 2019. On the application of machine learning techniques to derive seismic fragility curves. Computers & Structures 218, 108–122. https://doi.org/10.1016/j.compstruc.2019.03.004

Kibboua A, Naili M, Benouar D, Kehila F (2011) Analytical fragility curves for typical Algerian reinforced concrete bridge piers. Struct Eng Mech 39(3):411–442

Kim S-H, Shinozuka M (2004) Development of fragility curves of bridges retrofitted by column jacketing. Probab Eng Mech 19(1–2):105–112

Knudsen KL, Bott J (2011) Geologic and geomorphic evaluation of liquefaction case histories for rapid hazard mapping. Seismol Res Lett 82:334

Kontoes, C., Herekakis, T., Ieronymidi, E., Keramitsoglou, I., Papadopoulos, G.A., Paralikidis, S., Aifantopoulou, D., Deflorio, A.M., Iasillo, D., Kiranoudis, C.T., 2012. Mapping Seismic Vulnerability and Risk of Cities: The MASSIVE Project. Journal of Earth Science and Engineering 2, 496–513.

Kramer, S. L. (1996). Geotechnical Earthquake Engineering (Prentice-Hall International Series in Civil Engineering and Engineering Mechanics) (1 ed.). Prentice Hall.

Kurian SA, Deb SK, Dutta A (2006) Seismic vulnerability assessment of a railway overbridge using fragility curves. In: 4th international conference on earthquake engineering, Taipei

Kuribayashi E, Tatsuoka F (1975) Brief review of soil liquefaction during earthquakes in Japan. Soils Found 15(4):81–92

Kwon O, Sextos AG, Elnashai, AS (2009) Seismic fragility of a bridge on liquefaction susceptible soil. In: 10th international conference on structure safety and reliability, Osaka

Kwon O-S, Elnashai AS (2009) Fragility analysis of a highway over-crossing bridge with consideration of soil-structure interactions. Struct Infrastruct Eng 6(1–2):159–178

Lanzano G., Salzano E., Santucci de Magistris F., Fabbrocino G., ‘’An observational analysis of seismic vulnerability of industrial pipelines’’, Chemical Engineering Transactions, 26, 567-572, 2012.

Lanzano, G., E. Salzano, F. S. de Magistris, and G. Fabbrocino.“Seismic vulnerability of gas and liquid buried pipelines.” J. Loss Prev. Process Ind. 28 (Apr): 72–78, 2014.

Lanzano G., E. Salzano, F.S. Magistris and G. Fabbrocino, “Performance assessment of continuous buried pipelines under earthquake loadings,” Chem. Eng. Trans, vol. 31, no. 1, pp. 631-636, 2013.

Lee, D.H., Ku, C.S., Yuan, H., 2003 A study of the liquefaction risk potential at Yanlin. Taiwan, Engineering Geology 71, 97-117

Li J, Spencer BF, Elnashai AS (2012) Bayesian updating of fragility functions using hybrid simulation. ASCE J Struct Eng 139(7):1160–1171

Li, A.J., Merifield, R.S., Lyamin, A.V., 2008. Stability charts for rock slopes based on the Hoek–Brown failure criterion. Int. J. Rock Mech. Min. Sci. 45 (5), 689–700

Li., D.K, Juang, C.H., Andrus, R.D., and Camp, W.M. 2007. Index properties-based criteria for liquefaction susceptibility of clayey soils: a critical assessment, Journal of Geotechnical and Geoenvironmental Engineering, 133(1): 110-115

Lu, D. G., & Huang, M. G. (2020). Identification of the Most Fragile Component for a Typical RC Bridge Using Seismic Fragility Curves. Tehnički vjesnik, 27(1), 46-52.

Lupoi A, Franchin P, Pinto PE, Monti G (2005) Seismic design of bridges accounting for spatial variability of ground motion. Earthq Eng Struct Dyn 34(4-5):327–348

Lupoi G, Franchin P, Lupoi A, Pinto PE (2004) Seismic fragility analysis of structural systems. In: 13th world conference on earthquake engineering, Vancouver

Mackie K, Stojadinovic´ B (2004) Fragility curves for reinforced concrete highway overpass bridges. In: 13th world conference on earthquake engineering, Vancouver

Mackie K, Stojadinovic´ B (2007) R -factor parameterized bridge damage fragility curves. ASCE J Bridge Eng 12(4):500–510

Maio R., Tsionis G., 2015. Seismic fragility curves for the European building stock, JRC Technical Report, European Commission

Marano GC, Greco R, Mezzina M (2006) Analytical evaluation of fragility curves by using stochastic approach. In: 2nd fib international congress,

Martins, L., Silva, V., 2020. Development of a fragility and vulnerability model for global seismic risk analyses. Bull Earthquake Eng. https://doi.org/10.1007/s10518-020-00885-1

Matsuoka, M., K. Wakamatsu, M. Hashimoto, S. Senna, and S. Midorikawa (2015). Evaluation of liquefaction potential for large areas based on geomorphologic classification, Earthq. Spectra 31, 2375–2395

Maurer et al 2017. Assessing Liquefaction Susceptibility Using the CPT Soil Behavior Type Index. In Conference of Earthquake Geotechnical Engineering, PBD III Vancouner

Maurer, B., Green, R., Cubrinovski, M., Bradley, B., 2014. Evaluation of the liquefaction potential index for assessing liquefaction hazard in christchurch, New Zealand. J. Geotech. Geoenviron. Eng. 140 (7), 04014032

Mavrouli O., Fotopoulou S., Pitilakis K., Zuccaro G., Corominas J., Santo A., Cacace F., De Gregorio D., Di Crescenzo G., Foerster E., Ulrich T. (2014), "Vulnerability assessment for reinforced concrete buildings exposed to landslides", Bulletin of Engineering Geology and the Environment, vol. 73, no. 2, pp. 265-289, 10.1007/s10064-014-0573-0

Michel, C., Crowley, H., Hannewald, P., Lestuzzi, P., and Fäh, D. (2018). "Deriving fragility functions from bilinearized capacity curves for earthquake scenario modelling using the conditional spectrum." Bull. Earthq. Eng., 16(10), 4639–4660.

Moschonas IF, Kappos AJ, Panetsos P, Papadopoulos V, Makarios T, Thanopoulos P (2009) Seismic fragility curves for Greek bridges: methodology and case studies. Bull Earthq Eng 7(2):439–468

Moss R.E.S., & Chen, G. 2008. Comparing liquefaction procedures in the U.S. and China. Proceedings of the 14th World Conference on Earthquake Engineering. Beijing, China, October 12-17, 2008.

Naples Monti G, Nistico` N (2002) Simple probability-based assessment of bridges under scenario earthquakes. ASCE J Bridge Eng 7(2):104–114

Nateghi F, Shahsavar VL (2004) Development of fragility and reliability curves for seismic evaluation of a major prestressed concrete bridge. In: 13th world conference on earthquake engineering, Vancouver

Nielson BG, DesRoches R (2007) Seismic fragility methodology for highway bridges using a component level approach. Earthq Eng Struct Dyn 36(6):823–839

Noori, H. R., Memarpour, M. M., Yakhchalian, M., & Soltanieh, S. (2019). Effects of ground motion directionality on seismic behavior of skewed bridges considering SSI. Soil Dynamics and Earthquake Engineering, 127, 105820.

Nowicki M.A., Wald D., Hamburger M., Hearne M., Thompson E. 2014. Development of a globally applicable model for near real-time prediction of seismically induced landslides. Engineering Geology, 173, pp. 54-65

Ohtori, Y. and Hirata K., 2007. Conversion Methods of Ground Motion Index for Fragility Curve, CRIEPI Civil Engineering Research Laboratory Rep.No.N05053, Tokyo, Japan

Ordaz, M., A. Aguilar, and J. Arboleda (2007). Program for computing seismic hazard. CRISIS, V1.

O'Rourke M., "Analytical fragility relation for buried segmented pipe," 2009.

O'Rourke and E. Deyoe, "Seismic damage to segmented buried pipe," Earthquake Spectra, vol. 20, no. 4, pp. 1167-1183, 2004.

O'Rourke and G. Ayala, "Pipeline damage due to wave propagation," Journal of Geotechnical Engineering, vol. 119, no. 9, p. 1490–1498., 1993.

O'Rourke and S.S. Jeon, "Factors affecting the earthquake damage of water distribution systems," in 5th U.S. Conference on Lifeline Earthquake Engineering, Reston, 1999.

O'Rourke, E. Filipov and E. Uckan, "Towards robust fragility relations for buried segmented pipe in ground strain areas," Earthquake Spectra, vol. 31, no. 3, p. 1839–1858, 2015.

O'Rourke, S. Toprak and Y. Sano, “Factors affecting water supply damage caused by the Northridge earthquake,” in ProceedingsoftheSixthUSNationalConference on Earthquake Engineering, 1998.

O'Rourke, S.S. Jeon, S. Toprak, M. Cubrinovski, M. Hughes, M.V. Ballegooy and S. et al, “Earthquake response of underground pipeline networks in Christchurch, NZ. 30, .,” in Earthquake Spectra.

Padgett JE, DesRoches R (2009) Retrofitted bridge fragility analysis for typical classes of multispan bridges. Earthq Spectra 25(1):117–141

Papathanassiou G., Ganas Ath., Valkaniotis S. 2016. Recurrent liquefaction-induced failures triggered by 2014 Cephalonia, Greece earthquakes: Spatial distribution and quantitative analysis of liquefaction potential, Engineering Geology, Vol 200, pp 18-30, doi:10.1016/j.enggeo.2015.11.011

Papathanassiou G., Mantovani A., Tarabusi G., Rapti D., Caputo R. 2015. Assessment of liquefaction potential for two liquefaction prone areas considering the May 20, 2012 Emilia (Italy) earthquake, Engineering Geology, Vol 189, pp 1–16, http://dx.doi.org/10.1016/j.enggeo.2015.02.002

Papathanassiou G., Pavlides Sp. 2011. GIS-based database of historical liquefaction occurrences in the broader Aegean region, DALO v1.0, Quaternary International, Vol 242, 1, pp 115-125, DOI 10.1016/j.quaint.2011.03.049

Papathanassiou, G., 2008. LPI-based approach for calibrating the severity of liquefaction induced failures and for assessing the probability of liquefaction surface evidence. Eng. Geol. 96, 94–104

Papatheodorou K., Klimis N., Moutsokapas Pr., Koutrakis S., Margaris B. 2007. Geotechnical earthquake hazard assessment based on a GIS platform. Paper No 1441, 4th International Conference on Earthquake Engineering, Thessaloniki, Greece.

Park J, Choi E (2011) Fragility analysis of track-on steel-plate-girder railway bridges in Korea. Eng Struct 33(3):696–705

Park YJ, Ang AHS (1985) Seismic damage analysis of reinforced concrete buildings. ASCE J Struct Eng 111(4):740–757

Pitilakis K.D., Karapetrou S.T., Fotopoulou S.D. (2014), "Consideration of aging and SSI effects on seismic vulnerability assessment of RC buildings", Bulletin of Earthquake Engineering, vol. 12, no. 4, pp. 1755-1776, 10.1007/s10518-013-9575-8

Pitilakis, K., Alexoudi, M., Argyroudis, S., Anastasiadis, A., 2006. Seismic Risk Scenarios For An Efficient Seismic Risk Management: The Case Of Thessaloniki (Greece), in: Wasti, S.T., Ozcebe, G. (Eds.), Advances in Earthquake Engineering for Urban Risk Reduction, Nato Science Series: IV: Earth and Environmental Sciences. Kluwer Academic Publishers, Dordrecht, pp. 229–244. https://doi.org/10.1007/1-4020-4571-9_15

Pitilakis, K.D., Crowley, H., Kaynia, A.M. (Eds.), 2014. SYNER-G: typology definition and fragility functions for physical elements at seismic risk - buildings, lifelines, transportation networks and critical facilities, Geotechnical, geological and earthquake engineering. Springer, https://doi.org/10.1007/978-94-007-7872-6

Pomonis, A., Kappos, A.J., Karababa, F., Panagopoulos, G., 2009. Seismic vulnerability and collapse probability assessment of buildings in Greece, in: Second International Workshop on Disaster Casualties. University of Cambridge, UK.

Porras P. and M. Ordaz, “A New Seismic Intensity Parameter to Estimate Damage in Buried Pipelines due to Seismic Wave Propagation,” Journal of Earthquake Engineering, 2007.

Porras P. and M. Ordaz, “Seismic vulnerability function for high-diameter buried pipelines: MexicoCity’s primary water system case,” in Pipeline Engineering and Construction International Conference, Baltimore, 2003.

Porter, K., 2020. A Beginner’s Guide to Fragility, Vulnerability, and Risk. University of Colorado Boulder, https://www.sparisk.com/pubs/Porter-beginners-guide.pdf.

Prasad GG, Banerjee S (2013) The impact of flood-induced scour on seismic fragility characteristics of bridges. J Earthq Eng 17(6):803–828

Qi’ang W, Ziyan W, Shukui L (2012) Seismic fragility analysis of highway bridges considering multi-dimensional performance limit state. Earthq Eng Eng Vib 11(2):185–193

Rajah S., S. Nasr, K. Ferguson and J. Christopher , “Seismic fragility evaluation of water pipelines,” in Pipelines 2012: Innovations in Design, Construction, Operations and Maintenance—Doing More with Less, Miami, 2012.

Rajeev P., Tesfamariam S. (2012), "Seismic fragilities of non-ductile reinforced concrete frames with consideration of soil structure interaction", Soil Dynamics and Earthquake Engineering, vol. 40, pp. 78-86, https://doi.org/10.1016/j.soildyn.2012.04.008

Ramadan, O. M., Mehanny, S. S., & Kotb, A. A. M. (2020). Assessment of seismic vulnerability of continuous bridges considering soil-structure interaction and wave passage effects. Engineering Structures, 206, 110161.

Reiter, L. (1991). Earthquake hazard analysis: issues and insights. Columbia University Press.

Robertson P.K., Wride C.E. 1998. Cyclic liquefaction and its evaluation based on SPT and CPT, Proceedings NCEER Workshop of Evaluation of Liquefaction Resistance of Soils, Technical Report NCEER-97-0022, State University of New York as Buffalo, pp. 41-87.

Robertson, P.K. 1990.Soil classification using the cone penetration test. CanadianGeotechnical Journal,27(1): 151–158. doi:10.1139/t90-014.

Rossetto, T., D'Ayala, D., Ioannou, I., Meslem, A., 2014. Evaluation of Existing Fragility Curves, in: Pitilakis, K., Crowley, H., Kaynia, A.M. (Eds.), SYNER-G: Typology Definition and Fragility Functions for Physical Elements at Seismic Risk, Geotechnical, Geological and Earthquake Engineering. Springer Netherlands, Dordrecht, pp. 47–93. https://doi.org/10.1007/978-94-007-7872-6_3

Rovithis E., Kirtas E., Bliziotis D., Maltezos E., Pitilakis D., Makra K., Savvaidis A., Karakostas C., Lekidis V. (2017), "A LiDAR-aided urban-scale assessment of soil-structure interaction effects: The case of Kalochori residential area (N. Greece)", Bulletin of Earthquake Engineering, vol. 15, no. 11, pp. 4821-4850, doi:10.1007/s10518-017-0155-1

Saade A., Grace Abou-Jaoude G., Wartman J. 2016. Regional-scale co-seismic landslide assessment using limit equilibrium analysis. Engineering Geology, 204, pp. 53-64

Saez E., Lopez-Caballero F., Modaressi A. (2011), "Effect of the Inelastic Dynamic Soil-Structure Interaction on the Seismic Vulnerability Assessment", Structural Safety, vol. 33, no. 1, pp. 51-63, http://dx.doi.org/10.1016/j.strusafe.2010.05.004

Saxena V, Deodatis G, Shinozuka M, Feng MQ (2000) Development of fragility curves for multi-span reinforced concrete bridges. In: International conference on Monte-Carlo simulation, Monaco

Sedan O., C. Negulescu, M. Terrier, A. Roulle, T. Winter, D. Bertil (2013) Armagedom — a tool for seismic risk assessment illustrated with applications, J. Earthq. Eng. 17(2) 253-281.

Seed, H.B., & Idriss, I.M. 1982. Ground motions and soil liquefaction during earthquakes. Earthquake Engineering Research Institute, Berkeley, California.

Seed, H.B., Idriss, I.M., 1971. Simplified Procedure for evaluation Soil liquefaction potential, Journal Soil Mechanics and Foundation Div., ASCE, 97 SM9, 1249-1273.

Seed, H.B., Tokimatsu, K., Harder, L.F., Chung, R.M., 1985. The influence of SPT procedures in soil liquefaction resistance evaluations, Journal Geotechnical Engineering Division, ASCE, 111 (12), 1425-1445.

Seed, R.B., Cetin, K.O., Moss, R.E.S., Kammerer, A.M., Wu, J., Pestana, J.M., Riemer, M.F., Sancio, R.B., Bray, J.D., Kayen, R.E., Faris, A., 2003. Recent advances in soil liquefaction engineering: a unified and consistent framework, 26th annual ASCE L.A. Geotechnical Spring Seminar, Long Beach, California, 71 pp.

Shinozuka M, Feng MQ, Kim HK, Kim SH (2000b) Nonlinear static procedure for fragility curve development. ASCE J Eng Mech 126(12):1287–1295

Shinozuka M, Feng MQ, Lee J, Naganuma T (2000a) Statistical analysis of fragility curves. ASCE J Eng Mech 126(12):1224–1231

Shirazian S, Ghayamghamian MR, Nouri GR (2011) Developing of fragility curve for two-span simply supported concrete bridge in near-fault area. World Acad Sci Eng Technol 51:571–575

Soleimani, F. (2020). Propagation and quantification of uncertainty in the vulnerability estimation of tall concrete bridges. Engineering Structures, 202, 109812.

Soltanieh, S., Memarpour, M. M., & Kilanehei, F. (2019). Performance assessment of bridge-soil-foundation system with irregular configuration considering ground motion directionality effects. Soil Dynamics and Earthquake Engineering, 118, 19-34.

Sonmez, H., 2003. Modification of the liquefaction potential index and liquefaction susceptibility mapping for a liquefaction-prone area (Inegol, Turkey), Environmental Geology 44, 862-871.

Stewart J.P., Fenves G.L., Seed R.B. (1999), "Seismic Soil-Structure Interaction in Buildings. I: Analytical Methods", Journal of Geotechnical and Geoenvironmental Engineering, vol. 125, no. 1, pp. 26-37, doi:10.1061/(ASCE)1090-0241(1999)125:1(26)

Sullivan IT (2010) Analytical seismic fragility curves for skewed multi-span steel girder bridges. M.Sc. dissertation, Clemson University

Suzuki, A., and Iervolino, I. (2020). “Intensity measure conversion of fragility curves.” Earthquake Engng Struct Dyn. 49, 607–629.

Tanaka S, Kameda H, Nojima N, Ohnishi S (2000) Evaluation of seismic fragility for highway transportation systems. In: 12th world conference on earthquake engineering, Auckland

TC4 (1999) Manual for zonation on seismic geotechnical hazards, publ. JGS

Tinsley, J.C., Youd, T.L., Perkins, D.M., Chen, A.T.F, 1985, Evaluating Liquefaction Potential, in Ziony,J.I., ed., Evaluating earthquake hazards in the Los Angeles Region - an earth science perspective:U.S. Geological Survey Professional Paper 1360, 263-316

Tonkin, Taylor, 2013. Canterbury earthquakes 2010 and 2011. Land Report as at 29 February 2012. Earthquake Commission (108 pp., http://www.tonkin.co.nz/canterburyland- information/docs/downloads2592013/T&T-Stage-3-Report.pdf)

Toprak, S., Holzer, T.L., 2003. Liquefaction Potential Index: Field Assessment, Journal of Geotechnical and Geoenvironmental Engineering, ASCE 129 (4), 315-322.

Tormene, P., 2019. The Integrated Risk Modelling Toolkit: a QGIS plugin driving the OpenQuake Engine. https://doi.org/10.5446/40799

Trendafiloski, G.; Wyss, M.; Rosset, P. (2011) Loss estimation module in the second generation software QLARM. In Human Casualties in Earthquakes: Progress in Modeling and Mitigation; Spence, R., So, E., Scawthorn, C., Eds.; Springer: Dordrecht, The Netherland; pp. 381–391.

Tsionis, G., & Fardis, M. N. (2014). Fragility functions of road and railway bridges. In SYNER-G: Typology definition and fragility functions for physical elements at seismic risk (pp. 259-297). Springer, Dordrecht.

Tsuchida, H., 1971. Estimation of liquefaction potential of sandy soils, Proceedings of the 3rd Joint Meeting, US-Japan, UNJR.

Ulrich T., Negulescu C., Foerster E., Modaressi H., Auclair S. (2011), "Comparison of different numerical methodologies to derive fragility curves of RC buildings with soil-structure interactions", Proceedings of the EURODYN 2011, Eighth International Conference on Structural Dynamics, Leuven, Belgium

Van Ballegooy, S., Malan, P., Jacka, M.E., Lacrosse, V., Leeves, J.R., Lyth, J.E., 2012. Methods for characterizing effects of liquefaction in terms of damage severity, Proc. 15th WCEE, Portugal, Lisbon.

Varnes DJ (1984) Landslide hazard zonation: a review of principles and practice. Natural Hazard Series, vol 3. UNESCO, Paris.

Veletsos A.S., Meek J.W. (1974), "Dynamic Behaviour of Building-Foundation Systems", Earthquake Engineering and Structural Dynamics, vol. 3, no. 2, pp. 121-138

Villamor P, Almond P, Tuttle M, Giona-Bucci M, Langridge RM, Clark K, Ries W, Bastin SH, Ege A, Vandergoes M (2016) Liquefaction features produced by the 2010–2011 Canterbury earthquake sequence in southwest Christchurch New Zealand and preliminary assessment of paleoliquefaction features. Bull Seismol Soc Am. https://doi. org/10.1785/0120150223

Wakamatsu K. 1992. Evaluation of liquefaction susceptibility based on detailed geomorphological classification, Proceedings of the Technical Papers of Annual Meeting Architectural Institute of Japan,B, 1443-1444 (in Japanese)

Worden C.B., D. Wald, T. Allen, K.W. Lin, D. Garcia, G. Cua (2010) A revised groundmotion and intensity interpolation scheme for ShakeMap, Bull. Seismol. Soc. Am. 100 (6): 3083–3096.

Worden C.B., Wald D. (2020) ShakeMap Manual Online: Technical Manual, User's Guide, and Software Guide

Wang, W., 1979. Some findings in soil liquefaction, Research report water conservancy and hydroelectric power scientific research institute, Beijing, China, pp. 1-17.

Weatherill, G.A., Silva, V., Crowley, H., and Bazzurro, P. (2015), "Exploring the impact of spatial correlations and uncertainties for portfolio analysis in probabilistic seismic loss estimation" Bull. Earthq. Eng., 13(4), 1–25.

Witter CR, Knudsen LK, Sowers MJ, Wentworth MC, Koehler DR, Randolph CE (2006) Maps of Quaternary Deposits and liquefaction susceptibility in the Central San Francisco Bay Region, California, Open file report 2006-1037, USGS, pp 43

Wotherspoon L, Pender M, Orense RP (2012) Relationship between observed liquefaction at Kaiapoi following the 2010 Darfield earthquake and former channels of the Waimakariri River. Eng Geol 125:45–55. https://doi.org/ 10.1016/j.enggeo.2011.11.001

Xie, Y., & DesRoches, R. (2019). Sensitivity of seismic demands and fragility estimates of a typical California highway bridge to uncertainties in its soil-structure interaction modeling. Engineering Structures, 189, 605-617.

Yamazaki F, Motomura H, Hamada T (2000) Damage assessment of expressway networks in Japan based on seismic monitoring. In: 12th world conference on earthquake engineering, Auckland

Yi JH, Kim SH, Kushiyama S (2007) PDF interpolation technique for seismic fragility analysis of bridges. Eng Struct 29(7):1312–1322

Yi, F. 2014. Estimating soil fines contents from CPT data, Proceedings 3rd International Symposium on Cone Penetration Testing, Las Vegas, Nevada, USA

Youd T L (1998) Screening guide for rapid assessment of liquefaction hazard at highway bridge site. Technical report, MCEER-98-005 pp 58

Youd TL, Perkins DM (1978) Mapping of Liquefaction induced Ground Failure Potential. J Geotech Eng Div 104:433–446

Youd, T.L., 1984. Recurrence of liquefaction at the same site. In: Proceedings of the 8th World Conference on Earthquake Engineering, 3, pp. 231e238

Youd, T.L., Idriss, I.M., Andrus, R.D., Arango, I., Castro, G., Christian, J.T., Dobry, R., Finn, W.D.L., Harder, L.F., Hynes, M.E., Ishihara, K., Koester, J.P., Liao, S.S.C., Marcurson, III WF, Marti, G.R., Mitchell, J.K., Moriwaki, Y., Power, M.S., Robertson, P.K., Seed, R.B., Stokoe II K.H., 2001. Liquefaction resistance of soils: summary report from the 1996 NCEER and 1998 NCEER/NSF workshops on evaluation of liquefaction resistance of soils, Journal of Geotechnical and Geoenvironmental Engineering, ASCE 127 (10), 817-833

Zhang J, Huo Y, Brandenberg SJ, Kashighandi P (2008) Effects of structural characterizations on fragility functions of bridges subject to seismic shaking and lateral spreading. Earthq Eng Eng Vib 7(4):369–382

Zhang, G., Robertson, P.K., Brachman, R., 2002. Estimating liquefaction-induced ground settlements from the CPT for level ground. Can. Geotech. J. 39 (5), 1168–1180. http://dx.doi.org/10.1139/t02-047

Zhong J, Gardoni P, Rosowsky D (2012) Seismic fragility estimates for corroding reinforced concrete bridges. Struct Infrastruct Eng 8(1):55–69

Zhu et al. 2017. An Updated Geospatial Liquefaction Model for Global Application. Bulletin of the Seismological Society of America, Vol. 107, No. 3, pp. doi: 10.1785/0120160198

Zhu J, Daley D, Baise LG, Thompson EM, Wald DJ, Knudsen KL (2015): A Geospatial Liquefaction Model for Rapid Response and Loss Estimation. Earthq. Spectra, 31(3), 1813–1837